**UNIVERSITÁ DEGLI STUDI DI PADOVA**
**DIPARTIMENTO DI SCIENZE CHIMICHE**
**CORSO DI LAUREA MAGISTRALE IN CHIMICA**

**TESI DI LAUREA MAGISTRALE**

# Polymerization Catalysis in Confined Spaces

**Relatore: Prof. Cristiano Zonta**

**Controrelatore: Dott. Marzio Rancan**

**Laureanda: Greta Zuppardo**

**ANNO ACCADEMICO: 2021/2022**

**TABLE OF CONTENTS**

# 1 INTRODUCTION

## 1.1 Ligands in coordination chemistry

In coordination chemistry, ligands are used to control the environment around the metal centers to modulate their electronic and steric properties. One of the main challenges for the scientific community is to synthetize new molecular structures mimicking natural processes. In this context, synthetic complexes represent a large category of catalysts which are composed by organic ligands that surround a metal center. The activity of these catalysts is governed by both the characteristics of the metal ion and the ligand.[1] Beside the catalytic activity, metal complexes have also found several applications in supramolecular chemistry where they are used as building blocks for the synthesis of supramolecular structures able to perform both molecular recognition and catalysis.[2] Among many different ligands, polypyridines represent the widest groups of polydentate ligands reported in literature. In particular, a large class is represented by tripodal ligands having three pyridyl systems linked to a central nitrogen atom.[3] This tris-pyridyl amines have been extensively studied in catalysis and molecular recognition. More in detail, the possibility of modulating steric and electronic properties of the ligand by modifying the substituents of the pyridyl units, has led to the synthesis of a wide range of derivatives with different features, that are reflected on the chemical properties of the relative metal complexes.

### 1.1.1 Tris(2-pyridilmethyl)amine (TPMA) ligands

The most common ligands among the tris-pyridyl amines are the tris(2-pyridilmethyl)amines (**TPMA**), that have been extensively employed during the years due to their chemical stability and their capability to form stable complexes with a large variety of metals (Figure 1).[4]

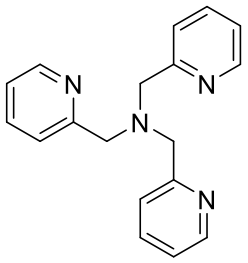


**1**

**Figure 1** Tris(2-pyridilmethyl)amine ligand.

The first synthesis of tris(2-pyridilmethyl)amine dates back to 1967 in the work of Andregg and Wenk.[5] The ligand was obtained by alkylation of primary (2-pyridyl)methylamine **3** with two equivalents of (chloromethyl)pyridine **2** in NaOH solution (Scheme 1) obtaining a brown solid after recrystallization from water (90 % yield). While along the years alkylation has remained the most studied method, in recent years reductive amination has shown to represent a valuable alternative in the presence of sensitive groups, using an aldehyde precursor **4** with ammonium acetate as nitrogen source and triacetoxyborohydride as reducing agent.[6]

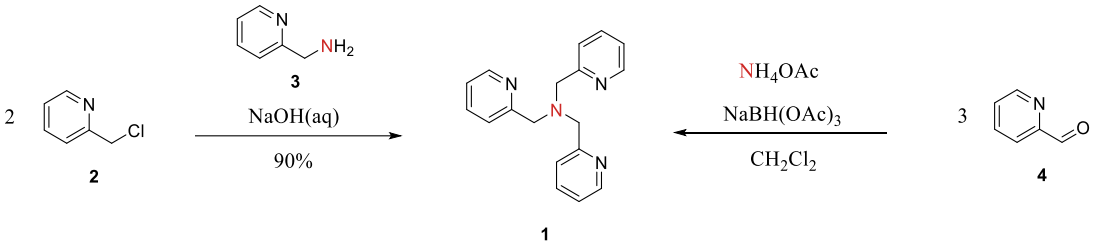


**Scheme 1** Main strategies adopted for **TPMA** synthesis: alkylation and reductive amination.

### 1.1.2 Tris(2-pyridilmethyl)amine (TPMA) complexes

Soon after the synthesis, in 1969, the first **TPMA** metal complex was reported with iron (II) and subsequently with other divalent metals such as copper, cobalt, zinc, nickel, ruthenium and manganese.[7] In general, a 1:1 stoichiometry metal to **TPMA** is observed. The most common geometry of metal based **TPMA** complexes is trigonal bipyramidal where one apical position is occupied by nitrogen of the tertiary amine, and the other one by a solvent molecule or a counter anion. The apical position is usually exploited to bind a monodentate ligand and this could allow to perform both molecular recognition or catalysis.[8,9]

## 1.2 Applications of Tris(2-pyridilmethyl)amine (TPMA) complexes in catalysis

As mentioned before, **TPMA** metal complexes have been extensively employed for catalytic purposes. As example, cobalt (II), iron (II) or nickel (II) **TPMA** complexes have been tested for hydrogen production,[10,11] atom transfer radical addition and polymerization with copper complexes,[12] and carbon dioxide reduction with cobalt complexes.[13,14] In the research group where this thesis has been carried out, **TPMA**-based systems have been extensively studied over the years in several applications including determination of enantiomeric excess of a wide range of substrates[15] and

reductive catalysis,[10,11,12] among which hydrogen evolution reactions (HER) and $CO_2$ reduction. While the work of this thesis is mainly focused on the application of a **TPMA**-based supramolecular cage complexed with copper (II) in atom transfer radical polymerization (ATRP) processes, also the other possible reactivities will be introduced in more details in the next paragraphs.

### 1.2.1 Hydrogen evolution reaction (HER)

Nowadays, hydrogen represents a more sustainable and promising alternative to fossil fuels to keep up with the growing demand for energy.[16] Its direct production from water (protons) has a complex mechanism and requires the use of a catalyst able to rapidly combine two protons and two electrons for the formation of H-H bonds.

$$2\ H^+ + 2e^- \longrightarrow H_2$$

Inspired by natural hydrogenases, in recent years several molecular catalysts have been developed for Hydrogen Evolution Reactions (HER) among which, cobalt polypyridine complexes have been widely employed. In particular, cobalt polypyridine complexes have played a prominent role as catalysts for both electrochemical and light-driven conditions, thanks to their capability to produce hydrogen in a purely aqueous environment avoiding decomposition products like heterogeneous cobalt nanoparticles. The photosynthetic hydrogen evolution under homogeneous conditions is conducted using a standard multi-component photochemical system made up of a photosensitizer ($Ru(bpy_3)$) **6**, a sacrificial electron donor (ascorbate) **7** and the Co-polypyridine complex **5** (Figure 2).

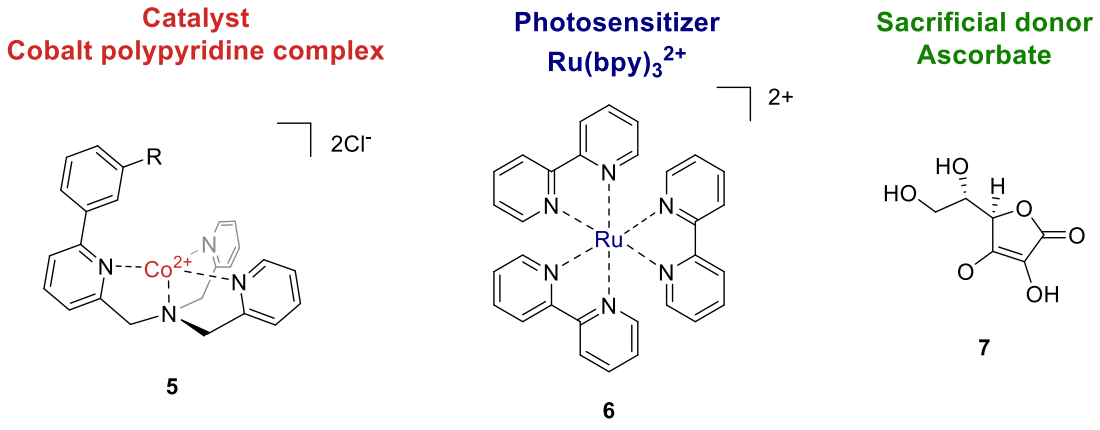


**Figure 2** Standard photochemical system for HER involving a catalyst based on cobalt polypyridine complex **5**, a photosensitizer based on $Ru(bpy)_3^{2+}$ **6,** and ascorbate **7** as sacrificial donor.

$Ru(bpy_3)^{2+}$ is a very efficient photosensitizer due to its strong absorption in the visible region with a long duration excited state that allows it to effectively participate in bimolecular reactions; its suitable reduction and oxidation potentials in the excited state (0.86 and +0.84 V vs. SCE in aqueous solution) to promote the photoinduced electron transfer process; and its ground state reduction and oxidation potentials (1.28 and +1.26 V vs. SCE) to facilitate catalyst activation or donor oxidation. Ascorbate is often used as sacrificial agent since it is water soluble, can be used in high concentrations and allows to work at acidic pH (pH = 4-6) that favors the reaction.

The reductive activation of the catalyst in the system can follow an oxidative or reductive pathway that involve bimolecular processes in homogeneous photochemical conditions.

In 2014, Thummel and coworkers introduced a new cobalt catalyst based on a planar polypyridine ligand with two axial chlorides ligands that catalyzed light-driven hydrogen reduction in aqueous environment. Under irradiation with blue light, at pH = 4 and utilizing $Ru(bpy)_3^{2+}$ and ascorbate as photosensitizer and sacrificial donor (Figure 3a).[17]

In 2016, in the research group where this thesis was carried out, new cobalt complexes based on **TPMA** ligands were developed to promote hydrogen production with a lower overpotential in aqueous solutions under photochemical condition. The presence of substituents with different hydrogen bond donor or acceptor abilities in the second coordination sphere, were investigated to understand the possibility to stabilize the catalytic unit (Figure 3b).[10]

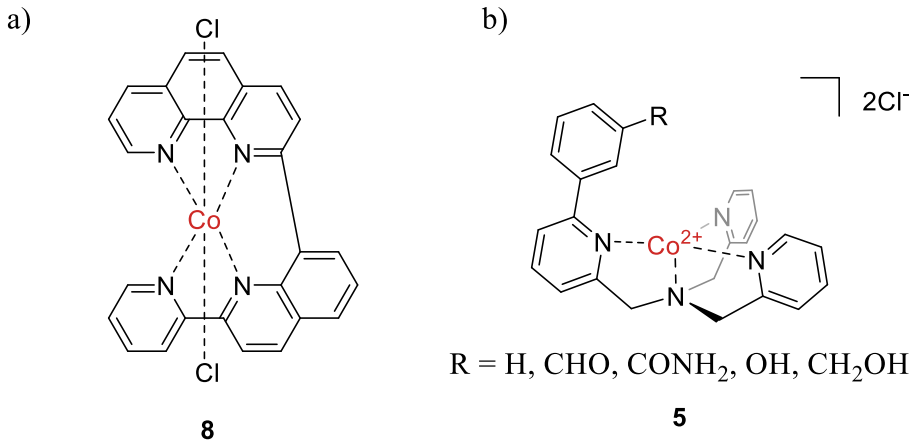


**Figure 3**: a) Thummel cobalt complex based on a planar polypyridine ligand with two axial chlorides **8** , b) **TPMA** cobalt complex based ligand **5** with different substituents on the phenyl ring for HER reaction.

### 1.2.2 Carbon dioxide reduction

Another recent innovation in the field of sustainability, is to convert $CO_2$ into methanol or ethanol, formate and CO through electrochemical methods, replacing hydrocarbon sources for petrochemical raw materials and chemicals. In this approach, catalysis is needed to find a new way to reuse $CO_2$ both by photo and electrochemical reduction. A good catalyst must have a good thermodynamic and kinetic stability, should be very selective to have high turnover number (TON) and should allow electrochemical reduction with a low potential in order to avoid the need to apply large voltages. Furthermore, in the case of electrocatalytic reduction of $CO_2$, also a good Faradic yield, defined as the selectivity of the catalyst to produce CO, it's necessary.

In 2015, Cheng et al reported a new catalyst based on **TPMA** ligands complexed with cobalt chloride **9** for carbon dioxide reduction.[13,14] The reduction potential of $Co^{II}/Co^{I}$ results more negative compared with other cobalt complexes supported by similar ligand scaffolds, and this may be crucial for an efficient carbon dioxide reduction. For a reasonable bond of $CO_2$ with metal complexes the peak of $Co^{II}/Co^{I}$ reduction should be more negative than 1,65 V. The electrocatalytic current at the $Co^{II/I}$ reduction potential observed in the $CO_2$ atmosphere shows a marked increase indicating that the complex can be a good catalyst for the reaction (Figure 4).

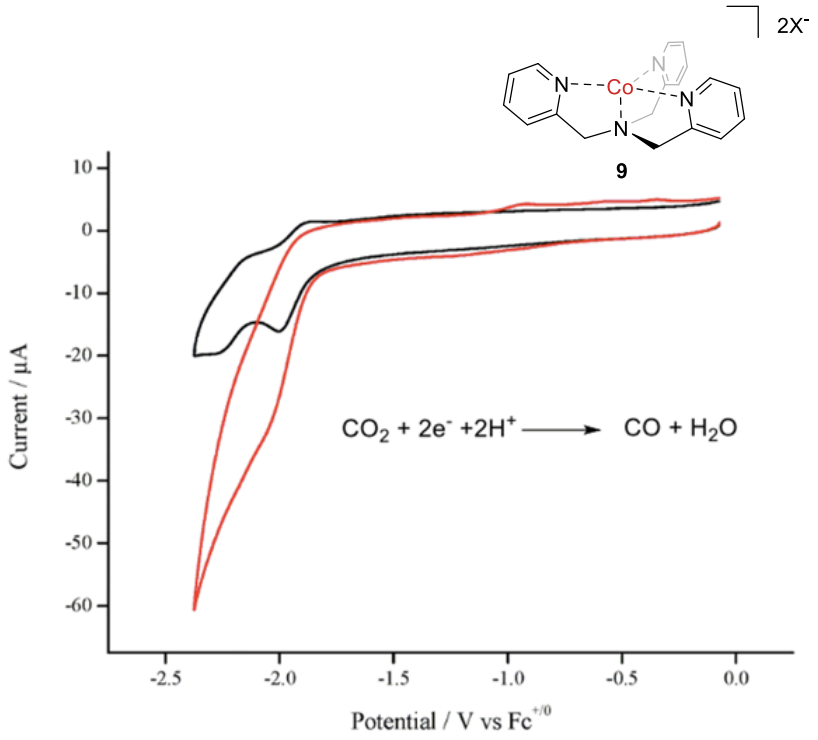


**Figure 4** Co-**TPMA** complex structure and cyclic voltammetry of Cheng's cobalt **TPMA** complex **9** under argon (black) and carbon dioxide (red) using a glassy carbon disk electrode, scan rate = 100 mV $s^{-1}$. Picture taken from reference [13]

## 1.3 Atom Transfer Radical Polymerization

Copper complexes based on **TPMA** ligands are among the most active catalysts in atom transfer radical polymerization.[18,19]

Controlled Reversible-Deactivation Radical Polymerizations (RDRP) are the most powerful methods to obtain polymers with well-defined properties. Traditional free radical polymerization processes are difficult to control because they are dominated by the kinetics of very fast reactions such as biradical termination and radical chain end transfer. In contrast, RDRP is propagated by radicals ($P_n^{\bullet}$) that are in a reversible active-dormant equilibrium (Scheme 2): radicals are deactivated reversibly by persistent radicals ($T^{\bullet}$) to form dormant radicals $P_n$-T.

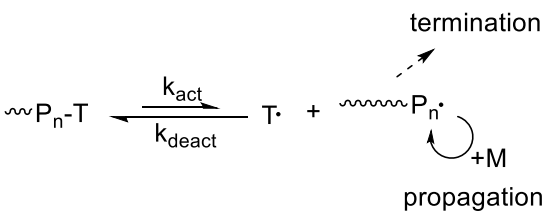


**Scheme 2** Activation-deactivation equilibrium in RDRP processes.

In particular in 1995, Matyjaszewski[20] and Sawamoto[21] independently reported the ATRP of methyl methacrylate (MMA), giving rise to the most used technique in the field of RDRP. This method had great success thanks to its versatility and simple setup, furthermore it allowed the synthesis of polymers with specific composition, architecture and position of functional groups. In ATRP, a metal complex in a low oxidation state $M^nL_m$ (typically a copper-polyamine system, $[Cu^IL]^+$) reacts with a dormant polymeric chain $P_n$-X (where X = Cl, Br) to produce radicals $P_n$• that can propagate the polymeric chain by addition to a monomer in the bulk of the solution. During this process, the copper complex is oxidized and binds to $X^-$ generating the deactivating species $[X\text{-}Cu^{II}L]^+$ which can trap the propagating radicals. The ATRP equilibrium is strongly shifted towards the dormant species $P_n$-X ($k_{act}/k_{deact} << 1$) so that $P_n$• concentration is very low and the probability of radical-radical termination processes is minimized (Scheme 3).

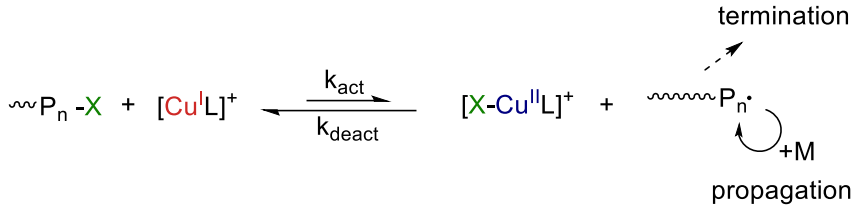


**Scheme 3** General ATRP mechanism.

The macromolecular growth begins almost simultaneously thanks to the utilization of very efficient alkyl halides (RX) as polymerization initiators (i.e very active towards C-X bond cleavage). In these conditions, chain growth is homogeneous and it is possible to obtain polymers with pre-determined molecular weight, narrow dispersity values defined as $D = M_w/M_n$, where $M_w$ is the weight-averaged molecular weight and $M_n$ is the number-averaged molecular weight, and C-X chain end fidelity.

ATRP reaction should exhibit the following characteristics in order to be defined "controlled": (*i*) fast and complete initiation, (*ii*) linear relationship between $M_n$ and monomer consumption, and (*iii*) $D < 1.5$. This enables the synthesis of well-defined polymers with narrow distributions and to predict molecular weights by the initial monomer concentration to initiator ratio ($C_M/C_I$).

A fundamental requirement of the catalyst is the reversible deactivation of dormant species with a terminal carbon-halogen bond, which involves one electron oxidation of the metal associated with an abstraction of a halogen atom. Thus, the metal catalyst should allow the formation of at least two oxidation states separated by a single electron transfer. Moreover, the complex should have good halogen affinity. For these aspects, late transition metals in a lower valence state are generally favorable. The most used catalyst is undoubtedly the $Cu^{I}/Cu^{II}$ redox couple.

By using ATRP, individual macromolecules can be prepared in the shape of stars, combs, bottlebrushes and rings or as networks with well-defined mesh size. Moreover, useful functionalities can be precisely incorporated into macromolecules by modifying either the end group, or reactive moieties at the center or specifically selected positions, to provide targeted properties (Figure 5).

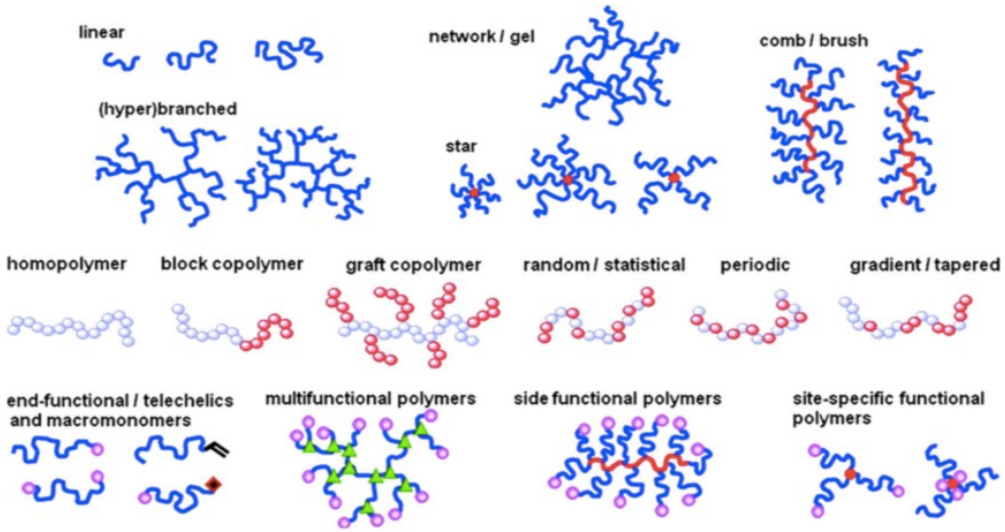


**Figure 5** From top to bottom, examples of polymers with controlled topology, composition and position of the functional group.

The rate of ATRP could be expressed by equation 1 and depends on the rate constant of radical propagation ($k_p$) and on the concentrations of monomer and growing radicals. The radical concentration depends on the ATRP equilibrium constant and the concentration of dormant species, activators and deactivators (Eqn. 1).

$$R_p = k_p C_M C_R = k_p \frac{k_{act}}{k_{deact}} C_M C_R \frac{C_{[Cu(I)L]^+}}{C_{[X-Cu(II)L]^+}} \qquad \text{Eqn. 1}$$

where:

$k_p$ = rate constant of propagation

$C_M$ = monomer concentration

$C_{RX}$ = initiator concentration

$C_{[Cu(I)L]^+}$ = concentration of Cu(I) complex

$C_{[X\text{-}Cu(II)L]^+}$ = concentration of Cu(II) complex

The structure of the Cu complex and monomer / dormant species as well as reaction conditions (solvent, temperature and pressure) can strongly influence the values of the rate constants $k_{act}$ and $k_{deact}$, and as a consequence their ratio $K_{ATRP}$;[22] generally the overall rate of ATRP increases with catalytic activity. Equilibrium constant in ATRP depend on; *i*) the structure of the catalyst, *ii*) alkyl halides (initiator and monomer), and *iii*) on the reaction medium.

*Cu / L complexes.* The range of activity for ATRP catalyst complexes covers over 6 orders of magnitude and the general order of Cu complex activity is tetradentate (cyclic-bridged) > tetradentate (branched) > tetradentate (cyclic) > tetradentate > tetradentate (linear) > bidentate ligands. The nature of nitrogen atoms in the ligands also influence the activity of the Cu complex and follows the order pyridine > aliphatic amine > imine < aromatic amine. The least active Cu-complexes show excellent control for the polymerization of highly reactive monomers that form stabilized propagating radicals. Instead, ligands that give more active complexes are suitable for less reactive monomers.

*Alkyl halide.* The reactivity of the alkyl halide in ATRP depends on the structure of the alkyl group and transferable halogen. Reactivity of alkyl halides follows the order of 3° > 2° > 1° and I > Br > Cl. In addition, $K_{ATRP}$ values increase with the addition of strong radical-stabilizing groups (aryl, carbonyl, ester, etc.) because of the resonance stabilization, polar and steric effects.

*Solvents.* ATRP has been successfully carried out in a broad range of solvents, including both common organic solvents and protic solvents such as alcohols and water. Solvents have much smaller effect on the propagation of radical polymerization than on ionic polymerization. However, the solvent strongly affects the activity of Cu complexes, which typically increases with solvent polarity. Qualitatively, this is due to the less polar character of $Cu^I$ complexes with respect of the cationic $Cu^{II}$ complexes, which are strongly stabilized in more polar solvents, thus shifting ATRP

equilibrium to the left. Controlling ATRP in water is highly desirable because water is an inexpensive and environmentally friendly solvent, with high thermal capacity. However, X-Cu$^{II}$L complexes in water are characterized by a low Cu-X bond energy, which destabilizes the deactivator.

### 1.3.1 Electrochemically mediated Atom Transfer Radical Polymerization (eATRP)

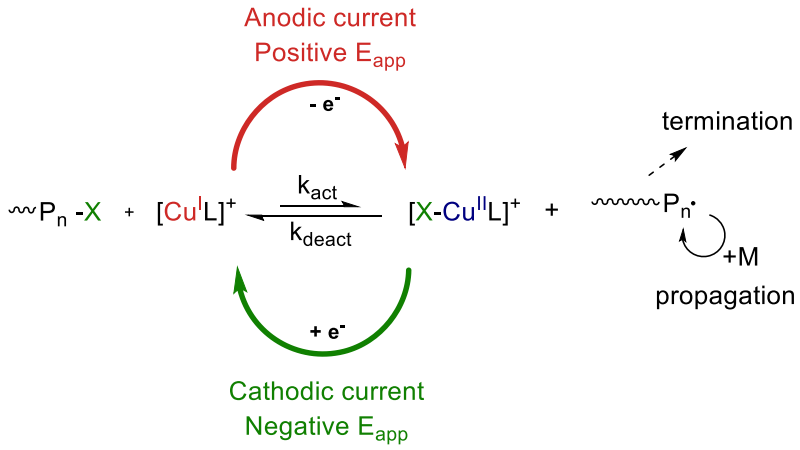


**Scheme 4** General mechanism of electrochemically mediated ATRP.

Electrochemically mediated Atom Transfer Radical Polymerization (*e*ATRP) represents a recently developed method, in which only a small amount of catalyst is used, thanks to the continuous reduction of the Cu$^{II}$ complex at the working electrode to reform the Cu$^I$ activator complex. A target amount of the air-stable Cu$^{II}$L catalyst complex can be electrochemically reduced to Cu$^I$/L activator to start controlled polymerization. In *e*ATRP the ratio of activator to deactivator is controlled by the potential applied by the working electrode ($E_{app}$). Several parameters, such as applied current, potential and total current passed can be controlled by changing the applied potential ($E_{app}$).[23] In proximity of the electrode surface, the Nernst equation (Eqn. 2) is considered valid, where $E_{1/2}$ is the half-wave potential of copper catalyst.

$$E_{app} = E_{1/2} + \frac{RT}{nF} \ln \frac{C_{Cu(II)}}{C_{Cu(I)}} \qquad \text{Eqn. 2}$$

$E_{1/2}$ = half-wave potential of the catalyst

R = gas constant

T = temperature

n = number of exchanged electrons

$C_{Cu(II)}$ = concentration of Cu(II) complex

$C_{Cu(I)}$ = concentration of Cu(I) complex

In the absence of mass transport limitations, the rate of reduction is directly dictated by the applied potential ($E_{app}$), a more negative potential induces an increase in the $C_{Cu(I)}$ / $C_{Cu(II)}$ ratio, resulting in a faster rate of polymerization. Exploiting the same principle, electrochemistry also permits a lower oxidation state catalyst ($Cu^{I}$/L) to be reverted back to its original higher oxidation state by simply shifting $E_{app}$ to more positive values.

## 1.4 Supramolecular Cages

The main objective of this thesis is to exploit the possibility to use supramolecular catalytic cages in ATRP chemistry. For this reason, a general introduction on supramolecular cages, the capabilities to exploit them in catalysis and a more specific description of the systems prepared in the last years in the laboratories where this thesis has been carried out will follow.

Over the last decade, species with well-defined inner void spaces able to accommodate guests, defined as molecular containers, have been increasingly studied within the context of complex chemical systems (Figure 6).[24]

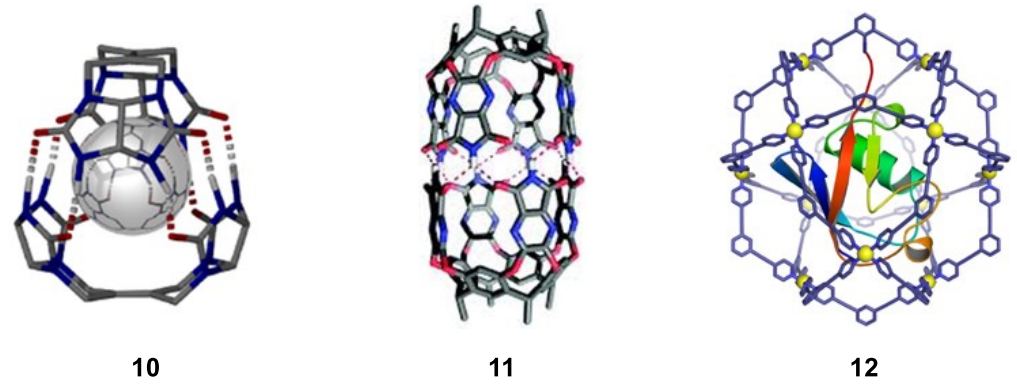


**Figure 6** Different supramolecular cages obtained by ionic hydrogen bonds **10**[25] and **11**[26] and ubiquitin-containing spheres **12**[27].

A cage compound is, according to the IUPAC definition, a ‘‘polycyclic compound with the shape of a cage’’. These shape-persistent architectures have a well-defined inner cavity, large enough to host other molecules called guests.[28] For this reason,

during the years cage-like systems have been extensively employed for molecular recognition and catalysis. The idea behind this concept is to emulate biological systems such as enzymes, that take advantage of non-covalent interactions to alter kinetic reaction profiles. To achieve this goal, many efforts have been dedicated to the development of novel supramolecular architectures, which could potentially control chemical reactions in order to obtain novel selectivities from confinement. More in detail, supramolecular systems usually present hydrophobic cavities which provide microenvironments that are distinct from the solution media. The host-guest interactions modulate the reactivity either by reducing the free energy of the reaction or by increasing the local concentration of reactants. These interactions have been exploited in two recent supramolecular coordination chemistry areas that take advantage of functional metal-organic architectures with confined spaces of different size and shape, namely, metal-organic cages (MOCs)[29], and metal-organic frameworks (MOFs)[30]. MOCs are discrete molecular architectures with well-defined shape, size and geometry, obtained through the self-assembly of metal ions and ligands that contain multiple binding sites with a specific geometry (Figure 7).[31]

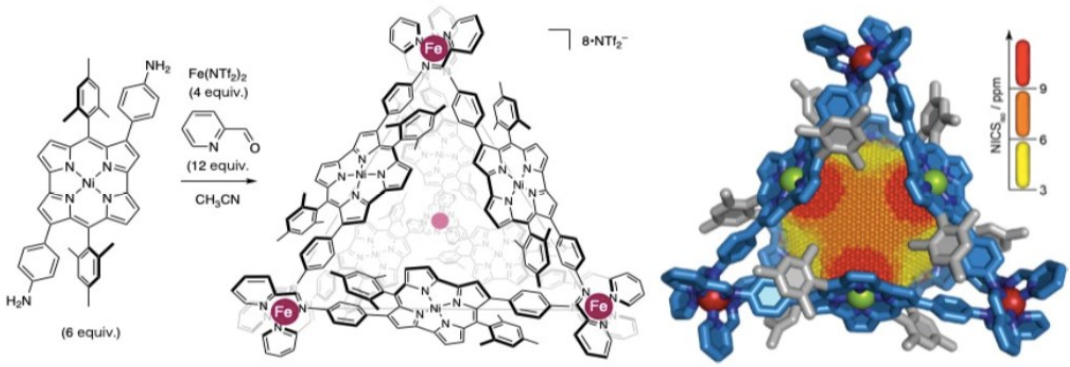


**Figure 7** Iron based self-assembled metal-organic cage with six identical aromatic walls. Figure adapted from reference **29**.

On the other hand, MOFs are crystalline materials consisting of ions coordinated with rigid organic ligands to form mono- bi- or three-dimensional structures with very high porosity (Figure 8).


**Figure 8** Metal-organic frameworks combine a cluster of metal ions and organic linkers to form a honeycomb-like structure. Figure adapted from reference 30.

In these cage-type structures, the cavity acts as a confinement site for a variety of reactions.[30] These systems usually present metal centers connected by organic linkers or organic molecules linked by non-covalent interactions. In this case, neither the metal centers nor the ligands alone catalyze the reaction only the resulting structure formed through the self-assembly of the subcomponent lead to novel catalytic properties. More in detail, the supramolecular structure could provide the preorganization of the reactants or the stabilization of the intermediates or the transition states.

## 1.5 Reactivity inside Molecular Cages

Inspired by the high efficiency and specificity of enzymes in living systems, many efforts have been dedicated to the development of cavities containing structures by exploiting non-covalent interactions to alter kinetic reaction profiles. The cavity provides a confined and isolated environment which differs from homogenous bulk solution. These systems usually present a metal center connected by organic linkers or non-covalent interaction and only the combination of these two components assembled together is able to catalyze reactions. The confined microenvironment governs the host-guest interactions, in terms of orientation of substrates and reactive conformation. The specific interaction between the guest and the cavity could modulate a chemical transformation either *i)* by reducing the free energy of the reaction *ii)* trapping unfavorable reaction intermediates to alter regio- and enantioselectivity, or *iii)* by increasing the local concentration of reactants enhancing the reactivity.

Supramolecular cages can act as catalysts in three main different ways: *i)* by preorganization of the reactants inside the cavity, *ii)* incorporating catalytic sites, and *iii)* by encapsulation of the catalyst within the cage.[32]

### 1.5.1 Preorganization of substrate

In recent years, metal-organic cages have emerged as artificial supramolecular reactors which provide a confined molecular space with a well-defined size and shape to modulate the arrangement and the reactivity of the encapsulated substrate. As example, while the [2+2] photocycloaddition of acenaphthylene (ACE), with the formation of the resulting *syn* and *anti* stereoisomers, is a well-known reaction, the enantioselective photodimerization of its 1-substituted derivatives was unexplored. In 2020 Guo and coworkers reported the possibility to perform the asymmetric cycloaddition reaction of a 1-substituted derivative of acenaphthylene (ACE) using a supramolecular photochirogenic approach that exploits the advantages of substrate preorganization in the ground state and manipulating subsequent photochemical transformation by weak but non-transient interactions in chiral supramolecular media (Figure 9).[33]

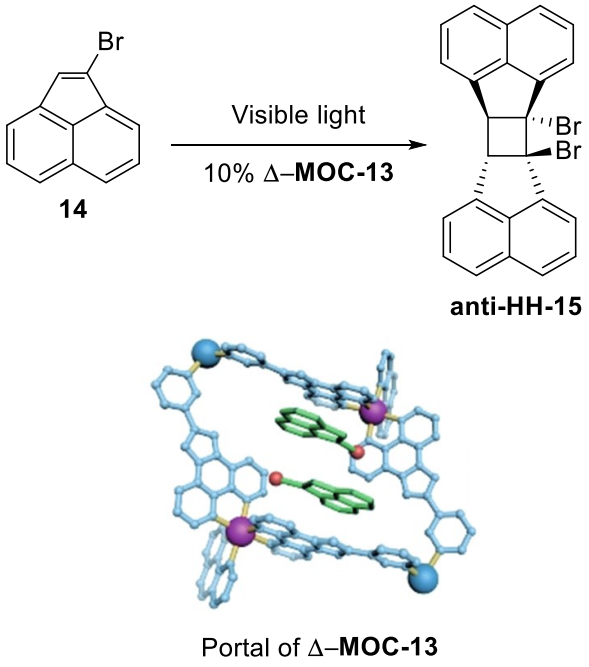


**Figure 9** Stereo- and regioselectivity in the formation of **anti-HH-15** with the homochiral **Δ-MOC-13** photocatalyst.

In order to obtain the stereoselective reaction, a homochiral and photoactive Δ-$[Pd_6(RuL_3)_8]^{28+}$ metal-organic cage (**Δ-MOC-13**) has been used as a supramolecular reactor for the enantioselective excited state photocatalysis of 1-Br-ACE **14**. Through

the confinement of the reactants inside the cavity of the molecular cage effect, the homochiral **Δ-MOC-13** photocatalyzed the dimerization of nonsymmetrical **14** to give exclusively and quantitative the formation of **anti-HH-15** with both stereo- and regioselectivity.

Between all the possible orientations of the two molecules of the substrate 1-Br-ACE, there is only one that is favored in energy. This means that all others imply disfavored preorganization arrangements upon encapsulation and are thus not preferred in the photoreactions. These results are consistent with host-guest mutual matching with regard to geometry and chirality and explains the absence of other reaction products.

### 1.5.2 Stabilizing transition state

Another way to obtain novel properties from confinement is the stabilization of transition state of the reaction provided by the interactions that are formed inside the cavity. Within this context, Raymond and coworkers synthetized water-soluble chiral tetrahedral cage **16** consisting of four metal centers located at the corners of a tetrahedron in an octahedral geometry joined by six naphthalene-based ligands (Figure 10).[34] The propeller-like arrangement of the ligands around the metal ion led to the formation of two enantiomers namely Δ and Λ. In the presence of $NR_4^+$ molecules as guests the exclusive formation of homochiral assemblies Δ,Δ,Δ,Δ and Λ,Λ,Λ,Λ of the tetrahedral architecture $[M_4L_6]^{12-}$**16**.

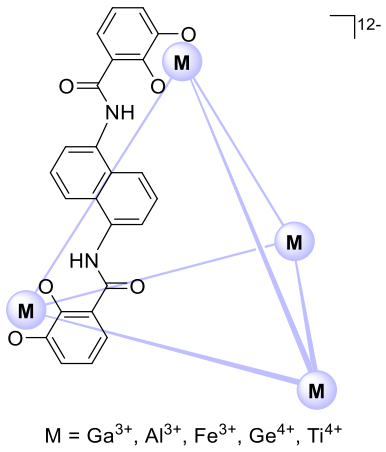


**16**

**Figure 10** Schematic representation of the tetrahedral $[M_4L_6]^{12-}$ assembly **16** synthetized by Raymond.

The addition of a competing guest like **17** led to the complete exchange with the release of the $NMe_4^+$ from the cavity. More in detail, the system **16·Ga** was able to confer a reactive conformation to the guest **17**, leading to an acceleration of the 3-aza-Cope rearrangement by up 3 orders of magnitude as compared to the free reaction (Figure 11).[35] Due to the lower affinity, after the reaction the product was released from the cavity, leading catalytic turnover. In this case. the electrocyclization was favored by the constrained environment of the host interior void cavity that recognize specific conformations suitable for the rearrangement.

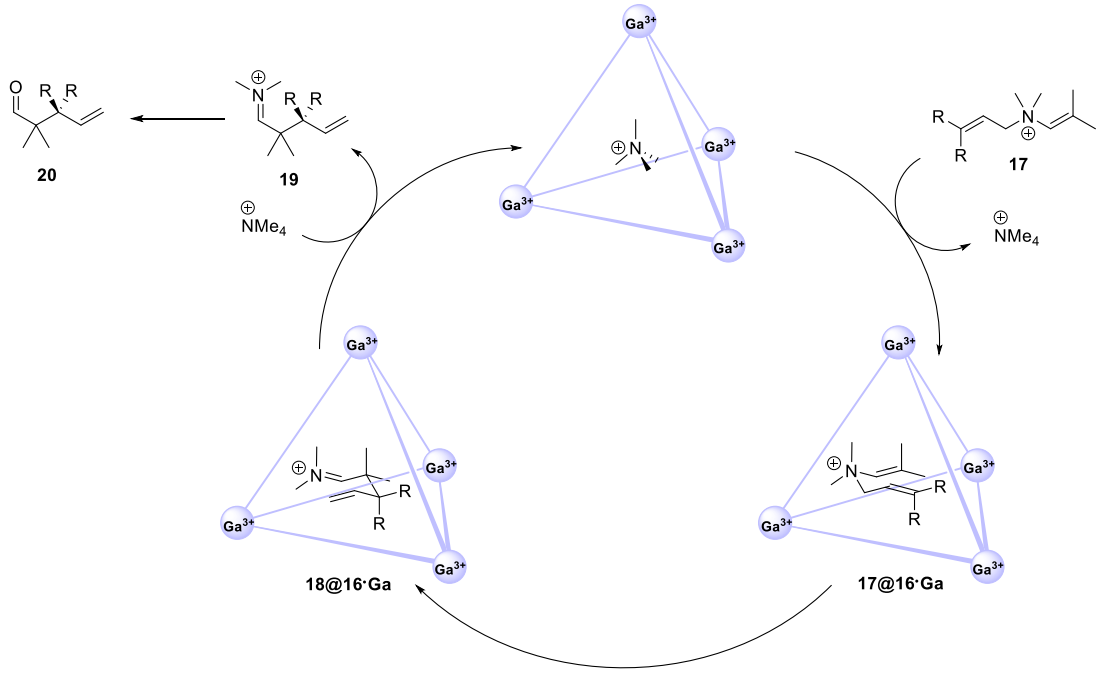


**Figure 11** Aza-Cope electrocyclization of allylenammonium cations **17** catalyzed by tetrahedral assembly **16·Ga**. Adapted from ref. [35].

### 1.5.3 Encapsulated catalyst within the cage

Another efficient way to speed up reaction or to alter the selectivity is to encapsulate the molecular catalyst inside the cavity. The catalyst can be introduced inside the cage either by covalent bonding or non-covalent interactions, whereas the cage behaves as a nanoreactor resulting in greater control over guest selectivity and product regio- and stereo-selectivity. This strategy has also the advantage of preventing self-quenching and deactivation of the catalyst. The concentration of the catalyst could be dramatically enhanced if the cage has the ability to encapsulate more than one catalyst molecules.

Moreover, even the morphology of the catalyst can be tuned by the cage framework, yielding a highly active species of the active species.

In 2015, the Raymond and Toste groups were the first to perform tandem catalysis combining natural enzymes and supramolecular cages for catalyzing organic reactions.[34] The reaction was performed using gold or ruthenium complexes encapsulated in cage **16** in combination with esterases, lipases or alcohol dehydrogenases. The reaction involved two steps catalyzed one by the enzyme and the other by the gold / ruthenium complex. When the reaction was performed in bulk solution, the enzyme often interacts with the metal catalyst leading to the deactivation of the active species resulting in a poor yield of the desired product. Nevertheless, the encapsulation of the metal catalyst into the coordination cage, prevents the interaction between the enzyme and the catalyst, avoiding the inhibition of enzymic activity. The supramolecular catalyst was obtained, by encapsulating $Et_3Pau^+$ and $(Me_3P)CpRu(NCMe)_2^+$ in the cavity of cage**s Au@16** and **Ru@16**.

The first reaction performed was a tandem enzyme-mediated acetate hydrolysis followed by **Au@16** or **Ru@16** mediated hydroalkoxylation or olefine isomerization (Figure 12).

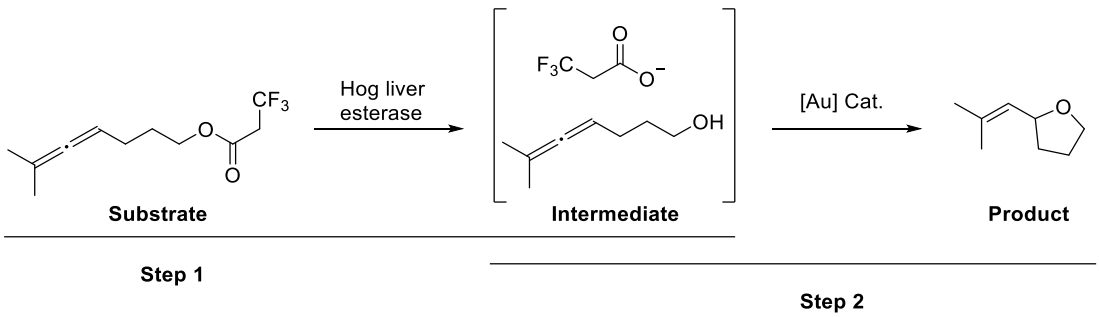


**Figure 12** Tandem-enzyme mediated acetate hydrolysis reaction catalyzed by Raymond cage **Au@16** or **Ru@16** coupled with enzymes.

Subsequently, the authors performed the **Ru@16**-mediated olefin isomerization of allyl alcohol to give propanal followed by reduction to propanol via ADH (Figure 13).[36] Even in this case, neither the enzymes nor the ruthenium catalyst can catalyze both reactions in sequence.

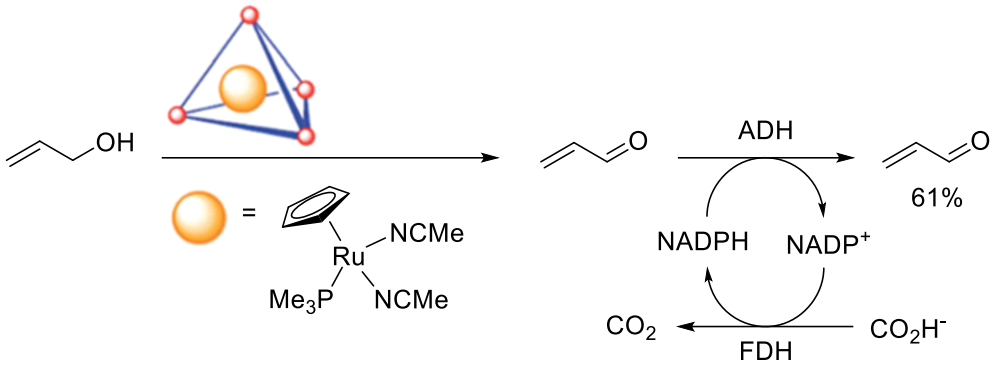


**Figure 13** Tandem-enzyme reaction of isomerization and reduction to propanol of allyl alcohol, catalyzed by Raymond cage **Ru@17** coupled with enzymes. Adapted from reference [36].

This research demonstrated that only the encapsulation of the ruthenium catalyst into a coordination cage could prevent adverse interactions between the catalyst and the enzyme, thus making the tandem reaction drastically more efficient.[37]

### 1.5.4 Embedded active sites within the cage

The second class of supramolecular catalysts consist of active sites, usually metal ions, incorporated in the structure of the cage. Also in this case, the cavity of the structure still plays an important role in the catalytic cycle activating the substrate, preventing aggregation of the catalysts and increasing the local concentration of the active center leading to an enhancement of the reactivity.

In this context the Su group developed a homochiral heterometallic coordination cage **21** and investigated the regio- and stereoselectivity of a coupling reaction (Figure 14).[38]

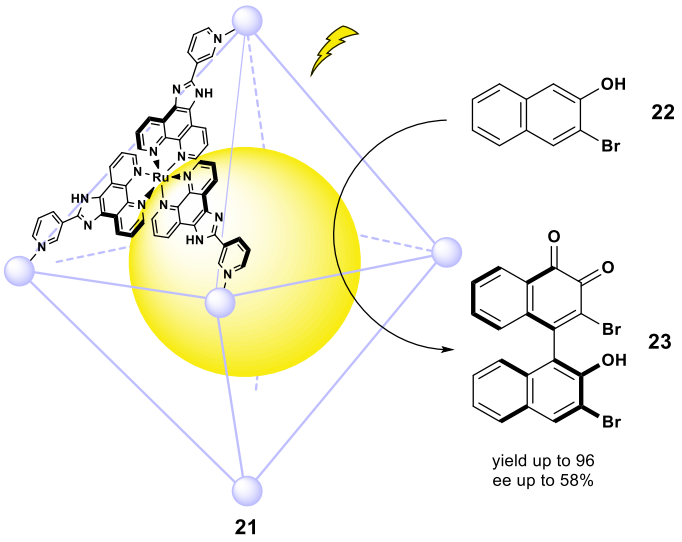


**Figure 14** Su chiral cage **21** formed through self-organization of ruthenium metalloligands and palladium metal knots. Photoinduced biaryl coupling of **22** to yield **23**. Adapted from ref [38].

More in detail, the cage had an octahedral geometry with palladium metal ions at the vertices and the photo-hydrogen evolving ruthenium complex placed at the faces, to give an $M_6L_8$ stoichiometry. The active site was the embedded ruthenium complex, that is a typical photo-driven hydrogen evolving catalyst. This system could encapsulate naphthol guests and perform an uncommon regiospecific 1,4-coupling to obtain 4-(2-hydroxy-1-naphthyl)-1,2-naphthoquinones in high yield (up to 96%) and good enantiomeric excess ratio (up to 58%). When the cage was irradiated with light a 453 nm, an electron transfer from a photoactive ruthenium center to a palladium ion leads to an intramolecular charge separation leading to the excited state of the cage **22** that can oxidize the naphthol **23** through single electron transfer to form a radical species. The only product obtained was the 1,4-coupled dimer, by inter- and intra-molecular radical transfer. Furthermore, the chiral environment influences the enantioselectivity. This reaction is a rare example of asymmetric induction in biaryl coupling exploiting cages both for photoredox reactivity and stereoselectivity.[38,39]

## 1.6 Tris(2-pyridilmethyl)amine based molecular Cages

Within the field of supramolecular cages, the research group in which this thesis has been carried out has reported the possibility to use tris(2-pyridyl)methylamine **TPMA** as building block for the synthesis of a supramolecular confined spaces to obtain a metal-organic architecture with an internal cavity able to accommodate guests. The novel self-assembled structure was built up through imine condensation between a modified **TPMA** zinc complex bearing three aldehyde groups and diamine molecules.[40] The cage was obtained exploiting dynamic covalent chemistry (DCC) starting from relatively simple building blocks, to build up large three-dimensional complex architectures.[41] In particular, since DCC works under thermodynamic control, allows easy synthetic pathways for a system of components to achieve its thermodynamically most favorable state.[42] In this case, the addition of ethylenediamine to a solution of the **TPMA** zinc complex **24**, led to the formation of the supramolecular cage **25** (Figure 15).

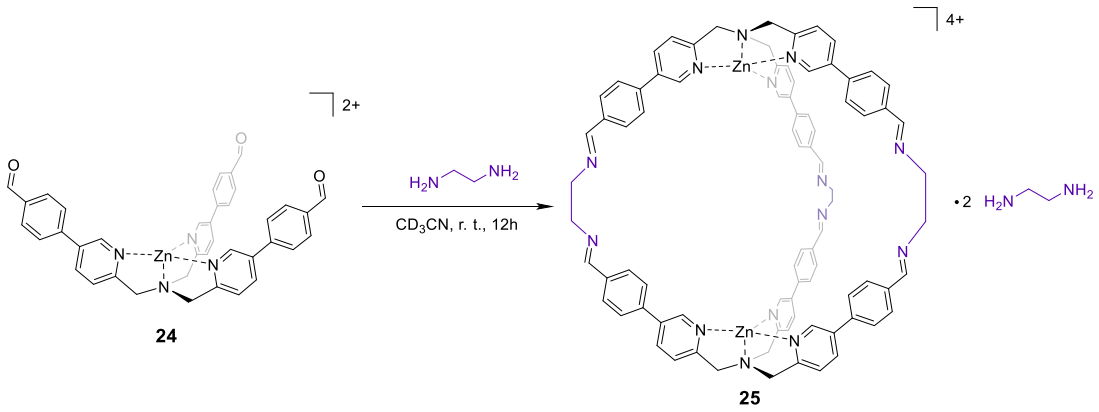


**Figure 15** Formation of the supramolecular cage **25** starting from complex **24** and using ethylenediamine as linker. The reaction was made in $CD_3CN$ at room temperature obtaining the product after 12 hours. Perchlorate counter anions are removed for clarity.

### 1.6.1 Binding and Recognition properties

Inspired by the work of Anslyn on the carboxylic acids by **TPMA**-based complexes,[43] dicarboxylate anions recognition within the novel developed cages were initially investigated by the group. Confinement processes are ruled by the complementarity and size and shape adaptability of the host, guest and solvent. The interplay of these parameters determines the thermodynamic and kinetics behaviour of the association process. Interestingly, the addition of a stoichiometric amount of dicarboxylic acid to

a solution of the empty cage resulted in the formation of the 1:1 host-guest complex, detectable by the appearance of a new set of $^{1}$H-NMR signals and confirmed by the resolution of a crystal structure of a similar system (Figure 16).

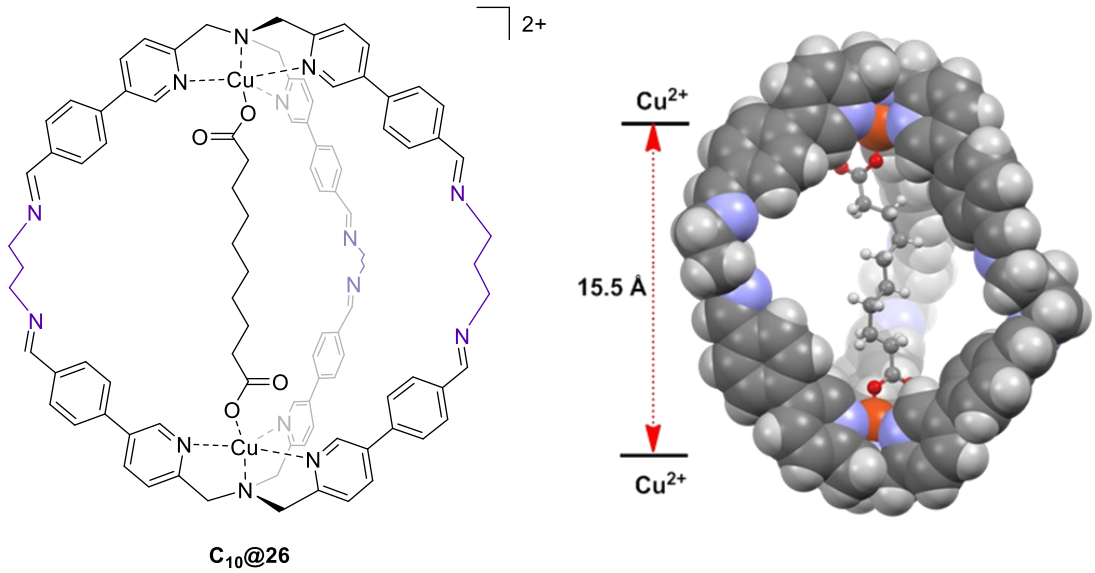


**Figure 16** X-ray crystal structure of **$C_{10}$@26**·Cu in CPK model displaying the entrapment of sebacic acid **$C_{10}$** (ball & stick model) inside the cage.

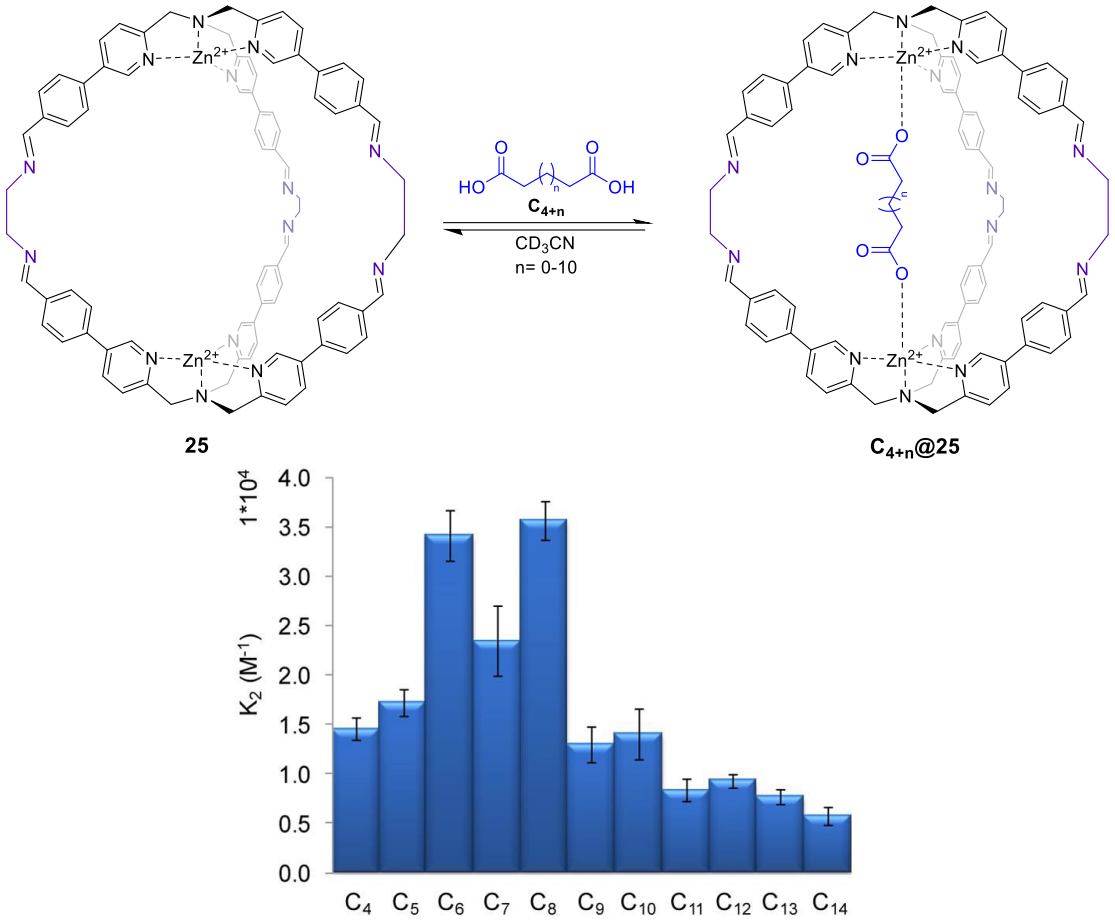


**Figure 17** $^{1}$H NMR binding constants ($K_2$) for the inclusion of diacids **$C_4$-$C_{14}$** within cage **25**. Perchlorate counteranions are removed for clarity.

After this preliminary result, the attention was focused on understanding the influence of minimal structural variations on the encapsulation phenomena. For this reason, the binding capability of the cage was studied in the presence of diacids ranging from succinic acid (**$C_4$**) to tetradecandioic acid (**$C_{14}$**) (Figure 17). The binding constants obtained via $^{1}$H-NMR for the series displayed a pseudo-Gaussian profile, typical for processes occurring in confined spaces centered on suberic acid (**$C_8$**). Since the guests are bind at both Zn metals, their presence induced deformation in the cage. These results showed that a change of the aliphatic chain length led to a higher thermodynamic cost for the conformational rearrangement for both the host and the guest.[44]

### 1.6.2 ESI-MS competition experiment

After the results on the recognition properties obtained with the cage using ethylenediamine as linker the research group investigated the influence of the amine linker on the binding capability of the system toward different dicarboxylic acids. More in detail, amines with different rigidity and chain length were employed as linkers to form the corresponding cages leading to the formation of structures with different cavity size. Since determination of the molecular-recognition properties of novel systems by $^{1}$H-NMR binding experiments required a titration for each guest, another method based on ESI-MS spectrometry was used.

A simultaneous competition methodology based on electrospray ionization mass spectrometry (ESI-MS) analysis, in which all the diacids were simultaneously present in solution, was used in order to get information about the binding capabilities of the novel cages. In particular, it was possible to evaluate how variations in the length of both diacid guest and diamine linker affects the binding process. The experiments were conducted adding equimolar amounts of the series of dicarboxylic diacids from (**C$_4$**) to (**C$_{14}$**) to a solution of the aldehyde zinc complex **24** and different diamine linkers (Figure 18). Leaving the solution to equilibrate for 24 hours the system could dynamically evolve towards the thermodynamically most favorable species. ESI-MS spectrometry was exploited for the determination of the relative ratio between all the inclusion species and the same experiment was repeated for all the series of diamine linkers.

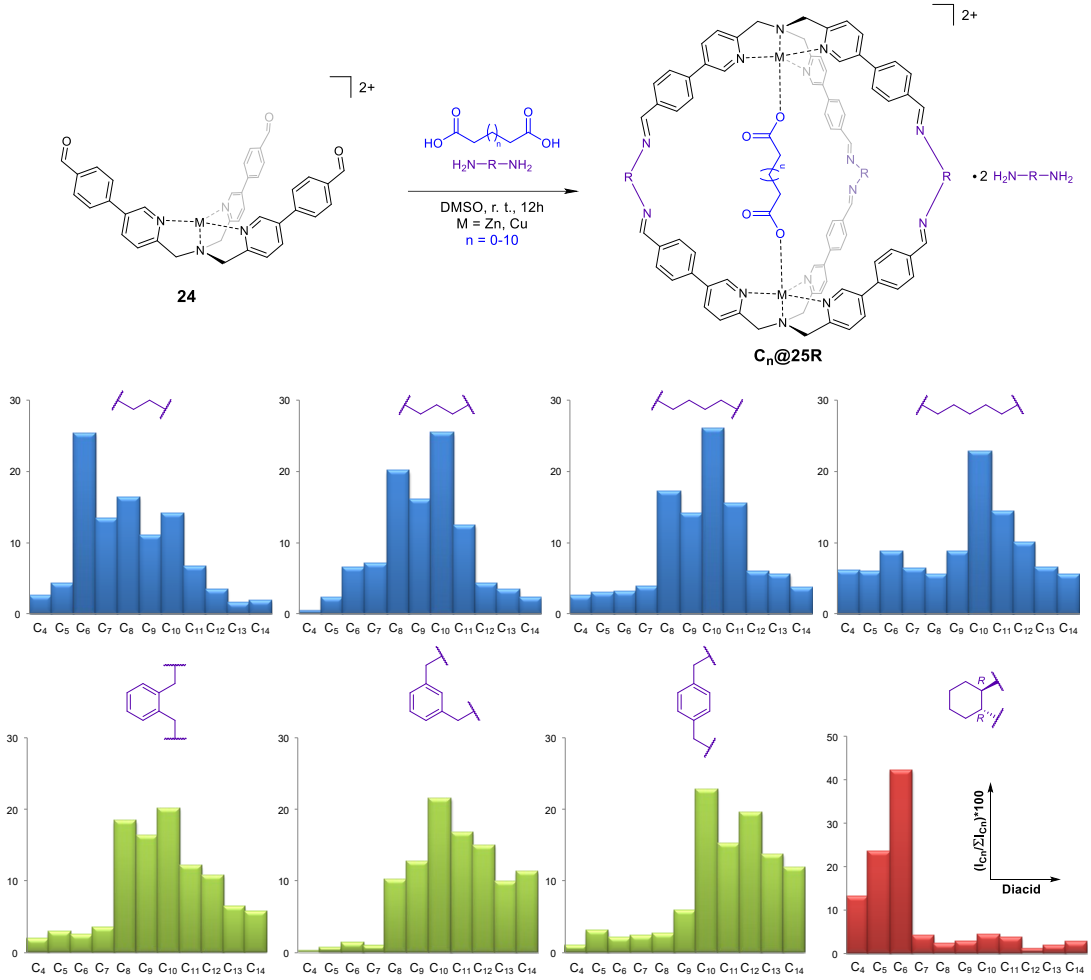


**Figure 18** Synthesis of the supramolecular cage **25R** with different dicarboxylic acids ranging from succinic acid $C_4$ to tetradecandioic acid $C_{14}$ as guests and using different diamine (a-h) as linkers. b) ESI-MS selectivity profiles for cage **25R** in the competition experiments using different diacids guests and different diamine linkers.

The ESI-MS spectra showed a series of m/z peaks that correspond to the different inclusion complexes. The obtained pattern has a trend like that obtained with the NMR experiments. A general observation for all the profiles is that the elongation of the diamine linker corresponds to longer dicarboxylic acids as more-suitable guests. In the same fashion, increased flexibility of the linker leads to a wider distribution of the preferential guests.

### 1.6.3 Supramolecular Cage's self-assembling in complex matrixes

Further studies highlight the high stability of the cage also in the presence of high amount of water.[45] In particular, the group reported the ability of these structures to self-assemble even in the presence of complex matrixes like wine and fruit juices. The idea behind this project was to exploit the presence of organic acids, like L-Tartaric and L-Malic, that are widely present in fruit juice matrixes, to template cages

formation. It should be noted that the process was very challenging due to the presence of many other organic compounds that could compete for the binding site, and the presence of water and ethanol that could prevent the formation of the imine bond (Figure 19).

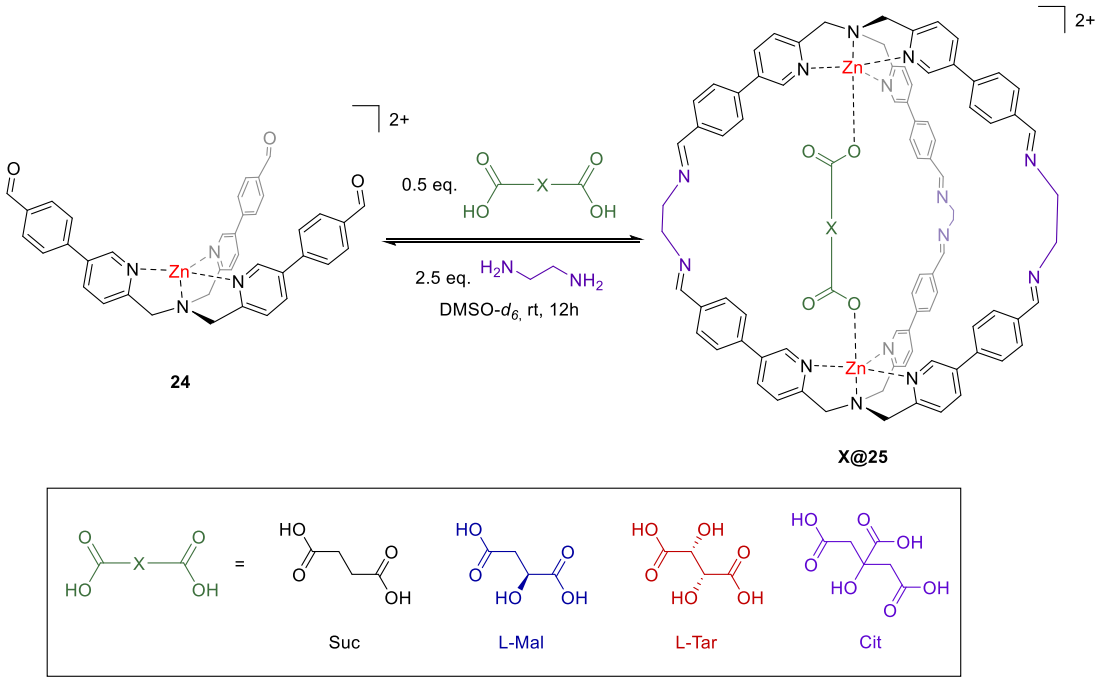


**Figure 19** Synthesis of **TPMA**-based cage **X@25** performed using dicarboxylic acids such as Succinic acid, L-malic acid, L-tartaric acid and citric acid, typically present in complex matrixes. Perchlorate anions are removed for clarity.

The experiment was initially performed by progressive additions of defined volumes ranging from 15 µl to 125 µl of red wine without any pre-treatment to a 0.5 mL solution of ethylenediamine and **TPMA** aldehyde precursor in DMSO-$d_6$. After 20 minutes, $^1$H-NMR of the different solutions were almost completely superimposable with those of the supramolecular architecture obtained using commercially available enantiopure tartaric acid. This indicate that the tartaric acid present in wine is able to template the self-assembly process also at high water contents (Figure 20).

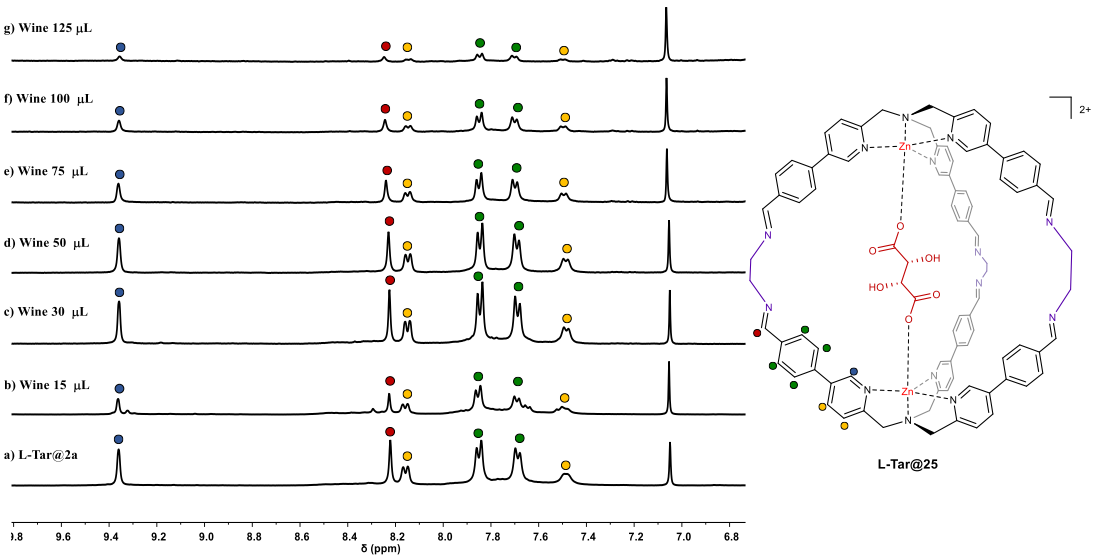


**Figure 20** Partial $^{1}$H-NMR spectra (400 MHz, 301 K, DMSO-$d_6$) of the supramolecular cage **25** formed by addition of a) commercially available L-tar acid, b) 15 µL, c) 30 µL, d) 50 µL, e) 75 µL, f) 100 µL, g) 125 µL of Valpolicella wine without any pre-treatment to 500 µL DMSO-$d_6$ solution containing 1 µmol of complex **24** and 2.5 µmol ethylenediamine. Internal standard p-xylene at 7.05 ppm.

The possibility to form cages in complex mixtures was also tested using 3 red wines, 3 white wines, 6 commercially available fruit juices and 3 freshly squeezed juices as sources of dicarboxylic acid for templation of the inclusion complex. Each reaction was attempted by adding 15µL of untreated mixture to a 0.5 mL solution of DMSO-$d_6$ (500 µL) containing 2.5 mmol of ethylenediamine and 1 mmol of aldehyde-**TPMA**-based complex, and then analyzed via $^{1}$H-NMR. From the obtained results, it was possible to discriminate and quantify the content of succinic, tartaric and malic dicarboxylic acids present in these matrixes using $^{1}$H-NMR (Figure 21).

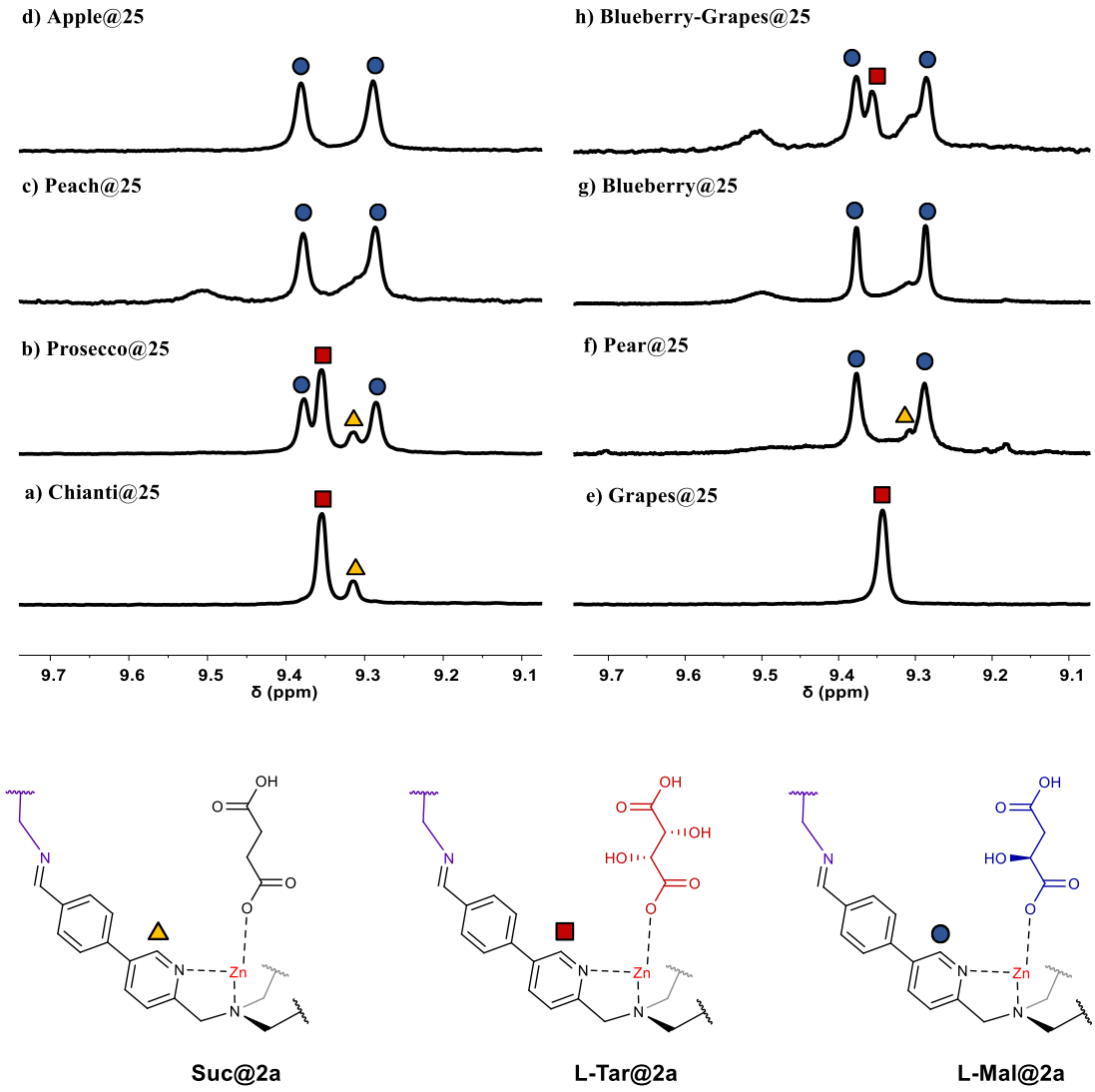


**Figure 21** $^{1}$H-NMR spectra (400 MHz, 301 K, DMSO-$d_6$) of the supramolecular cage **25** formed upon adding (a) Chianti wine, (b) Müller–Thurgau wine, (c) peach juice, (d) apple juice, (e) freshly squeezed grape juice, (f) pear juice, (g) blueberry juice, and (e) blueberry–grape juice without pre-treatment to a 500 mL DMSO-$d_6$ solution containing complex **24** and ethylenediamine. The signals at 9.5 ppm and 9.33 ppm in (c), (g) and (h) are ascribed to citric acid encapsulated inside the cage.

### 1.6.4 Chiral Diaza-Cope Rearrangement for the preparation of novel cages

Imine condensation chemistry is largely employed for the formation of organic cages with a well-defined shape and size. This process can guide the system towards the formation of a specific product from a set of possibilities. Furthermore, due to the dynamic nature of the reversible bond, this chemistry is able to equilibrate through an error-checking and self-correct them towards the most stable product. However, the reversibility of imine bond formation can also create chemical instability because the presence of an acid, or high amounts of water could lead to the hydrolysis of the C=N

bond.[46] This somehow limits the applications of imine based supramolecular systems in molecular recognition and catalysis. More in details, attempts within the group where this thesis was carried out to use in catalysis imine cages previously shown have failed.

These negative results prompted the group to apply a different strategy based on a [3,3]-sigmatropic rearrangement, a powerful tool for the stereoselective formation of stable C-C bonds. Among the different reactions the attention has been focused on Diaza-Cope rearrangement which has been largely used in formation of chiral enantiopure diamines.[47] In this reaction, after imine formation between enantiopure 1,2-Bis(2-Hydroxyphenyl)ethylenediamine **(R,R)-HPEDA** and two generic aldehydes, the rearrangement occurs to form the C-C bond among them stereospecifically (Scheme 5). The driving force of the reaction is the formation of a strong resonance-assisted hydrogen bond (RAHB) that allows the shift of the equilibrium toward the rearranged product which is released after hydrolysis.[48]

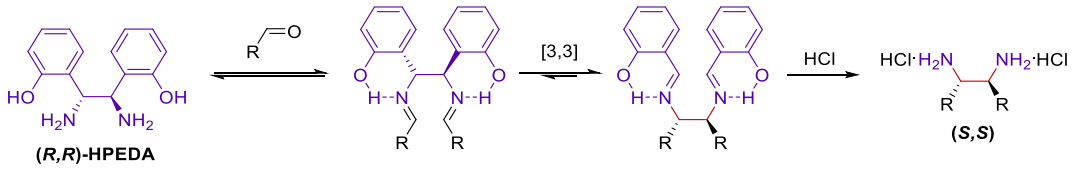


**Scheme 5** Reaction scheme of Diaza-Cope Rearrangement for the synthesis of chiral diamines.

Inspired by the possibility to obtain a novel synthetic procedure for the synthesis of a covalent chiral structure in one step, the formation of the cage was attempted using **(R,R)-HPEDA** as diamine linker (Scheme 6).

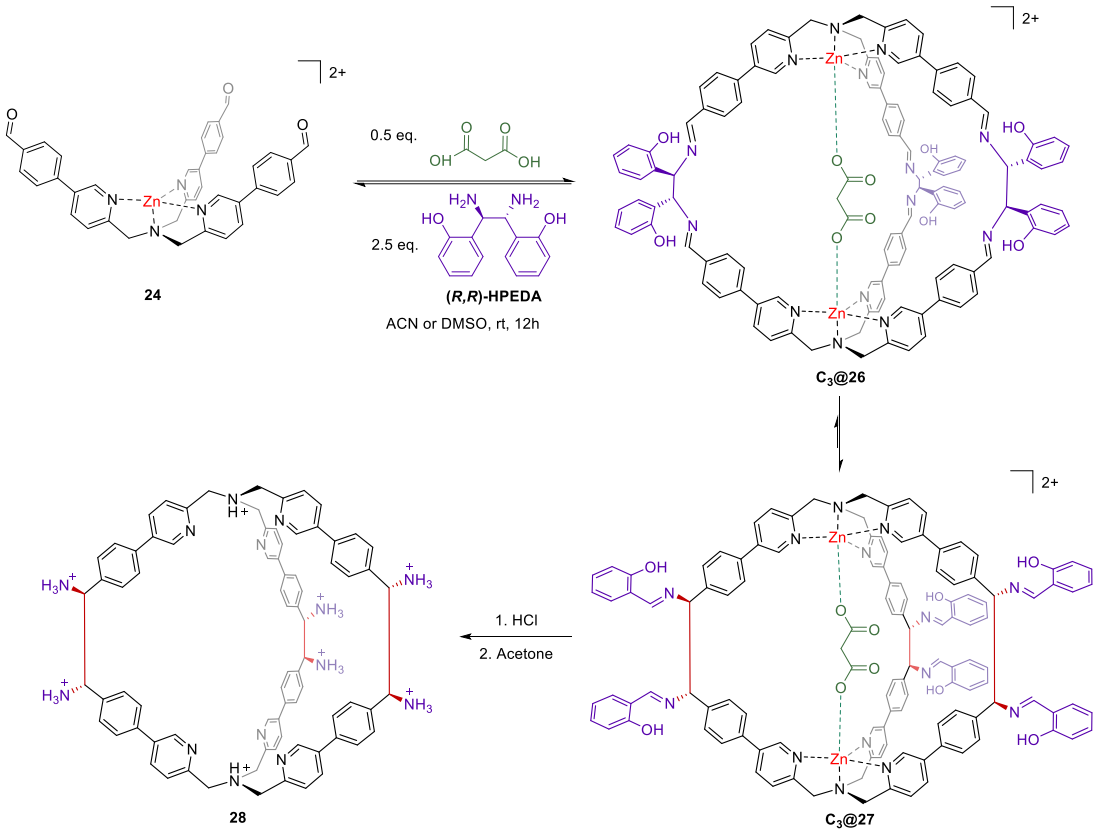


**Scheme 6** Representative scheme of the synthesis of covalent supramolecular cage **28** using **(*R*,*R*)-HPEDA** as diamine linker and dicarboxylic acid guests with different chain length. Perchlorate and Chloride anions are removed for clarity.

After a preliminary study on the effect of the chain length on the rearrangement process, malonic acid **C3** was chosen as guest. More in detail, starting from the aldehyde Zn complex **24** (1 eq.), **(*R*,*R*)-HPEDA** (2.5 eq.) was mixed in the presence of malonic acid **C3** (0.5 eq.) in a mixture of acetonitrile and 5% of DMSO (Scheme 6). After 24 hours, the formation of a sharp peak at 13 ppm, characteristic of the phenolic proton of the rearranged product **C3@27** was observed (Figure 22).

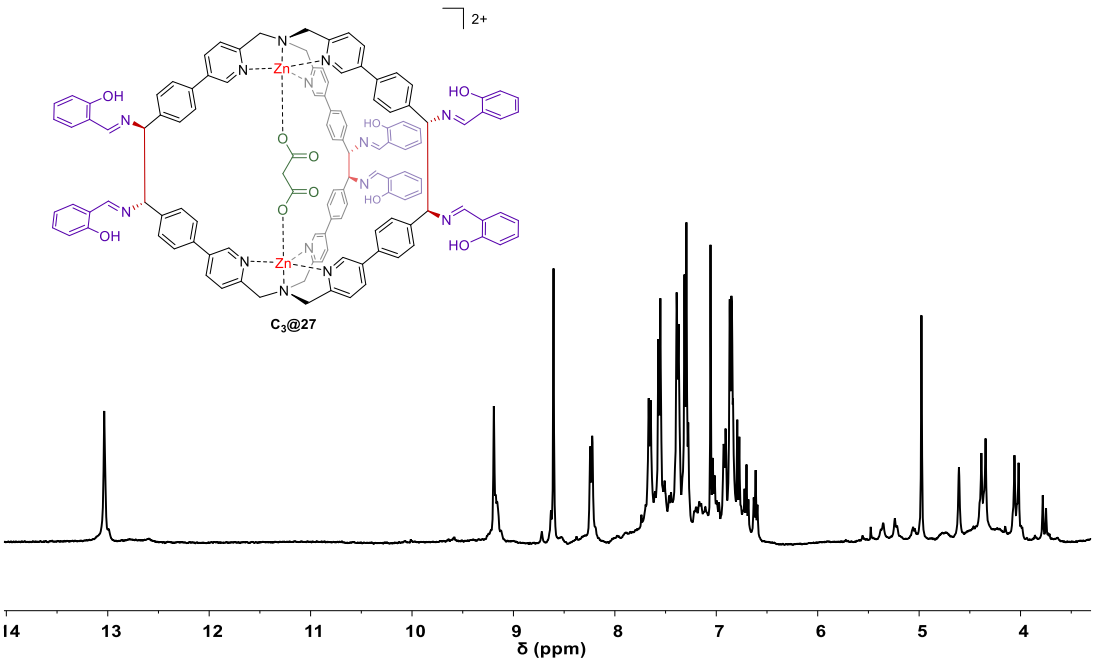


**Figure 22** $^{1}$H-NMR (400 MHz, 301 K, DMSO-$d_6$) spectra in time progression of complex **24** after the addition of 2.5 equiv. of **(*R*,*R*)-HPEDA** and 0.5 equiv. of **C**$_3$. The signal at 13 ppm corresponds to the O-H phenolic proton of cage **C**$_3$**@27**.

For the recovery of the covalent system, HCl 37% was added to the solution of cage **C**$_3$**@27** to hydrolyze the imine bonds of the rearranged product, then addition of acetone led to the isolation of the ammonium salt of the cage **28** in both high yield (>80%) and purity. Interestingly, the addition of concentrated HCl led to the complete decomplexation of the two **TPMA**-based complexes and the formation of the completely water soluble ligand with six novel stereocenters.

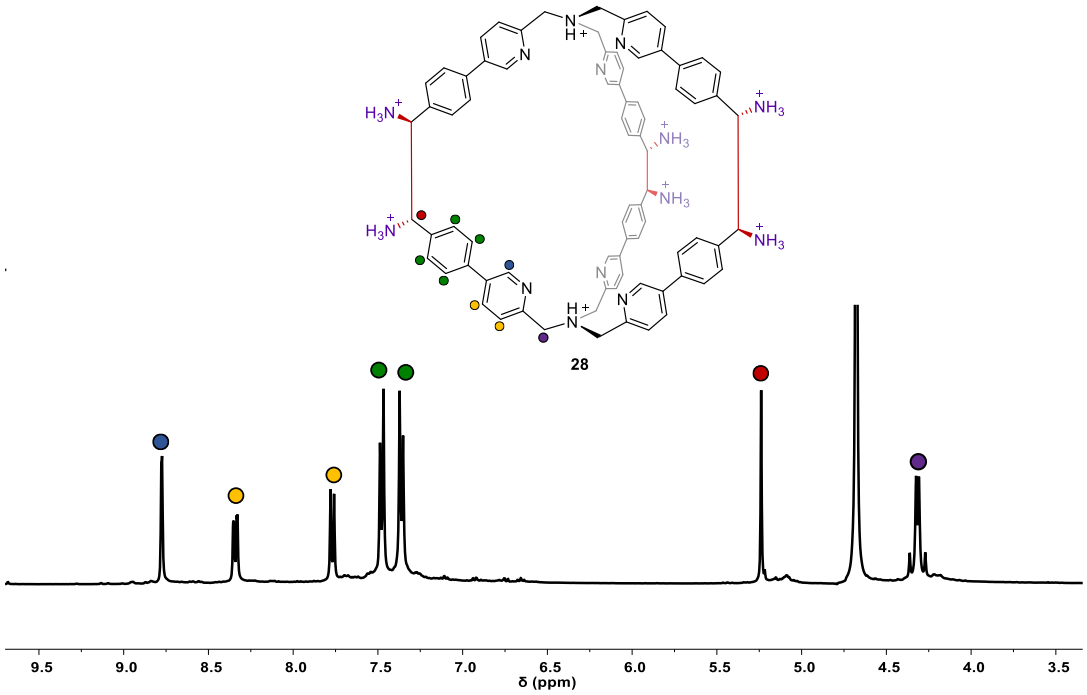


**Figure 23** $^{1}$H-NMR spectra (400 MHz, 301 K, $D_2O$) of cage **28**. Chloride anions are removed for clarity.

# 2 AIM OF THE THESIS

During the years, the **TPMA**-based molecular cages developed in the research group where this thesis has been carried out have been extensively employed for molecular recognition applications. However, the catalytic properties and applications of these architectures still remain unexplored. For this reason, the main objective of this work is to complex the novel **TPMA**-based supramolecular cage with copper and to apply the system in electrochemically mediated atom transfer radical polymerization (*e*ATRP). In particular, stereoselective radical reactions taking advantage of chiral confined cages will be investigated to reveal if a confined space is sufficient to control the stereochemistry of a radical polymerization. It will be also investigated if the confined space can alter the reactivity of Cage **Cu-28** catalyst compared to the traditional Cu/**TPMA** catalyst.

The study will be directed toward the investigation of aqueous *e*ATRP of poly(ethylene glycol) methyl ether methacrylate (OEOMA) monomers with different chain lengths, dimensions and steric hinderance, and as a consequence different molecular weight (Mw = 2000 g/mol, Mw = 950 g/mol, Mw = 500 g/mol, Mw = 300 g/mol).

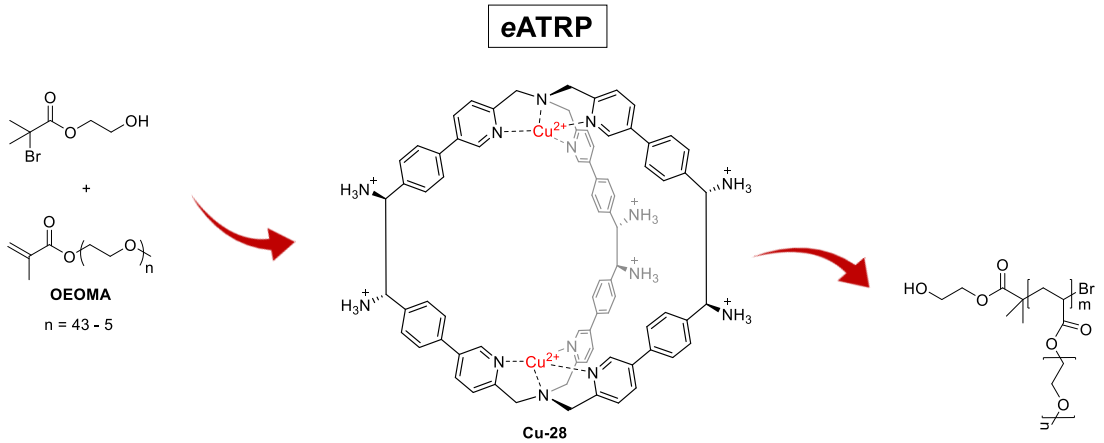


**Figure 24** Reaction scheme for aqueous eATRP of poly(ethylene glycol) methyl ether methacrylate (OEOMA) monomers with different chain lengths using copper cage **Cu-28** as catalyst.

# 3 RESULTS AND DISCUSSION

As expressed in the aim of the thesis, this work was focused on the optimization of the synthesis of a new **TPMA**-based chiral supramolecular cage complexed with copper, in order to investigate its electrochemical behavior and its catalytic activity in *e*ATRP processes. One of the biggest challenges in chemistry in this century is to master intermolecular interactions and their relationship with chemical reactivity. For this reason, knowing the high efficiency of **TPMA** complexes as catalysts in eATRP and the recognition properties of the **TPMA**-based chiral supramolecular cage synthetized by the research group, the goal is to try to develop stereoselective radical reactions.

In order to obtain these results, the first part of the study was dedicated to the synthetic preparation of the desired complex. The synthesis of the zinc complex, as previously optimized, requires three steps: i) formation of the tripodal bromide ligand **29**, ii) Suzuki coupling **30**, and iii) complexation with zinc perchlorate in order to obtain complex **24** (Scheme 7).

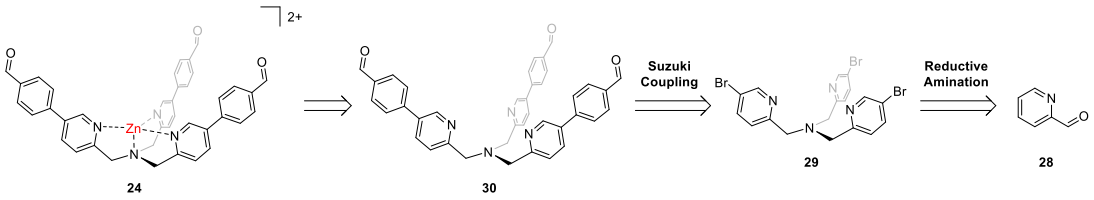


**Scheme 7** Retrosynthetic approach adopted for the synthesis of the Zn complex **24**.

## 3.1 Synthesis of the supramolecular Cage

As mentioned before, supramolecular cage synthesis started from the formation of tris-bromide-**TPMA 29** system performing the reductive amination of three equivalents of 5-bromide-2-pyridinecarboxaldehyde **28** and ammonium acetate (Scheme 8).

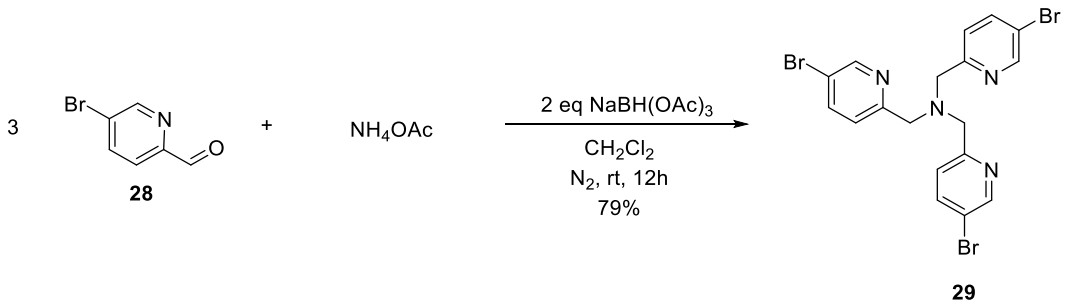


**Scheme 8** Reductive amination for the synthesis of tris((5-bromopyridin-2-yl)methyl)amine **29** starting from 5-bromide-2-pyridinecarboxaldehyde **28** and ammonium acetate.

The reaction proceeds through the formation of imine bonds that are consequently reduced using three equivalents of sodium triacetoxyborohydride. The product was obtained as a pale brown solid in 80% yield after crystallization using THF/Hexane mixture. The product was characterized via $^{1}$H-NMR spectroscopy obtaining a high symmetric spectrum in which the formation of the product was confirmed by the presence of a peak at 3.86 ppm referred to the six $CH_2$ benzylic protons of the **TPMA** scaffold (Figure 25). Moreover, identity was confirmed ESI-MS spectra which showed one main peak at 524.88 m/z with the typical pattern of a species bearing three bromine atoms.

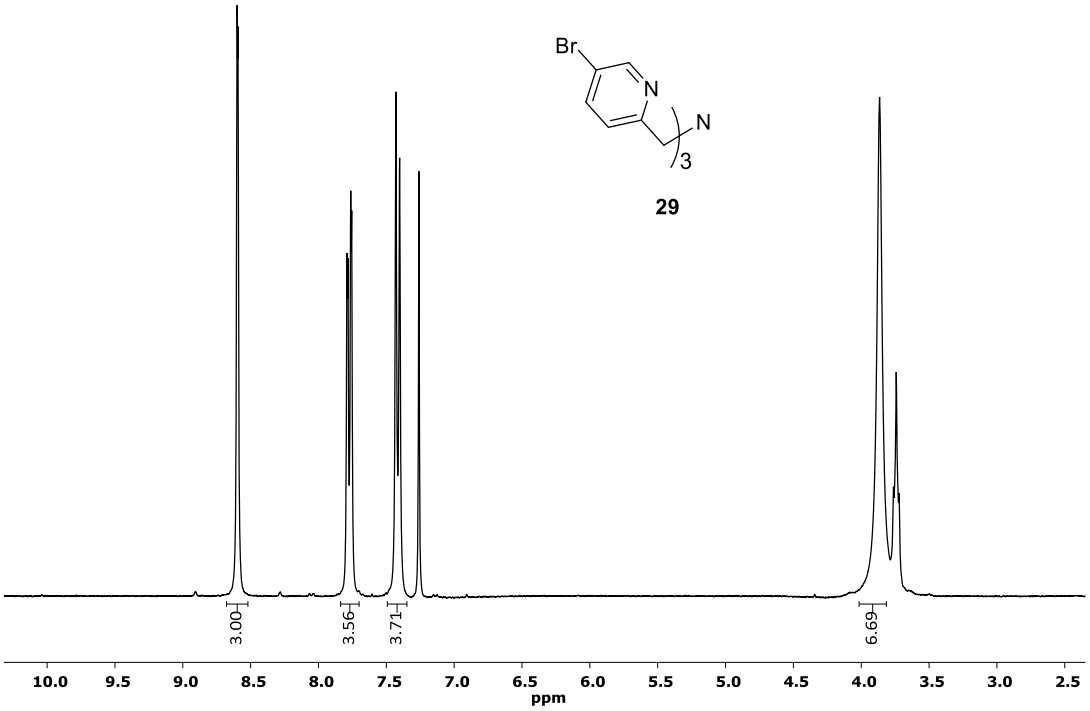


**Figure 25** $^{1}$H-NMR ($CDCl_3$, 300MHz) spectrum of the tris((5-bromopyridin-2-yl)methyl)amine ligand **29**. THF residual solvent peak at 3.7 ppm.

The tribromo substituted **TPMA** ligand **29** obtained in the first step has been then used for the subsequent Suzuki-Miyaura cross-coupling reaction for the preparation of ligand **30** which bears three aldehyde groups. In particular, one equivalent of the tribromo derivative **29** was mixed with three equivalents of 4-formylphenylboronic acid **31** in the presence of tetrakis(triphenylphosphine)palladium(0) as catalyst (Scheme 9). The reaction was stirred for 48 hours at 100 °C under inert atmosphere.

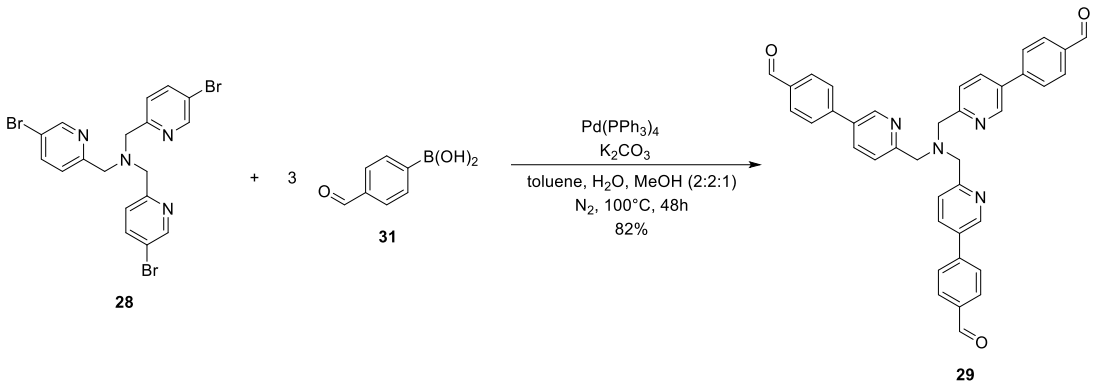


**Scheme 9** Suzuki-Miyaura coupling reaction between tribromo substituted **TPMA** ligand **28** and 4-formylphenylboronic acid **31** to form tri-aldehyde substituted **TPMA 29**.

The identity of the product was confirmed by the presence of the peak at 10.11 ppm related to the three aldehydic protons in the $^{1}$H-NMR spectrum (Figure 26). The identity of the product was confirmed also by ESI-MS technique obtaining only one main peak at 603.24 m/z.

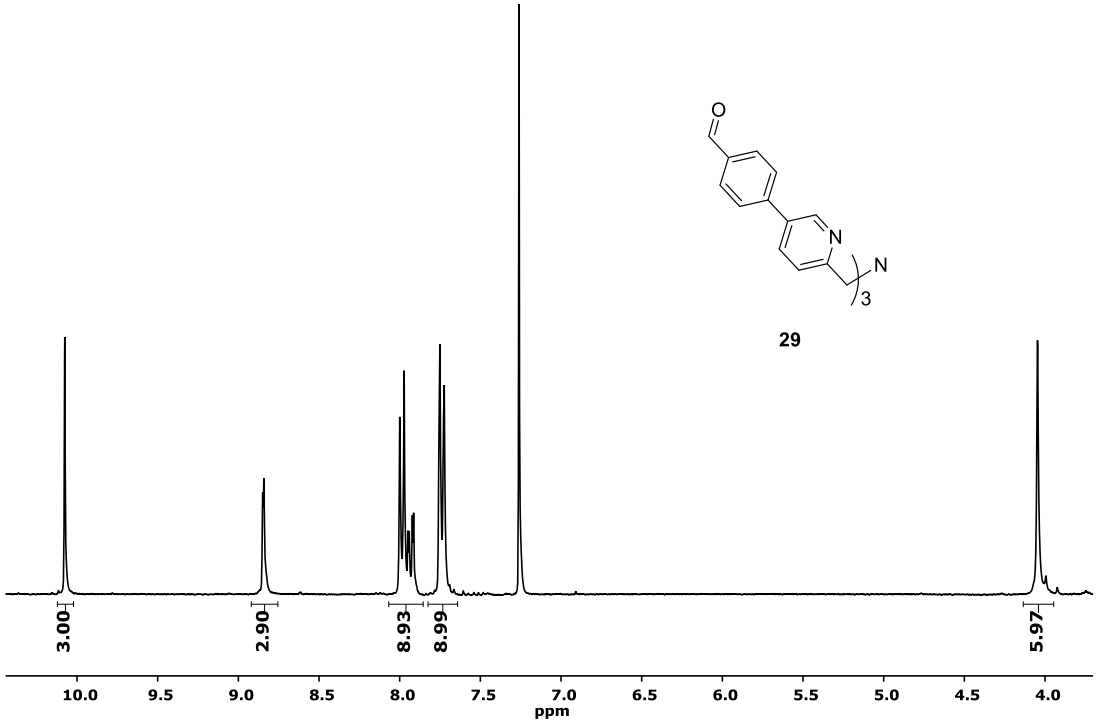


**Figure 26** $^{1}$H-NMR ($CDCl_3$, 300MHz) spectrum of the tri-aldehyde substituted **TPMA 29** ligand.

The following step of the synthesis was ligand complexation using zinc(II) perchlorate hexahydrated. The zinc salt was added stoichiometrically to a stirred suspension of ligand **29** in acetonitrile. After one hour, the zinc complex was precipitated with diethyl ether and obtained as perchlorate salt **24** in quantitative yield (Scheme 10).

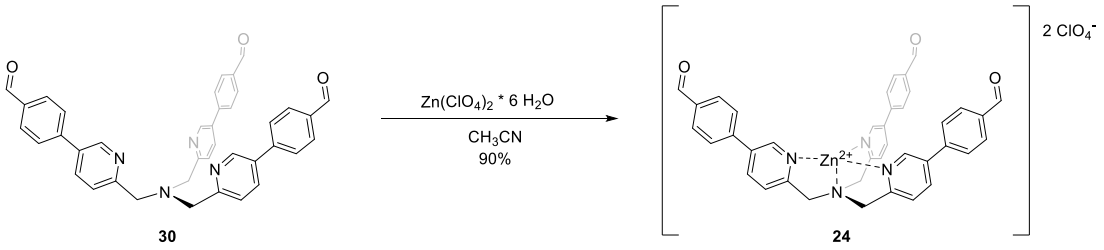


**Scheme 10** Complexation of the ligand **30** with zinc(II) perchlorate hexahydrated to form the **TPMA**-based Zinc complex **24**.

After the complexation, the $^{1}$H-NMR signals of the ligand a shift to higher ppm values for all the signals (Figure 27). The product was characterized also by ESI-MS analysis, the spectrum showed a main peak at 765.11 m/z corresponding to $[M+ClO_4]^+$ adduct.

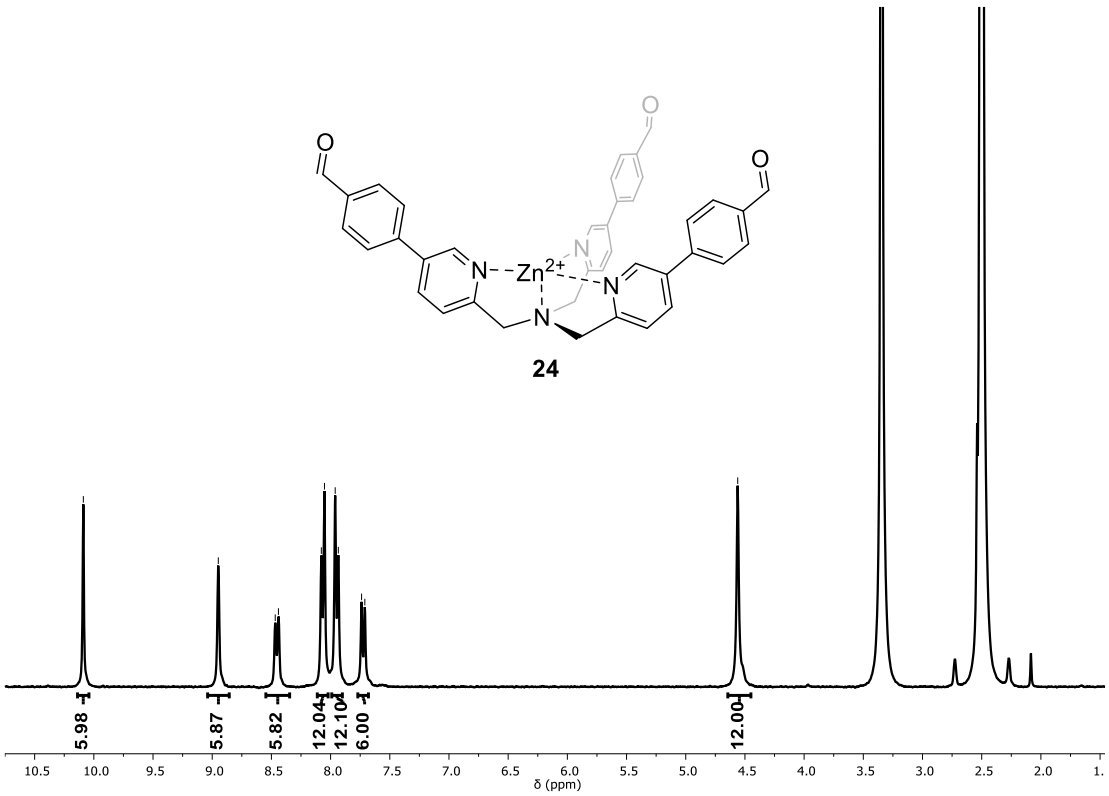


**Figure 27** $^{1}$H-NMR (300 MHz, $CD_3CN$) spectrum of the **TPMA**-based complex **24**.

At this point, the main building block for the formation of the supramolecular cage was formed and could be exploited in the Diaza-Cope rearrangement reaction for the synthesis of the cage. This synthetic strategy involves the use of 2.5 equivalents of (1*R*,2*R*)-1,2-bis(2-hydroxyphenyl) ethylenediamine **(*R*,*R*)-HPEDA** as linker and malonic acid **C$_3$** as templating agent (Scheme 11).

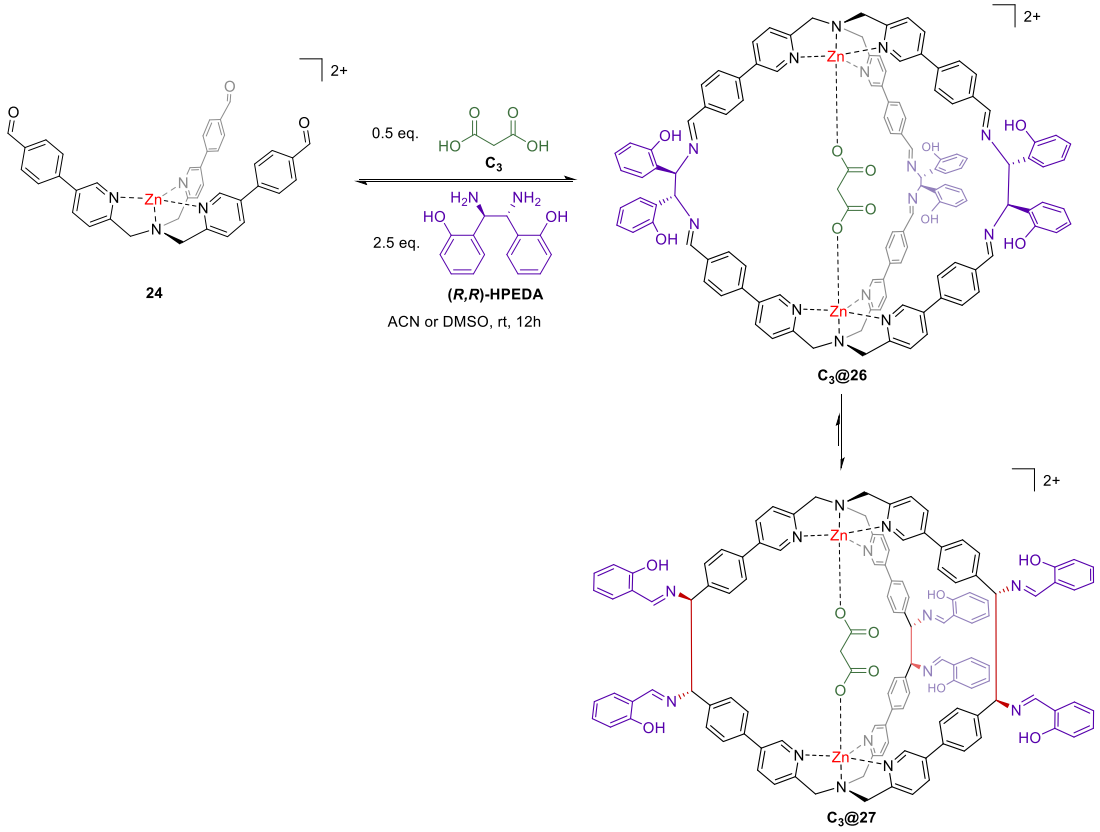


**Scheme 11** Diaza-Cope rearrangement of the cage using malonic acid **C3** as templating agent and **(*R*,*R*)-HPEDA** as diamine linker.

The reaction takes advantage of an imine condensation reaction between two functionalized **TPMA** units and three diamine molecules as linkers, that leads to the formation of the supramolecular cage in which three newly formed C-C bonds among components are formed. After that, the cage undergoes a concerted [3,3]-sigmatropic rearrangement, thermally allowed, with the shift of a σ-bond. This reaction is an equilibrium between the two structures, that is shifted to the product due to the stabilization given by the formation of a resonance assisted hydrogen bond (RAHB) between the alcohol hydrogen and the amine nitrogen.

In addition, the linking carbon atoms are novel stereocenters defined by the initial configuration of the amine as a consequence of the concerted nature of the Diaza-Cope rearrangement.

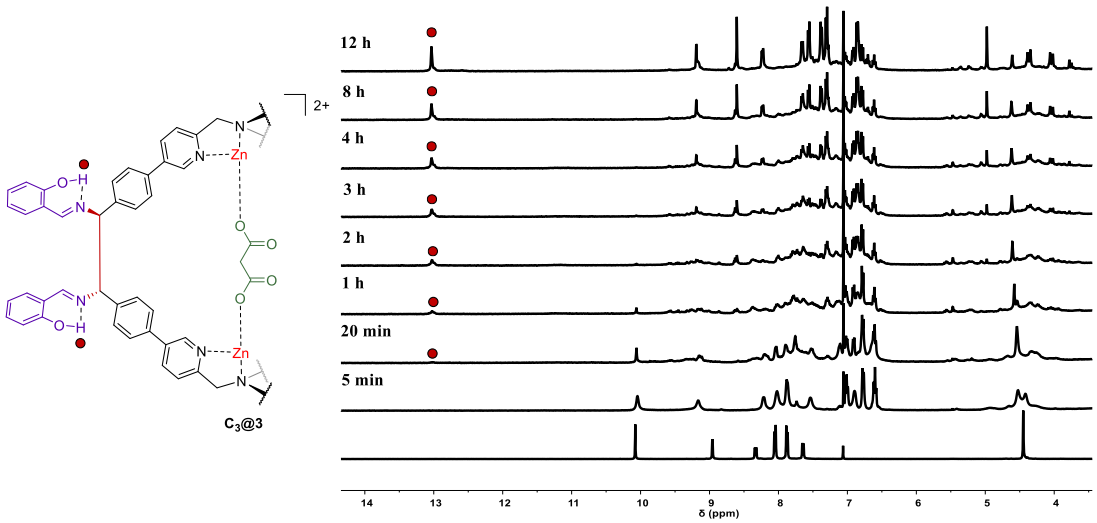


**Figure 28** $^{1}$H-NMR (400 MHz, 301 K, DMSO-*d*$_6$) complex **24** after the addition of 2.5 equiv. of **(*R*,*R*)-HPEDA** and 0.5 equiv of **C$_3$**.

Experimentally, it was possible to follow the reaction by $^{1}$H-NMR spectroscopy observing the disappearance of the aldehyde peak at 10.06 ppm and the simultaneous appearance of the characteristic phenolic signal (δ = 13.00 ppm) of the rearranged product **C$_3$@27** (Figure 28).

The cage was then hydrolyzed adding small volumes of hydrochloric acid solution and in this step the six imines undergo hydrolysis to six free primary amine groups (Scheme 12).

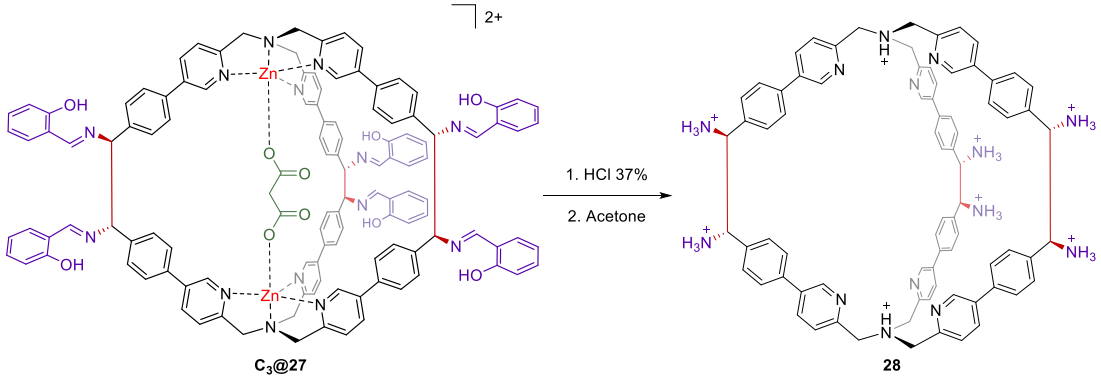


**Scheme 12** Hydrolysis with HCl of the rearranged product **C$_3$@27** in order to obtain the covalent cage **28**.

This novel system **28** was precipitated as chloride salt in quantitative yield and purified washing the solid with acetone. The $^{1}$H-NMR analysis was made dissolving a small amount of the powder compound in deuterium oxide. A highly ordered spectrum, with pyridine and phenyl protons well separated in the aromatic region is observed in which

the signal at 4.30 ppm referred to the $CH_2$ benzylic protons of the **TPMA** arms (Figure 29). An ESI-MS analysis was also performed in order to confirm the novel synthetized structure. As shown in Figure 30 a peak at 603.4 m/z was observed (Figure 30).

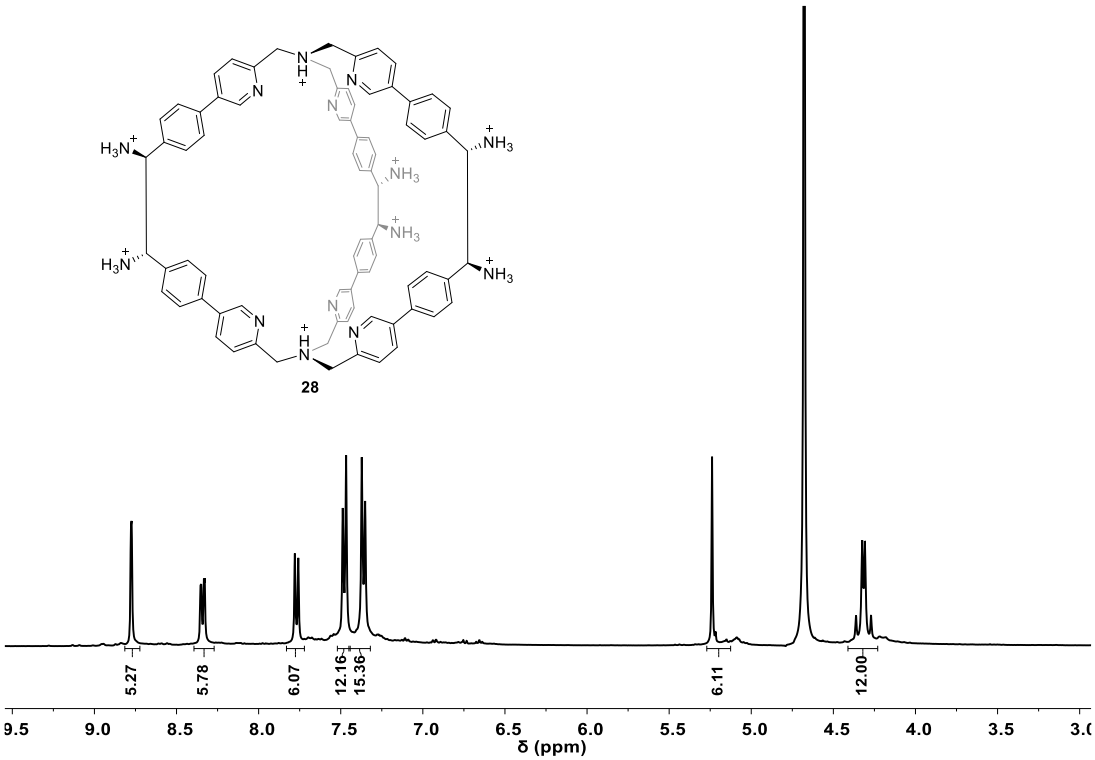


**Figure 29** $^1$H-NMR (400 MHz, 301 K, $D_2O$) spectrum of cage **28**.

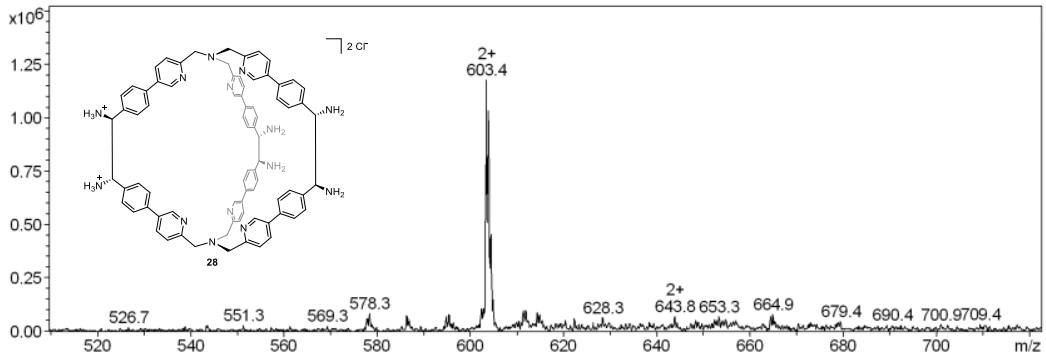


**Figure 30** Experimental ESI-MS pattern of cage **28**.

## 3.2 Complexation of the Cage with different metals

In order to study the capability of the system to bind metals such as zinc and copper, and to consequently obtain different metal complexes (Scheme 13), the attention was initially focused on Zn(II) for ease of analysis. Indeed, being Zn(II) diamagnetic leads to more clear $^{1}$H-NMR spectra compared to those that can be obtained for Cu(II) paramagnetic complexes.

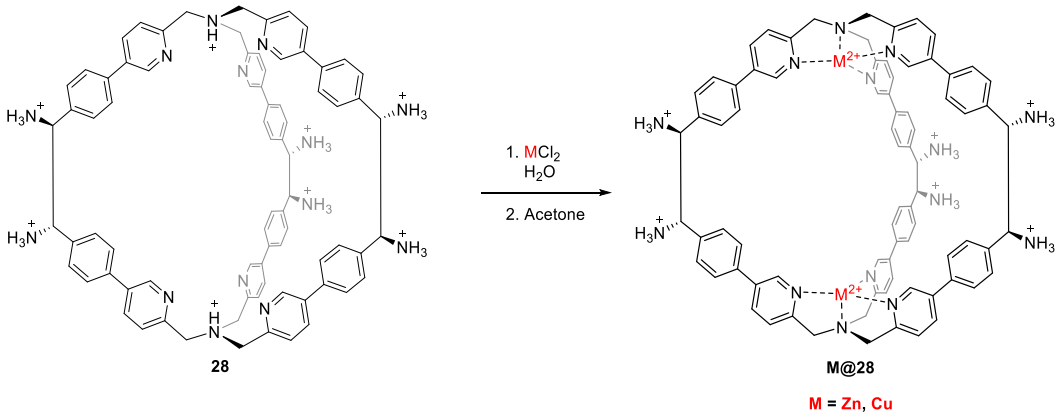


**Scheme 13** General scheme for the complexation of the cage **28** with different metal ions.

Experimentally, to a solution of the cage **28** in water, a stoichiometric quantity of hydrated zinc chloride salt was added and stirred at room temperature for 1 hour. Then, the addition of acetone led to the precipitation of a crystalline solid that was centrifuged and dried. The $^{1}$H-NMR was performed in $D_2O$ and confirmed the complexation by the splitting of the signal related to the **TPMA** arms $CH_2$ protons into two new signals located at 4.19 and 4.45 ppm, characteristic for this kind of complexes (Figure 31). From ESI-MS spectroscopy only one main peak was obtained at 703.66 m/z, consistent with the calculated value (Figure 32).

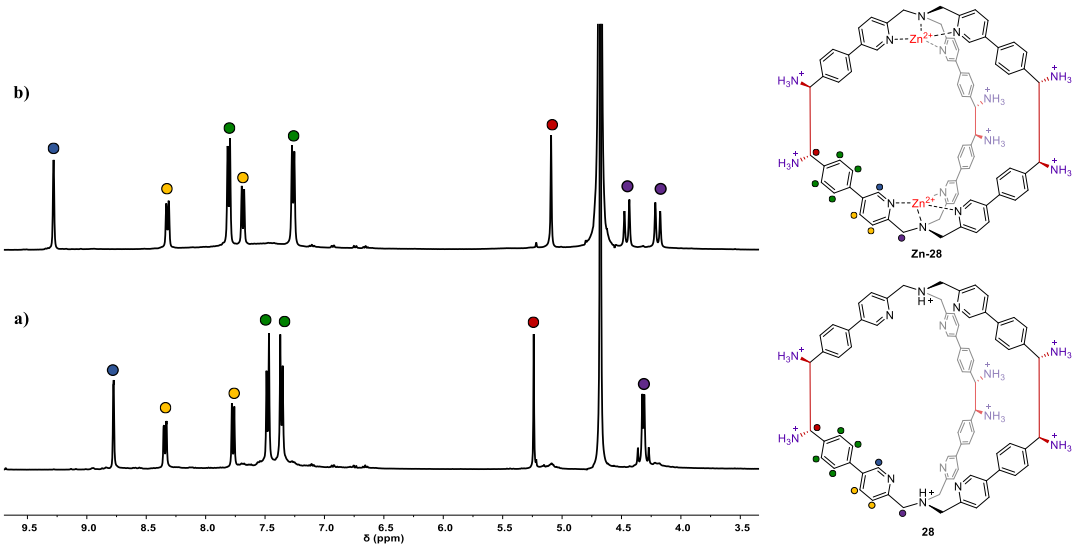


**Figure 31** $^{1}$H-NMR spectra (400 MHz, 301 K, $D_2O$,) of a) cage **28**, and b) cage **Zn-28** obtained after complexation of cage **28** with $ZnCl_2$. Chloride ions are removed for clarity.

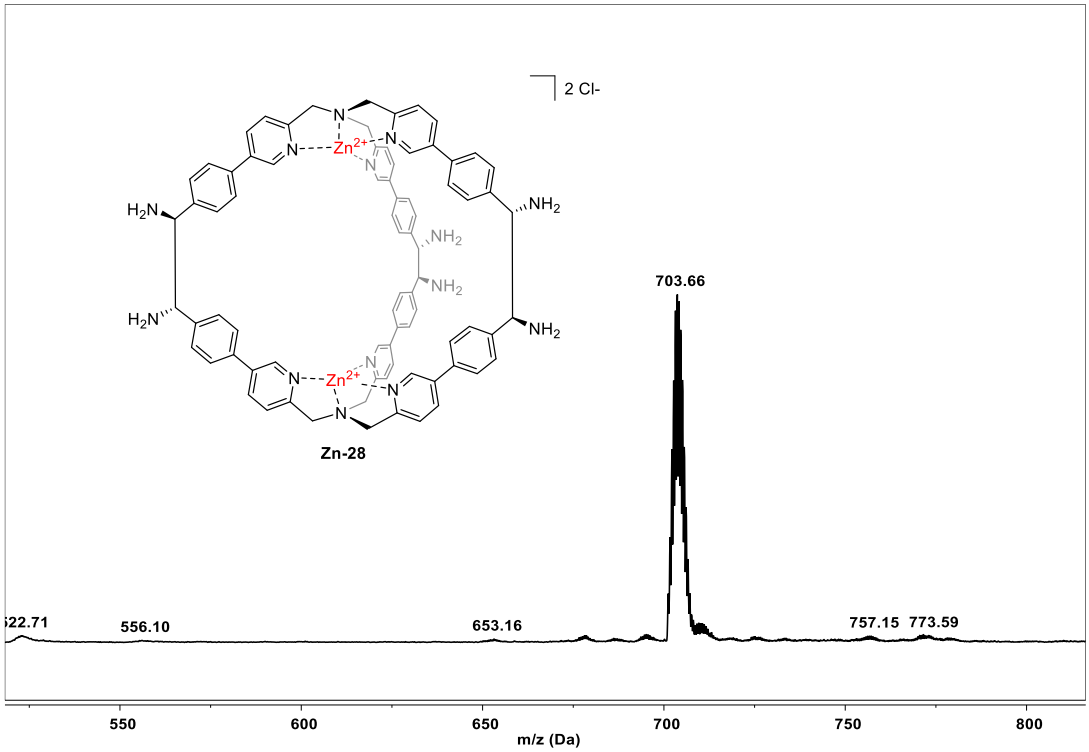


**Figure 32** ESI-MS spectrum of cage **Zn-28**.

The same procedure was used for the complexation of **28** cage with hydrated $CuCl_2$ however in this case, not being NMR analysis effective, only ESI-MS spectrometry was performed obtaining a main signal at 701.22 m/z that confirmed the hypothesis of the entire complexation of the cage (Figure 33).

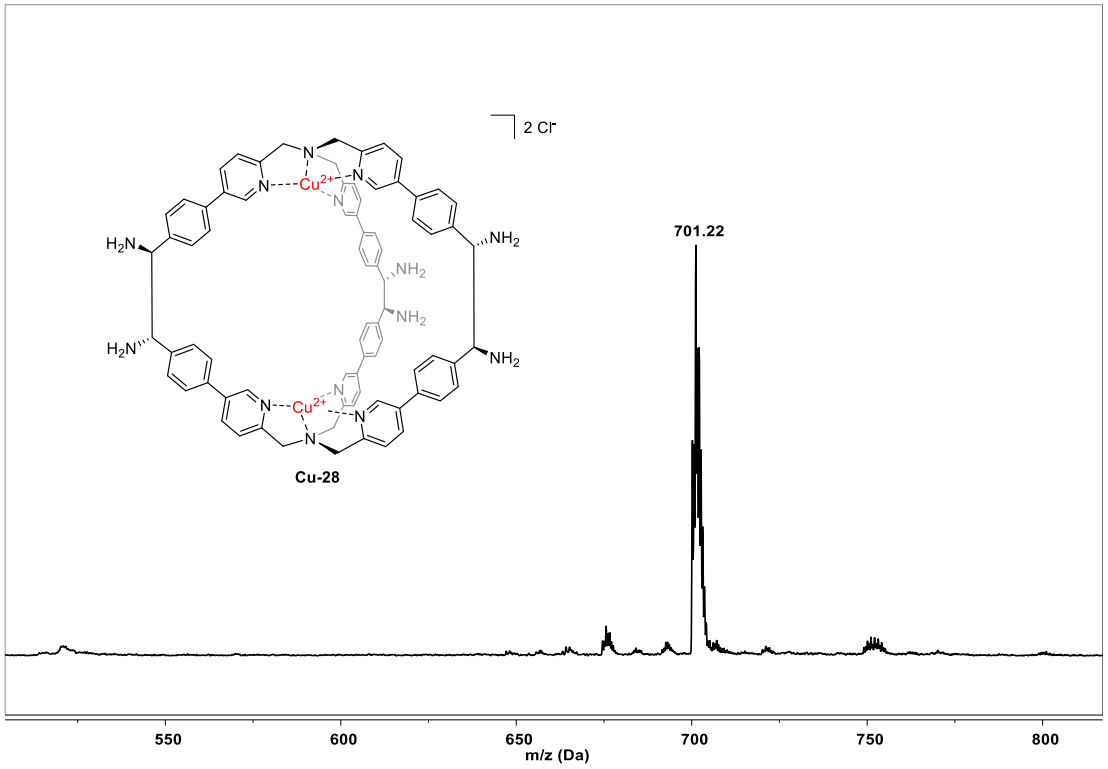


**Figure 33** ESI-MS spectrum of cage **Cu-28**.

Moreover, single-crystal suitable for X-ray diffraction has been obtained for cage **Cu-28**. As shown in Fig. 34, the structure of the system has been confirmed. As expected, the reaction furnished the enantiopure product with six novel stereocenters.

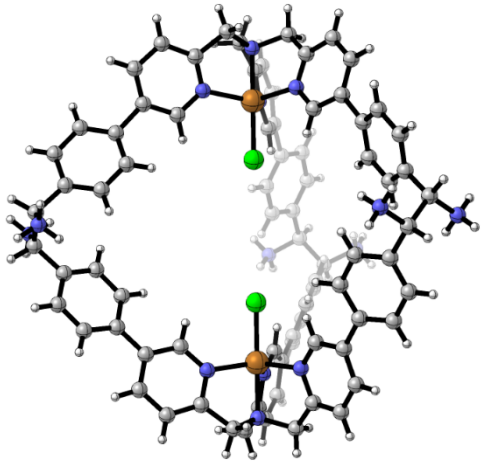

**Figure 34** Single-crystal X-Ray structure of cage **Cu-28**. Chloride ions are removed for clarity.

Furthermore, the complete complexation of cage **28** with $CuCl_2$, an electrochemical titration was performed before applying it in polymerization experiments.

### 3.2.1 Electrochemical titration of cage 28 with Cu

To have a further confirmation of the complexation of cage **28** with copper, an electrochemical titration was setup using a 0.1 M $CuCl_2$ solution. For the electrochemical investigations of the cage complex, a three-electrode setup was used with a Glassy Carbon disk as working electrode, a saturated calomel as reference electrode, and a graphite rod as counter electrode (separated from the working electrode compartment by a glass frit and a methylcellulose layer saturated with 0.1 M *n*-$Bu_4NBF_4$ in dimethylformamide, DMF). Experimentally, first cyclic voltammetries (CVs) of the cage were recorded in the absence of copper, using tetraethylammonium tetrafluoroborate ($Et_4NBF_4$) as supporting electrolyte. In this case no electrochemical signals were obtained confirming the absence of electrochemical activity of the ligand. By progressively adding 5-10 μL aliquots of $CuCl_2$ solution, the recorded CVs started to show the typical reversible peak due to the reversible reduction of Cu centers. The signal increases up to a total volume of 50 μL that corresponded to the calculated stoichiometric ratio 1 : 2 of Cage **28** : Cu. After this point, the recorded voltammetries showed a new peak couple at -0.03 V (reduction) and +0.2 V vs SCE (oxidation), which corresponds to the presence of free copper in solution meaning that the cage was totally complexed at a 1 : 2 ratio (Figure 35).

This experiment confirmed the formation of the complexed cage **28** with copper(II) and its reversible electrochemical activity in order to apply it as catalyst in *e*ATRP processes.

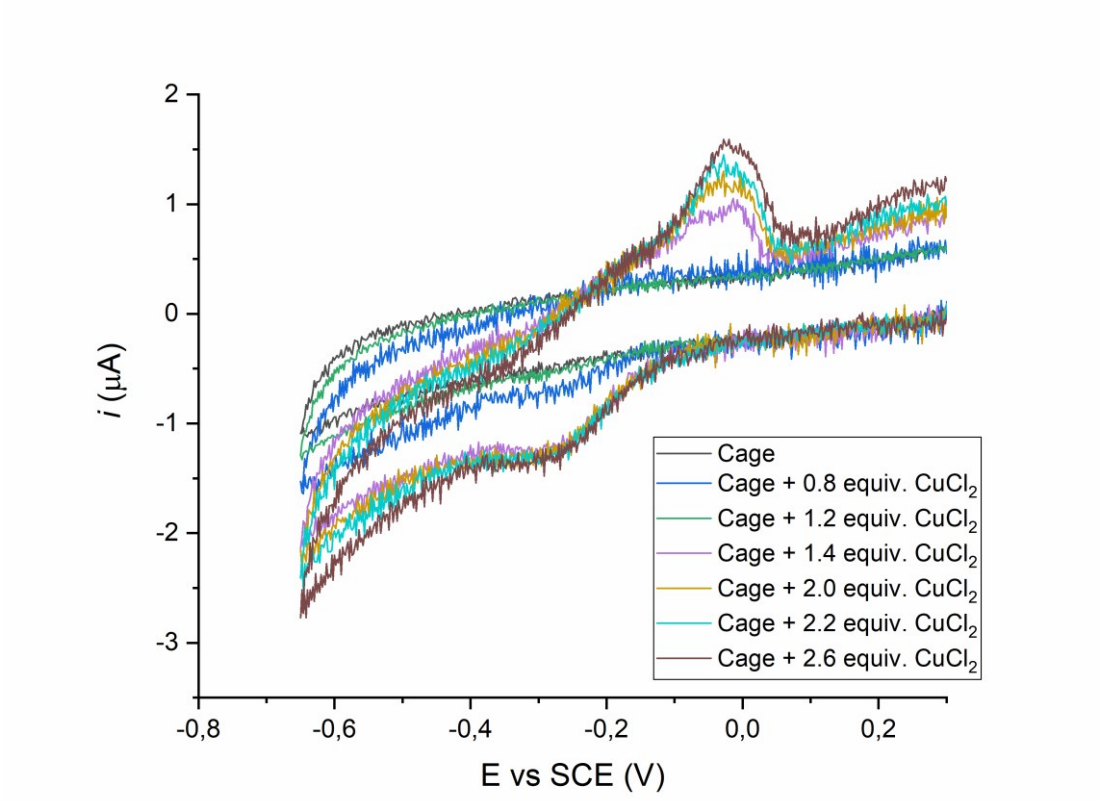


**Figure 35** Electrochemical titration for the complexation of the cage **28** with increasing amounts of $CuCl_2$.

### 3.3 Electrochemical investigation of the catalytic system and comparison with traditional Cu catalysts for ATRP

The CV of **Cu-28** was compared to that of Cu/**TPMA**, a typical copper complex for ATRP. The CVs were recorded in water with NaBr as supporting electrolyte, which favors the formation of ternary $[CuL\text{-}Br]^{n+}$ complexes. The halfwave potential of the **Cu-28** is -0.18 V vs SCE, while that of Cu(II)/**TPMA** is -0.27 V vs SCE. Therefore, **Cu-28** is a slightly weaker reducing agent than the highly active Cu(I)/**TPMA** under these conditions.

Another observation regards the different pH of the solution of the two complexes. Cu(II)/**TPMA** is a very weak acid and the record pH is ca. 6. Conversely, 1 mM solution of **Cu-28** are rather acidic at pH 2.5. This could be due to the multiple ammonium groups present in the cage but also to small residual traces of acid present in the sample. The role of pH in the ATRP polymerization will be further discussed below.

However, a significant different between the CV of the two catalysts was the recorded current, which was much smaller for **Cu-28** as compared with typical Cu/**TPMA** system, although in the cage there are two copper(II) sites (Figure 36). This experimental evidence led to the assumption of aggregation of the **Cu-28** system. The possibility of formation of aggregates was also suggested by the hazy appearance of some Cu/cage solutions.

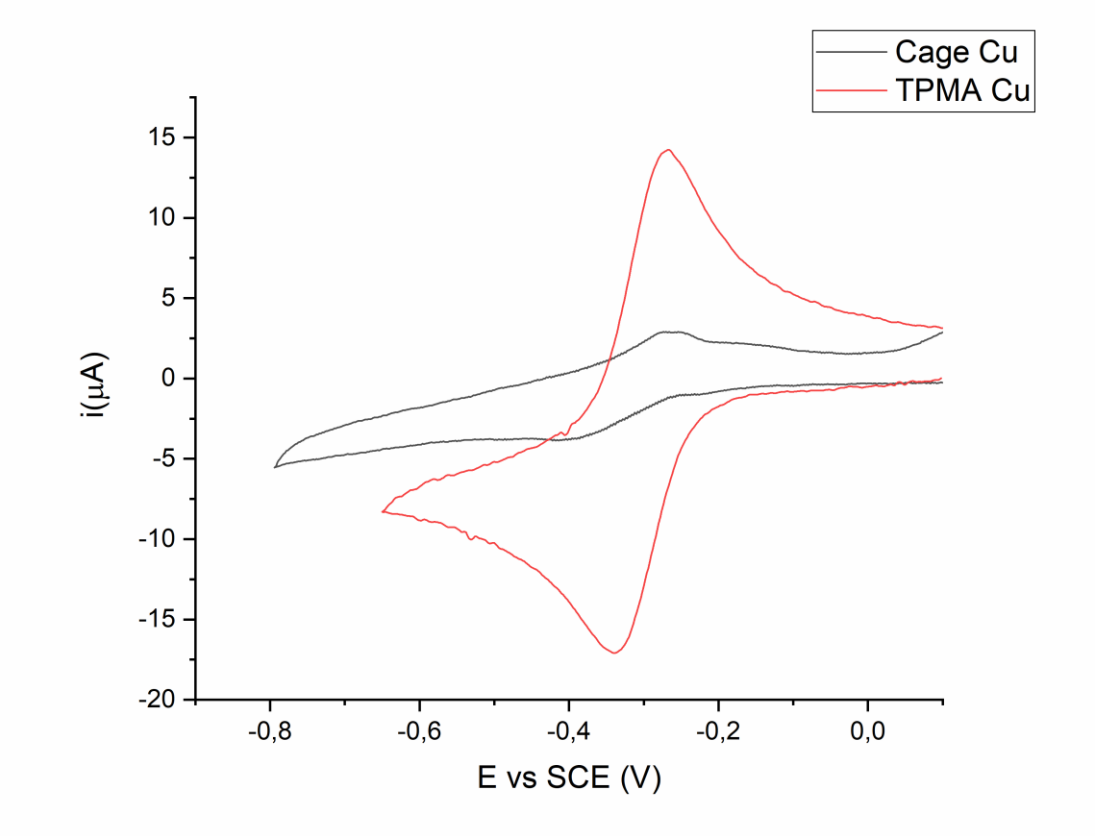


**Figure 36** Cyclic voltammetry of a) **TPMA-Cu** (red line) b) Cage **Cu-28** (black line).

To explore this hypothesis two different experiments were performed in order to calculate the Diffusion coefficient ($D$) and the Hydrodynamic radius ($R_{hyd}$) of the cage using the Randles-Sevcik and Stokes-Einstein equations respectively. More in detail, cyclic voltammetries at different scan rates and cyclic voltammetries at different concentration of the catalyst were carried out.

### 3.3.1 Cyclic voltammetries at different scan rates

As first experiment, the estimation of Diffusion coefficient from experimental cyclic voltammetry was carried out. The Diffusion coefficient (*D*) is an important physical parameter of the species involved in an electrochemical reaction, that describes diffusional transport. This value can be calculated for simple diffusional-controlled one-electron transfer electrode reactions using the Randles-Sevcik equation (Eqn.1):

$$\mathrm{I_p} = 0{,}4463\ \mathrm{nFAC}\sqrt{\frac{\mathrm{nFv}D}{\mathrm{RT}}} \qquad \text{Eqn. 1}$$

Where:

n = 2 number of exchanged electrons per cage

F = 96485,34 C $mol^{-1}$ Faraday constant

A = 6,24 x $10^{-2}$ $cm^2$ WE area

C = 1 mM catalyst concentration

v = V/s scan rate

R = 8,314 J $K^{-1}mol^{-1}$ gas constant

T = 298 K temperature

*D* = $cm^2$/s diffusion coefficient

This expression defines the peak current ($I_p$) as a function of the scan rate ($v$). The prediction is that $I_p$ increases for higher scan rates because the number of exchanged electrons in the time unit is greater. During voltametric experiments the current was measured, while all other parameters are known or under experimental control, therefore *D* of the electrochemical species can be determined.

A water solution containing 1 mM of cage **28**, 2 mM of $CuCl_2$ and 0.2 M of NaBr was analyzed starting from a scan rate of 20 mV/s up to 1000 mV/s. With the values of $I_p$ obtained for each trial, a graph was made as a function of the corresponding scan rate that should have a linear pattern (Figure 37).

Experimentally, the Diffusion coefficient was calculated from a linear regression of the plot of cathodic peak current ($I_p$) vs square root scan rate ($v^{1/2}$) (Figure 37).

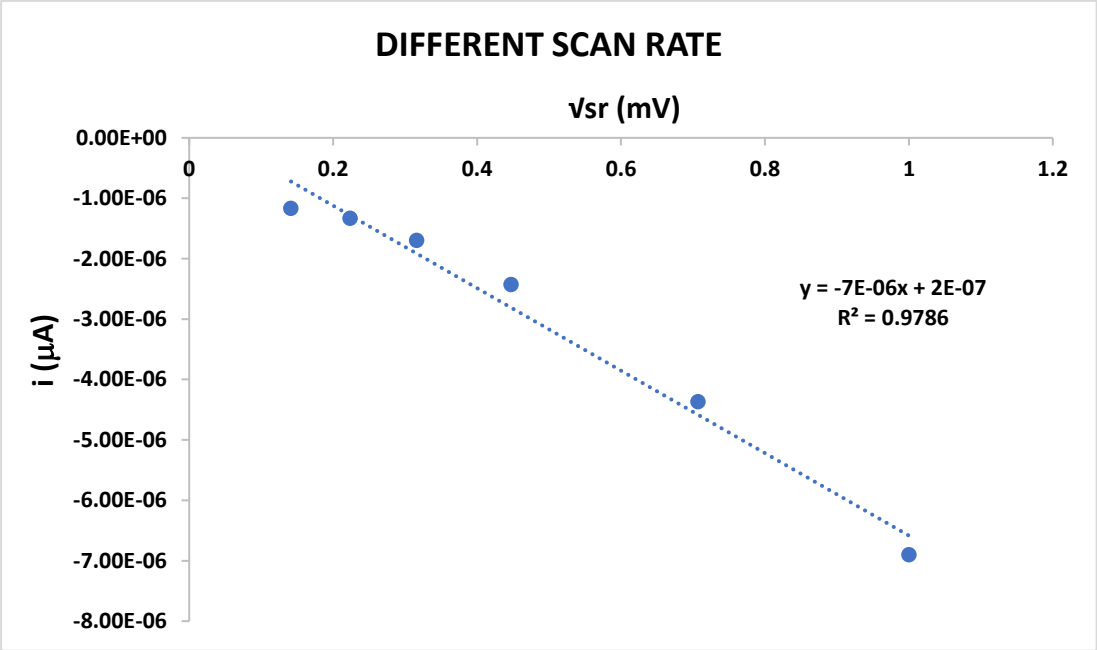


**Figure 37** Graph obtained from cyclic voltammetries at different scan rate. Current (i) variation as a function of the scan rate.

From the obtained results, the diffusion coefficient (D) found for the cage was 1.4 $10^{-8}$ $cm^2/s$.

Once the value of D was determined, it was used to calculate the Hydrodynamic radius ($R_{hyd}$), defined as the radius of an equivalent hard-sphere diffusing at the same rate as the molecule under observation, using the Stokes-Einstein equation (Eqn. 2):

$$D = \frac{K_b \mathrm{T}}{6\pi\eta R_{hyd}} \qquad Eqn.2$$

Where:

$K_b$ = 1.38 x $10^{-23}$ J $K^{-1}$ Boltzmann constant

T = 298 K temperature

η = 0.89 mPa/s medium viscosity ($H_2O$)

$R_{hyd}$ = nm hydrodynamic radius

From the Stockes-Einstein equation the value obtained for $R_{hyd}$ of the cage was 181 nm. The high value for the hydrodynamic ratio confirmed the initial hypothesis of the aggregation of the catalyst in the reaction conditions. A possible explanation could be attributed to the presence of salts in the reaction medium that could probably favor the aggregation phenomenon. It should be noted that with a such high radius of the

aggregates, the electrochemical methods might detect only the Cu/cage present at the surface of the aggregate particles, and thus the measured *D* and $R_{hyd}$ must be considered an estimation.

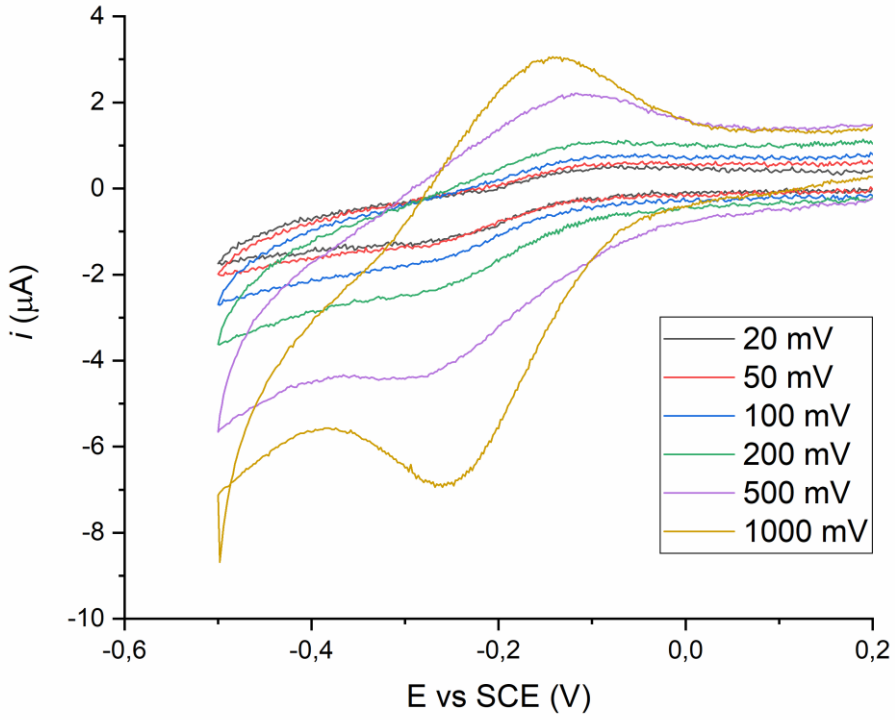


**Figure 38** Cyclic voltammetry at different scan rate of the Cage **Cu-28**.

### 3.3.2 Cyclic voltammetries at different concentrations of the catalyst

The observed aggregation phenomenon should be disfavored by dilution of the catalyst. Therefore, the same solution was then used to calculate $R_{hyd}$ by performing cyclic voltammetries while decreasing the concentration of the **Cu-28** catalyst starting from 1 mM **28** and 2 mM $CuCl_2$, down to 0.0625 mM of cage **28** and 0.125 mM $CuCl_2$ (Figure 39). Some examples of CVs are plotted in Figure 39A. Plotting a graph of the resulting *D* vs [Cu] (Figure 39B), it is apparent that the diffusion coefficient had a strong dependance on concentration, as typical for an aggregation phenomenon. At the same time, the calculated hydrodynamic radius (Figure 39C) sharply decreased with decreasing [Cu]. This trend could be due to the fact that at high concentrations the molecules tend to aggregate resulting in lower current at the electrode.

At [Cu] < $6\times10^{-5}$ M, the calculated $R_{hyd}$ reached a value typical of a free molecule in solution (1 nm), suggesting that the aggregation phenomenon was suppressed at these very diluted concentrations.

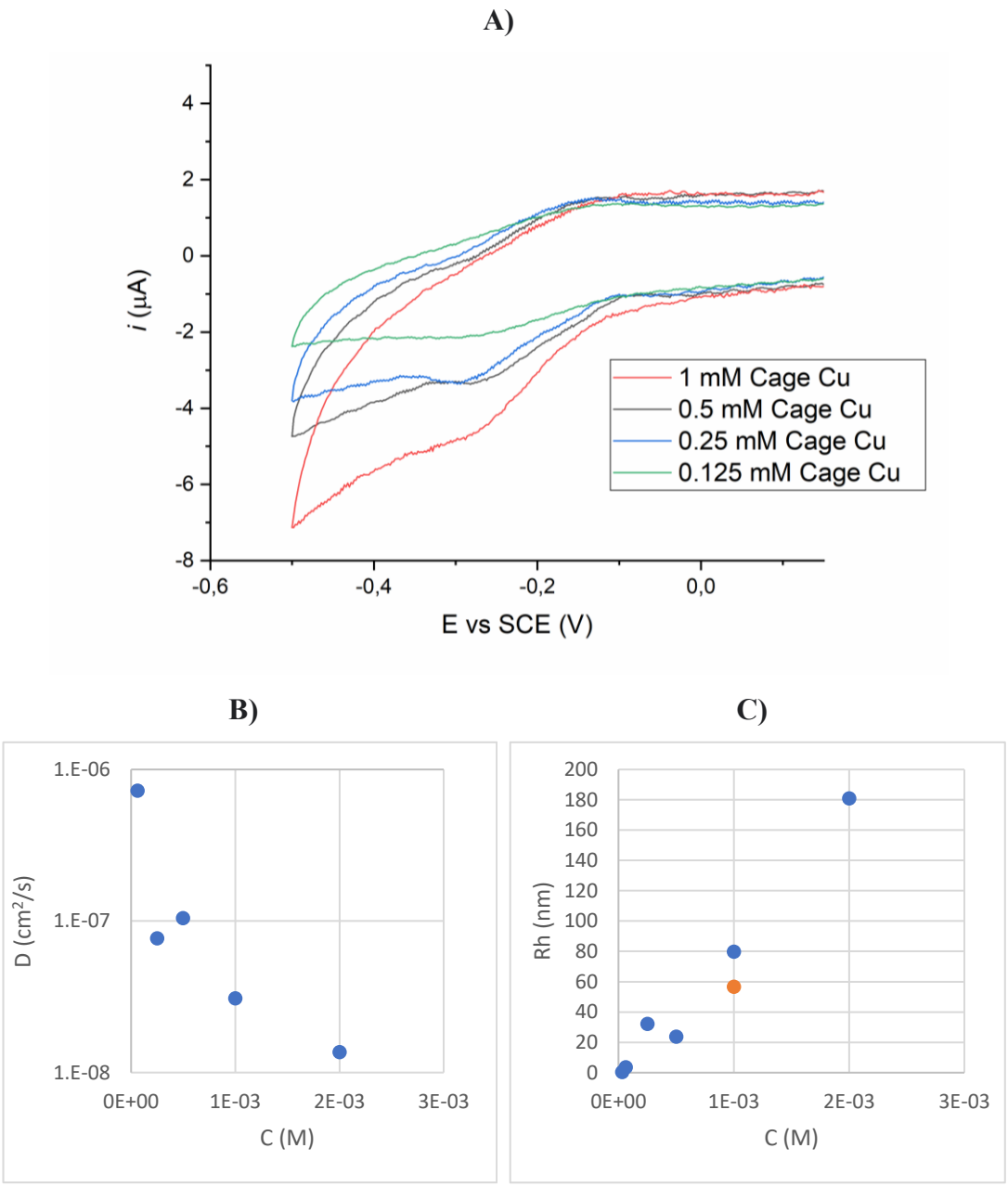


**Figure 39** A) Cyclic voltammetry at different concentrations of the Cage **Cu-28** catalyst. B) Diffusion coefficient and C) $R_{hyd}$ as a function of Cu concentration. The data in blue dots were determined from electrochemical measurements, while the data in orange was determined from dynamic light scattering.

### 3.3.3 Dynamic light scattering (DLS) analysis of the catalyst

To further investigate the aggregation behavior of the **Cu-28** cage with a complementary technique, a DLS analysis was performed to determine the size distribution profile of the cage copper complex. In this technique the sample is irradiated by a laser beam and variations of the scattered light are measured as a function of time. The intensity variations measured by the detector are generated by the Brownian motion of particles, at the same temperature and viscosity smaller particles move faster giving sharper variations in the intensity of scattering while bigger ones will create slower variations.

A standard water solution containing 1 mM Cu and 0.1 M of NaBr as supporting electrolyte, was analyzed through dynamic light scattering, giving an average particle size of 59 nm. This is well in agreement with the $R_{hyd}$ calculated from electrochemical measurement (Figure 39C), again confirming the aggregation behavior of this complex.

While DLS and electrochemical studies are consistent, DOSY NMR experiments of the cage **Zn-28** at 1 mM concentration showed a hydrodynamic radius in $D_2O$ corresponding to the size of the molecular cage ($7.43 \times 10^{-10}$ m). This indicated that the Zn complex did not aggregate at concentration value where the equivalent $CuBr_2$ complex was significantly aggregated.

## 3.4 Electrochemically mediated Atom Transfer Radical Polymerization of OEOMA monomers using Cage Cu-28 as catalyst

After the electrochemical studies, the catalyst was applied in Electrochemically Mediated Atom Transfer Radical Polymerization (*e*ATRP) processes. Poly(ethylene glycol) methyl ether methacrylate (OEOMA) was chosen as the model monomer, as it represents one of the most studied monomers in aqueous ATRP. In particular, OEOMA with different chain length of the side chain were chosen for the purpose of examine both the catalytic activity of the cage and the influence of the molecular size (viz. length of the ethylene glycol lateral chain) on the activation/deactivation processes into the cavity. The molecular weight of the monomer was varied between 2000 and 300, which corresponded to side chain length between 43 and 5 units of ethylene glycol ($OEOMA_{2000}$, $OEOMA_{950}$, $OEOMA_{500}$ and $OEOMA_{300}$) (Scheme 14).

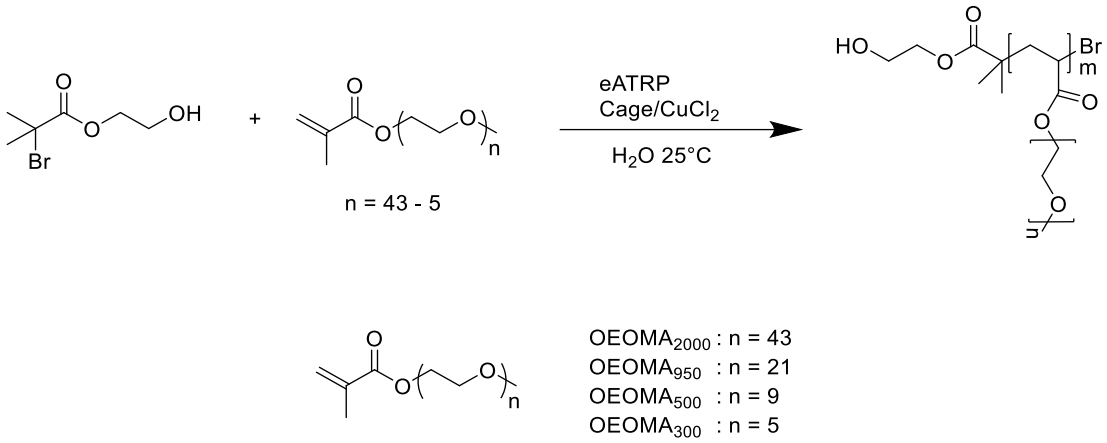


**Scheme 14** General scheme for the electrochemical polymerization of OEOMA monomers catalyzed by Cage **Cu-28**.

The electrochemical polymerization procedure was carried out as follows: All electrodes, electrolyte, solvent and reagents, except the initiator, were introduced into the cell, thermostated at 25 °C. After degassing, cyclic voltammetry of **Cu-28** cage was recorded using a small Glassy Carbon disk as WE, to measure the standard reduction potential of the catalyst and select the suitable $E_{app}$ value for each monomer (Figure 40). A reversible peak couple was observed corresponding to one electron transfer.

$$[Cu^{II}L]^{2+} + e^- \longrightarrow [Cu^{I}L]^{+}$$

$$[Cu^{I}L]^{+} \longrightarrow [Cu^{II}L]^{2+} + e^-$$

With the addition of the initiator (R-X) there is a high increase of the cathodic current for the Cu(II)/Cu(I) reduction that indicates high catalytic activity of the **Cu-28** in the activation of the carbon-halogen bond. Additionally, the voltammetry becomes irreversible (Figure 40). The process can be described by the following electrocatalytic cycle:

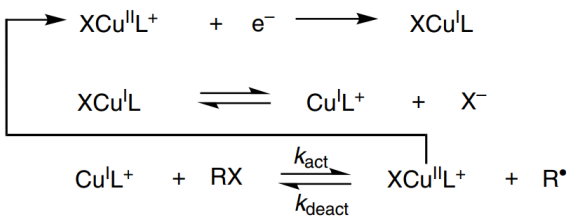

The $XCu^{II}L^{+}$ complex is reduced to $XCu^{I}L$ at the WE, after which it can partially dissociate to $Cu^{I}L^{+}$, the ATRP activator complex. $Cu^{I}L^{+}$ quickly reacts with the alkyl halide to for a radical and to reform $XCu^{II}L^{+}$, closing the catalytic cycle. $XCu^{II}L^{+}$ is reduced again at the WE, explaining the cathodic current enhancement and the irreversible wave upon scan reversal. We can conclude that despite the partial aggregated state of the Cu-cage, it is an active catalyst in the activation of R-X initiators.

Last, to start the electrochemical polymerization a large (bulk) Platinum mesh is connected to the potentiostat and the selected potential was applied for the polymerization under continuous magnetic stirring.

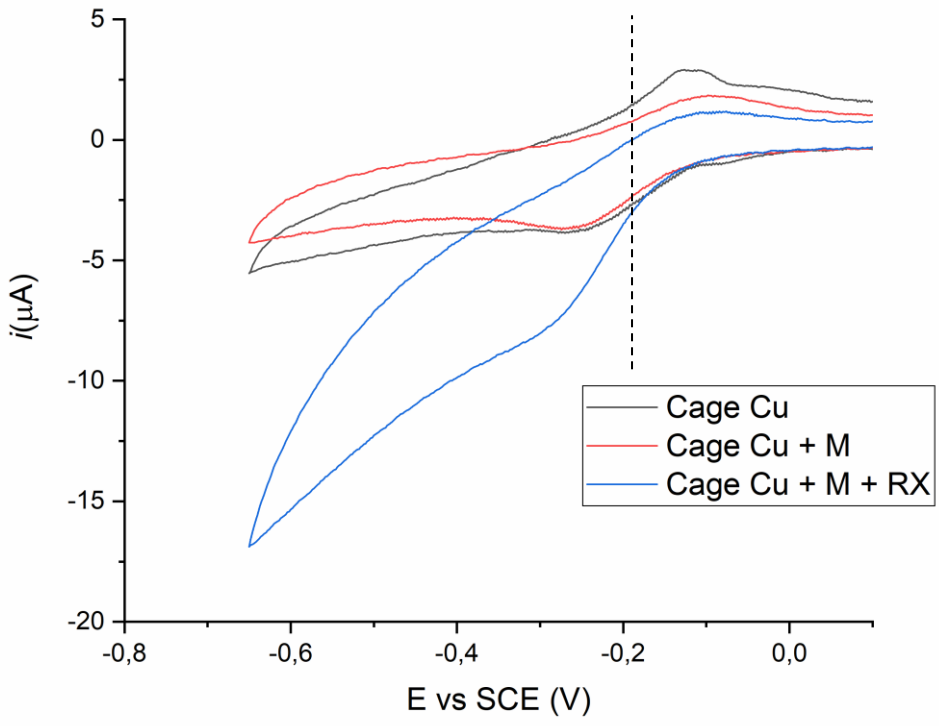


**Figure 40** Cyclic voltammetry of a) 1 mM Cage **Cu-28** (black line) b) 1 mM Cage **Cu-28** + 10% v/v $OEOMA_{950}$ monomer (M) (red line) c) 1 mM Cage **Cu-28** + 10% v/v $OEOMA_{950}$ monomer + 2 mM HEBiB initiator (RX) (blue line). The dashed line represents the applied potential for the polymerization of $OEOMA_{950}$.

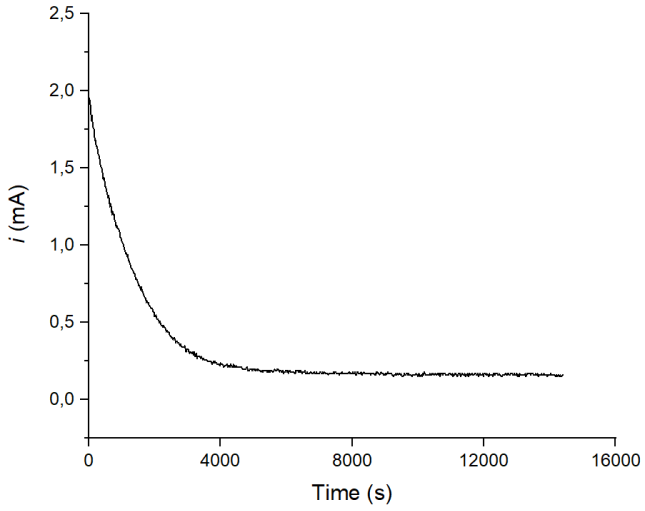


**Figure 41** Cathodic current recorded during electrochemical polymerization of $OEOMA_{950}$ catalyzed by Cage **Cu-28**.

Figure 41 displays a chronoamperometry curve recorded during electrolysis with **Cu-28**. The curve is divided into two regions. In the first hour, a large current was recorded, which corresponds to the bulk reduction of Cu(II) species to form the activator Cu(I) form of the catalyst. After about 1 hour, a constant current was recorded, which is due to the continuous reduction of Cu(II) species that accumulate in solution following radical-radical termination reactions.

Aliquots of the sample were periodically picked up for four hours in order to determine polymer molecular weight by GPC analysis (see example in Figure 42) and conversion via $^1$H-NMR.

All conversions were calculated by $^1$H-NMR integrals of monomer and polymer signals over time using DMSO-$d_6$ as internal standard (Figure 43).

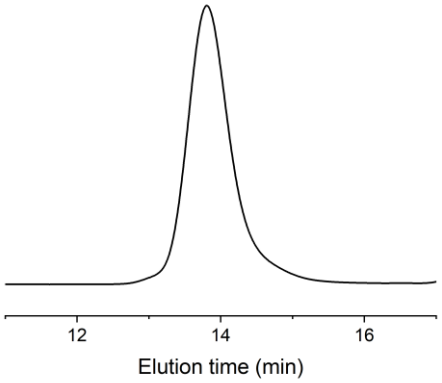


**Figure 42** GPC trace for eATRP of $OEOMA_{950}$ (10% v/v) in $H_2O$ + 0.1 M NaBr catalyzed by Cage **Cu-28**.

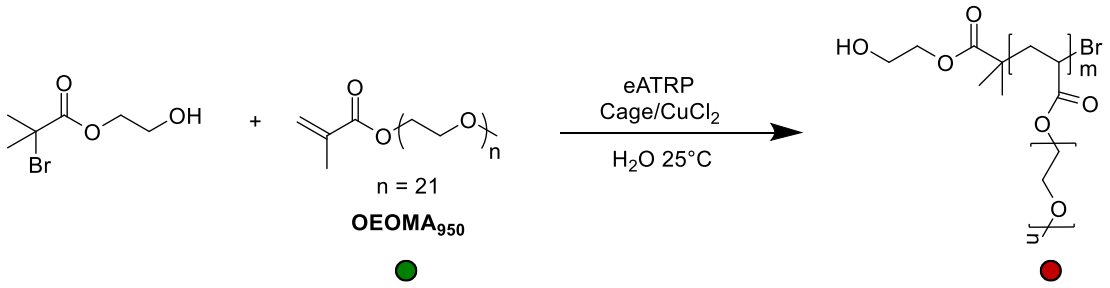


*$OEOMA_{950}$:*

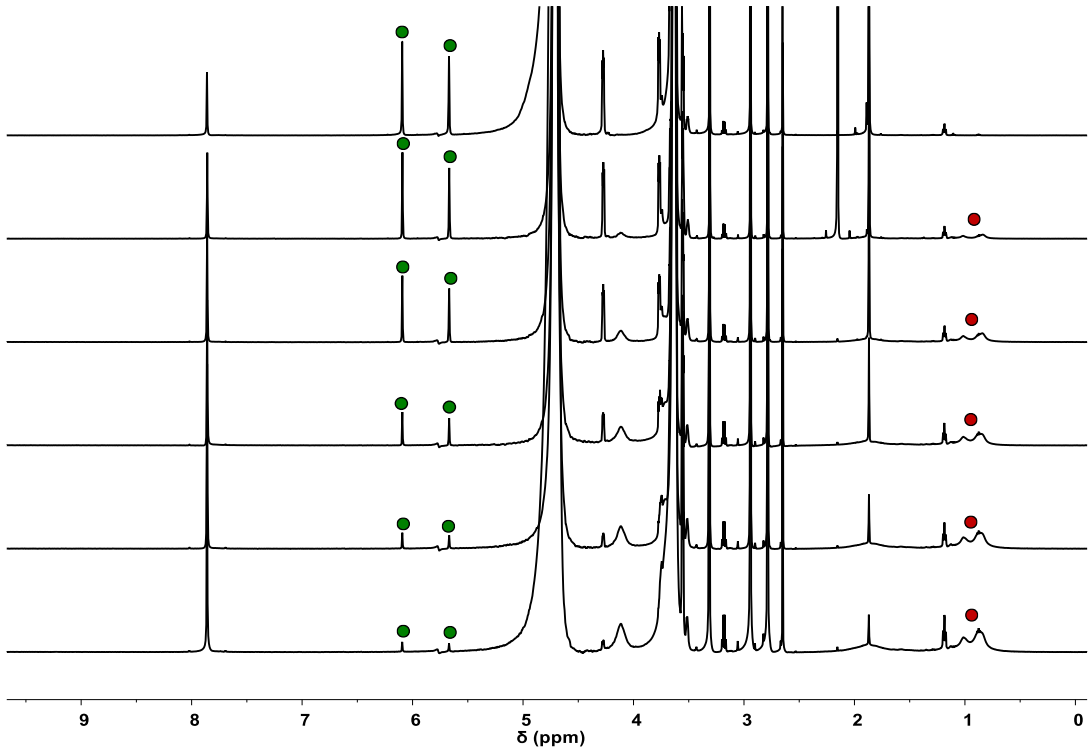


**Figure 43** 600 MHz $^1$H-NMR spectra stacking for the polymerization reaction of $OEOMA_{950}$ monomer catalyzed by Cage **Cu-28**. From top to bottom spectra recorded at time = 0.5 hour, 1 hour, 2 hours, 3 hours and 4 hours. Integrals corresponding to the monomer, 6.10 ppm and 5.67 ppm signals, and polymer, signals between 1.3-0.7

ppm, have been used to determine the conversion. Integrals are referred to the external standard DMSO-$d_6$ signal at 2.67 ppm.

| *Entry* | *Monomer* | Conv (%) | $Mn_{th}$ ($10^{-3}$) | $Mn_{exp}$ ($10^{-3}$) | D | Q (C) |
|---|---|---|---|---|---|---|
| *1* | $OEOMA_{2000}$[a] | 60 | 32705 | 30385 | 1.08 | 1.44 |
| *2* | $OEOMA_{950}$[b] | 95 | 52294 | 32155 | 1.07 | 0.50 |
| *3* | $OEOMA_{500}$[a] | 81 | 44186 | 37202 | 1.13 | 0.9 |
| *4* | $OEOMA_{300}$[b] | 82 | 42067 | 36127 | 1.19 | / |

**Table 1** Potentiostatic eATRP of different monomers catalyzed by Cage Cu. Reaction Conditions: Solvent $H_2O$; 0,5mM ligand Cage **Cu-28** : 1mM $CuCl_2$ : 96mM NaBr as supporting electrolyte : 10% v/v Monomer. Reaction time 4h. rt. [a] $E_{app} = E_{1/2} - 120$ mV. [b] $E_{app} = E_{1/2}$.

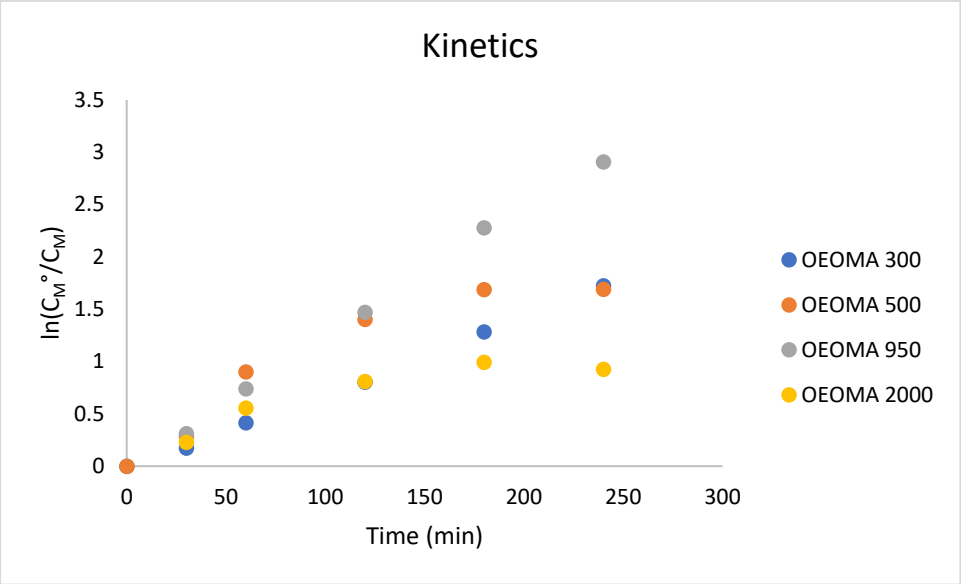


**Figure 44** Polymerization kinetics for OEOMA monomers catalyzed by Cage **Cu-28**, given by the logarithm of the concentration of the monomer over time. $C°_M$: initial concentration of the monomer, $C_M$: monomer concentration at different times.

For all monomers high conversions values were reached meaning that the system has good catalytic properties. As shown in the kinetic profiles in Figure 44, the logarithm of the concentrations of the monomers varies linearly over time for the first 2-3 hours of reaction, which implies a constant generation of radicals. The conversion of $OEOMA_{2000}$ is limited to ca 60% because of the bulky size of the monomer, which reaches cannot polymerize further after reaching a critical size.

Low dispersity values were observed by GPC analysis that highlights efficient activation/deactivation abilities and furthermore, experimental molecular weights of polymers are in accordance with theoretical ones.

### 3.5 Electrochemically activated Atom Transfer Radical Polymerization of OEOMA monomers using $Cu^{II}$/TPMA as catalyst

Copper complexes with **TPMA**-based ligands are among the most active catalyst in ATRP. In particular, $Cu^{II}$/**TPMA** is the best performing catalyst in aqueous media. For this reason, all polymerizations were performed also with $Cu^{II}$/**TPMA** to have a significative comparison of the obtained results.

All electrodes, electrolyte, solvent and reagents, except the initiator, were introduced into the cell, thermostated at 25 °C. After degassing, cyclic voltammetry of $Cu^{II}$/**TPMA** was recorded using Glassy Carbon as WE, to measure the standard reduction potential of the catalyst and select the suitable $E_{app}$ value for each monomer. A second voltammetry was recorded after the addition of the initiator obtaining an irreversible voltammetry with a high anodic current increase (Figure 45).

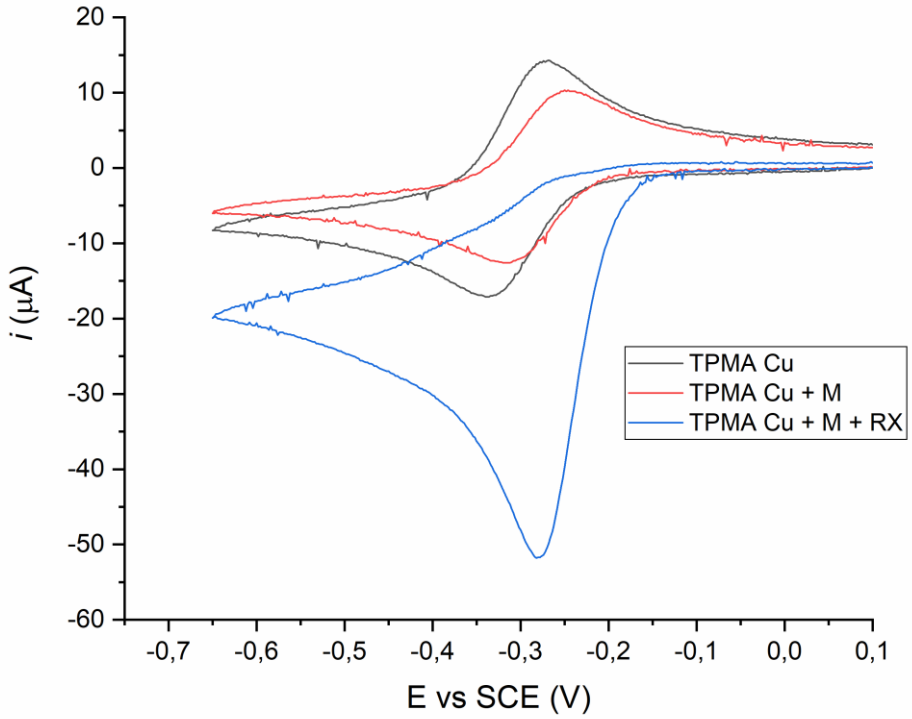


**Figure 45** Cyclic voltammetry of a) 1mM **TPMA** Cu (black line), b) 1 mM **TPMA** Cu + 10% v/v $OEOMA_{950}$ monomer (M) (red line), c) 1mM **TPMA** Cu + 10% v/v $OEOMA_{950}$ monomer + 2 mM HEBiB initiator (RX) (blue line).

The chosen potential was applied for the chronoamperometric experiment using a Platinum mesh as WE under continuous magnetic stirring. Samples were withdrawn

periodically for four hours to determine polymer molecular weight by GPC analysis and conversion via $^1$H-NMR.

All conversions were calculated by $^1$H-NMR integrals of monomer and polymer signals over time using DMSO-$d_6$ as external standard.

| *Entry* | *Monomer* | Conv (%) | $Mn_{th}$ ($10^{-3}$) | $Mn_{exp}$ ($10^{-3}$) | D | Q (C) |
|---|---|---|---|---|---|---|
| *1* | *OEOMA$_{2000}$* | 28 | 30310 | 15005 | 1.13 | 2.23 |
| *2* | *OEOMA$_{950}$* | 60 | 47887 | 33328 | 1.5 | 2.25 |
| *3* | *OEOMA$_{500}$* | 93 | 50406 | 45980 | 1.36 | 1.95 |
| *4* | *OEOMA$_{300}$* | 54 | 27611 | 55146 | 1.38 | 1.81 |

**Table 2** Potentiostatic eATRP of different monomers catalyzed by **TPMA** Cu. Reaction Conditions: Solvent $H_2O$; 1 mM **TPMA** ligand : 1mM $CuCl_2$ : 96mM NaBr as supporting electrolyte : 10% v/v Monomer. Reaction time 4h. rt. $E_{app} = E_{1/2} + 60$ mV.

From the obtained results it was possible to see that using the cage catalyst, higher conversions were obtained for $OEOMA_{2000}$, $OEOMA_{950}$, and $OEOMA_{300}$ and a similar conversion was obtained for $OEOMA_{500}$. Moreover, better dispersity values were obtained using the supramolecular system (Figure 46).

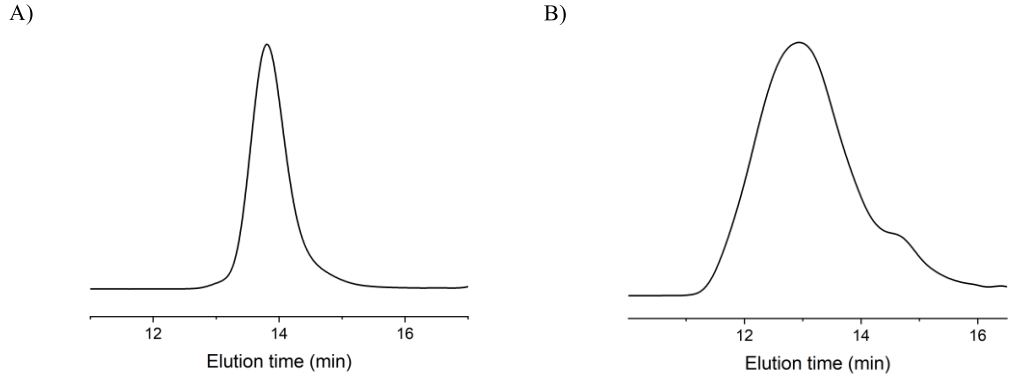


**Figure 46** GPC traces comparison of: eATRP of $OEOMA_{950}$ (10% v/v) in $H_2O$ + 0.1 M NaBr catalyzed by Cage **Cu-28** (A), and eATRP of $OEOMA_{950}$ (10% v/v) in $H_2O$ + 0.1 M NaBr catalyzed by Cu/**TPMA** (B).

Future studies will be carried out in order to explain the higher performances of the cage catalyst.

## 3.6 Electrochemically activated Atom Transfer Radical Polymerization of methacrylic acid using Cage Cu-28 as catalyst

Thanks to the promising results obtained in polymerization reactions with the OEOMA monomers using Cage **Cu-28** as catalyst, and because of the natural acidic pH around 2.5 of the complex, the polymerization of acidic monomers was explored using methacrylic acid.

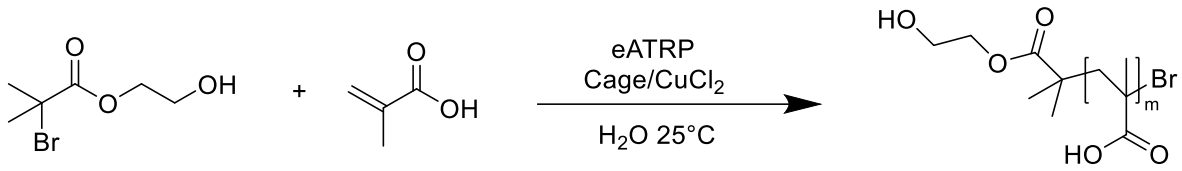


**Scheme 15** General scheme for the electrochemical polymerization of Methacrylic acid monomer catalyzed by Cage **Cu-28**.

Polymerization of acidic monomers is one of the biggest challenges in ATRP because of an intramolecular cyclization reaction that leads to the loss of the C-X chain-end functionality causing the partial termination of the growing polymer chains (Scheme 15). As reported in literature for $Cu^{II}$/**TPMA**, a good strategy to avoid this side-reaction is to lower the pH from neutral pH of **TPMA** up to 0.8 using hydrochloric acid, to reduce the concentration of carboxylate anions.

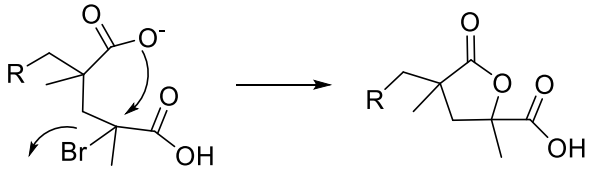


**Scheme 16** Intramolecular cyclization side-reaction of methacrylic acid.

The first polymerization experiment was performed at natural acidic pH of Cage **Cu-28** complex, already much lower than $Cu^{II}$/**TPMA**. Under these conditions, a conversion less than 10% was obtained, and this could be an indication of fast cyclization reaction under these weakly acidic conditions.

In a second attempt, the literature procedure for **TPMA** was followed, lowering the pH of the solution of the cage to 0.8 using HCl. The recorded cyclic voltammetry showed a broad reversible peak couple (Figure 47), indicating that the **Cu-28** catalyst has been degraded by the addition of HCl, resulting in a strong loss of activity. In

support of this hypothesis, knowing that during the synthetic procedure of the cage, HCl is used to decomplex the system, it is possible that the addition of HCl also in this case has led to the same effect. Only 18% of conversion was obtained for the polymerization process. The chain end cyclization was suppressed at this pH, but the catalyst activity was too low to generate high conversions.

To lower the pH without causing the **Cu-28** catalyst decomposition, triflic acid was used obtaining higher conversion values (28%) already at pH 1.1. More in detail, the cyclic voltammetry of the **Cu-28** catalyst after the polymerization remained unchanged, confirming the stability of the system in this reaction conditions.

To have a comparison in the same reaction conditions, a further experiment was performed at pH 0.8 with HOTf. The cyclic voltammetry displayed its typical reversible peak couple meaning that the catalyst is stable even at strongly acidic pH, and 25% of conversion was obtained for the polymerization of methacrylic acid. Despite the conversion was not so high, the kinetics of the reaction was linear even after four hours (Figure 48) indicating that the reaction could be carried out for longer times in order to try to achieve higher conversions. Conversely, the kinetics of the polymerization with HCl completely stopped at 18% conversion after 2 hours.

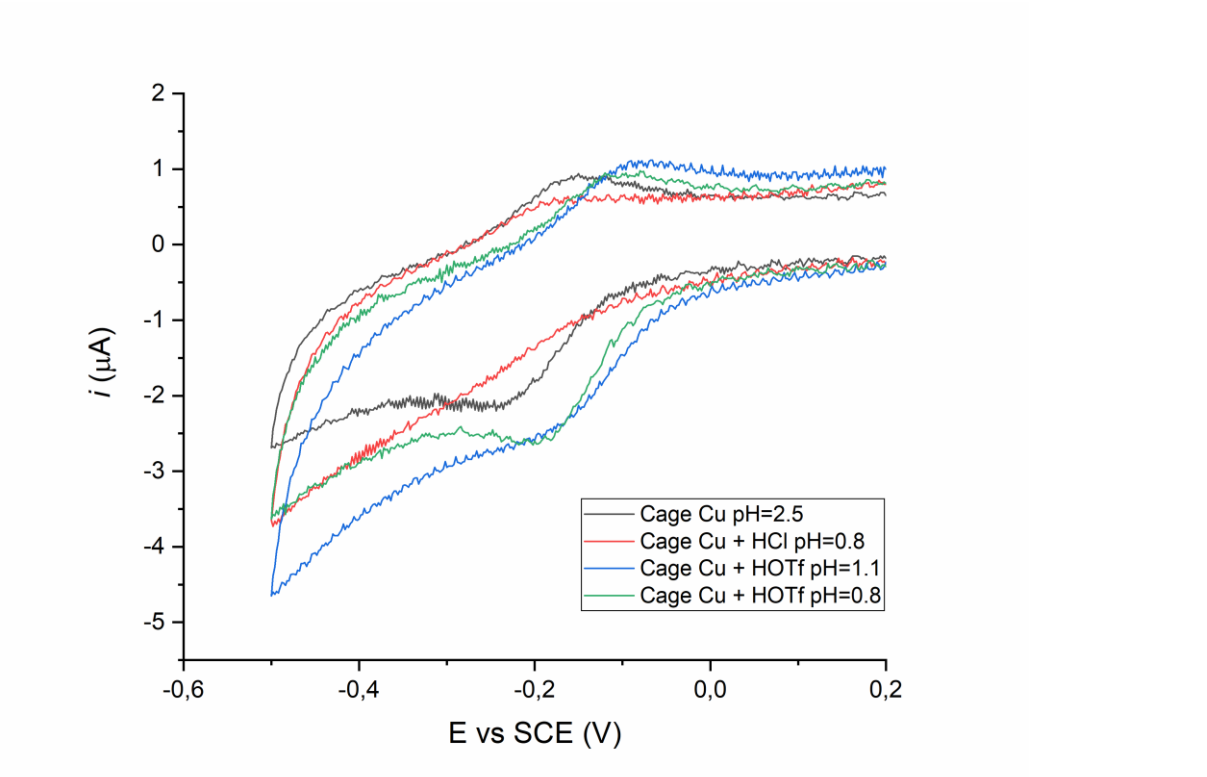


**Figure 47** Cyclic voltammetry at different pH of the solution using triflic and hydrochloric acids.

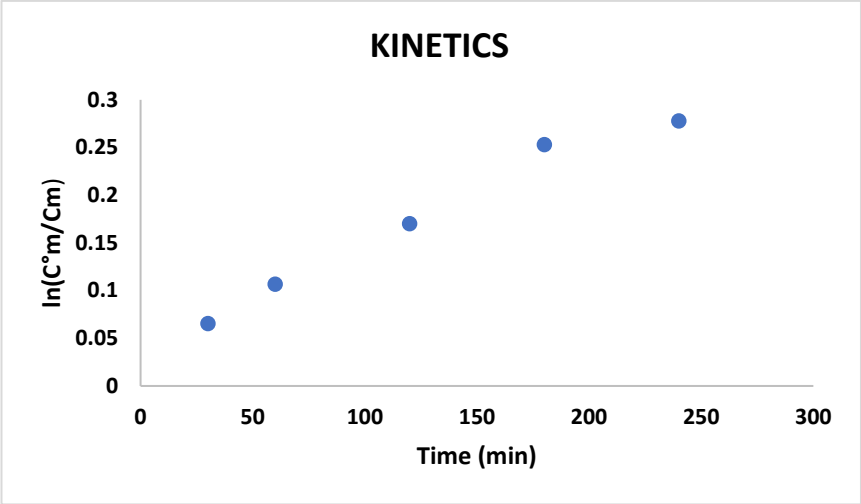


**Figure 48** Linear kinetics for methacrylic acid polymerization using Cage **Cu-28** as catalyst at pH = 0.8.

# 4 CONCLUSIONS

In this thesis, the procedure for the synthesis of a new **TPMA**-based supramolecular Cage **28** was optimized. The new system was complexed with zinc and with copper and relative complexes, **Zn-28** and **Cu-28** respectively, were characterized confirming the formation of the desired products. Catalytic properties of Cage **Cu-28** were investigated, and the system was applied in aqueous electrochemically mediated atom transfer radical polymerization. In particular, the polymerization of OEOMA monomers with different chain lengths, $OEOMA_{2000}$, $OEOMA_{950}$, $OEOMA_{500}$ and $OEOMA_{300}$, was studied. High conversions were obtained, that showed the ability of the system to catalyze the reaction, and small dispersity values, that indicates the efficiency of the activation/deactivation process allowing the formation of polymers with high control over molecular weights. All polymerizations were also compared to the traditional Cu/**TPMA** catalyst, highlighting best performances of the **Cu-28** system in particular as regard the dispersity of the formed polymers.

Furthermore, the **Cu-28** system was applied in the *e*ATRP of methacrylic acid, investigating the influence of different acids (HCl and HOTf) and pHs on the polymerization of acidic monomers. The best reaction conditions turned out to be the use of HOTf to lower the pH of the solution up to 1.1. The natural pH of Cage **Cu-28** solution resulted not acid enough to achieve high conversions, while the use of HCl instead of HOTf led to the degradation of the catalyst.

# 5 EXPERIMENTAL SECTION

## 5.1 General methods

All NMR spectra were recorded at 301 K in Bruker AVIII 600-z grad 5mm, Bruker 400 Avance III BBi-z grad 5mm, Bruker Avance 300 or Avance-DPX 200 MHz instruments. All $^{1}H$ NMR spectra were referenced to residual isotopic impurity of DMSO-$d_6$ (2.50 ppm), $CD_3CN$ (1.94 ppm) or $CDCl_3$ (7.26 ppm). The following abbreviations are used to describe briefly multiplicity of the signals: s=singlet, d=doublet, t=triplet and m=multiplet. Low resolution electrospray ionization mass spectrometry LRMS (ESI-MS) experiments were carried out in positive mode with Agilent Technologies LC/MSD Trap SL AGILENT instrument (mobile phase acetonitrile/0.1 % formic acid) with the following settings: Nebulizer = 15 psi, Dry gas = 5 L/min, Dry Temp = 325°C. The NMR and ESI-MS data were processed using MestReNova 10.0.2. Kinetic data were processed using OriginPro 2018. CVs were performed either by an Autolab PGSTAT30 potentiostat (Eco-Chimie, Utrecht, The Netherlands) interfaced to a PC running GPES 4.9 software, or a PARC 173 potentiostat. Gel permeation chromatography (Gel Permeation Chromatography, GPC, Agilent 1260 Infinity) has been used to determine the mean molecular weights and dispersions of polymers obtained via eATRP. The instrument is equipped with two columsn (Agilent PLgel 5µm MIXED-C 300 x 7.5 mm) with stationary phase consisting of a styrene-divinilbenzene lattice, and a universal refractive index detector (RID). For the analysis of the polymer samples the eluent used is a 10 mM LiBr solution in DMF, with a flow of 1 ml/min; the columns are thermostated to 70 ºC, while the temperature of RID is 50 ºC. The system has been calibrated using 12 standard linear PMMA samples (Agilent EasiVial) with Mn between 540 and 2210000. Chemicals were purchased from Aldrich or Fluorochem and used without further purification.

## 5.2 Synthesis of tris-functionalized TPMA based molecules

### 5.2.1 Synthesis of Tris(5-Bromopyridil)-Methylamine

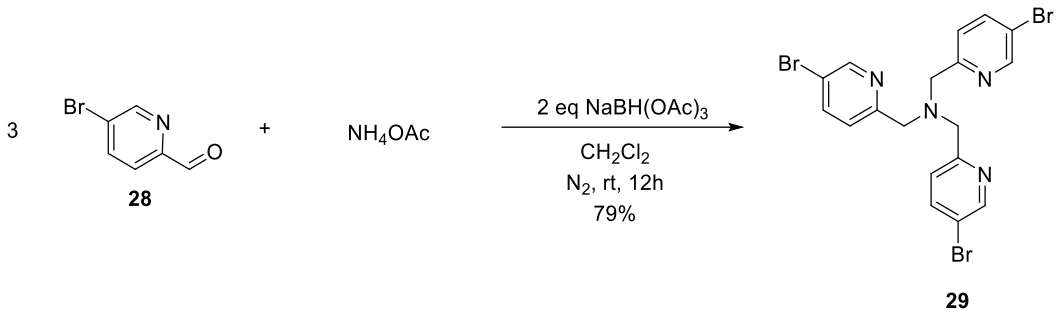


In a 250 ml double neck flask, anhydrous $NH_4OAc$ (1.38 g, 17.9 mmol) and 5-bromo-2-pyridinecarboxaldehyde **28** (10.00 g, 53.7 mmol) were dissolved in dry $CH_2Cl_2$ (170 mL) under $N_2$ and left under stirring for 1 hour. Three aliquots of $NaBH(OAc)_3$ (3.80 g, 17.9 mmol) were added waiting one hour between each addition. After that, the reaction was stirred for 12 hours at room temperature. The solvent was removed under reduced pressure. The resulting white solid was dissolved in AcOEt and the solution extracted with 0.1 M solution of KOH (3x100 ml). The organic phases were dried on anhydrous $MgSO_4$ and the solvent was removed under reduced pressure. The resulting solid was precipitated by crystallization from THF/hexane to yield a white solid (7.43 g, 79%).

*$^1$H-NMR (300 MHz, $CDCl_3$)* δ (ppm): 8.60 (d, 3H, *J* = 2.0 Hz, ArH),7.78 (dd, 3H, *J* = 2.0 Hz, *J* = 8.0 Hz, ArH), 7.41 (d, 3H, *J* = 8.0 Hz, ArH), 3.81 (s, 6H, $CH_2$).

*(ESI-MS)* (m/z): $[M+H]^+$ calculated for $[C_{18}H_{15}Br_3N_4+H]^+$ = 524.89; found = 524.88

### 5.2.2 General procedure for the synthesis of ligand 29

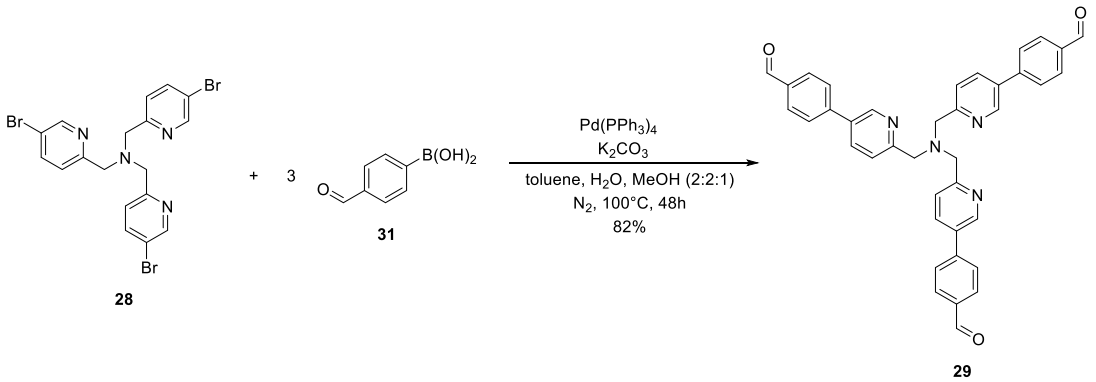


In a Schlenk apparatus a mixture of **28** (3.00 g, 5.69 mmol), 4-formylphenylboronic acid **31** (3.84 g, 25.6 mmol), $Pd(PPh_3)_4$ (65 mg, 0,0057 mmol, 1 mol%) and $K_2CO_3$ (5.51 g, 39.8 mmol) was dissolved in 60 ml of $H_2O$/toluene/$CH_3OH$ (1:1:0.5). The mixture was stirred under $N_2$ for 48 hours at 100°C. The solvent was removed under reduced pressure. The resulting yellow oil was dissolved in $CHCl_3$ and the solution extracted with $H_2O$ (3x50 mL). The organic phases were dried on anhydrous $MgSO_4$, filtered on celite and then the solvent was removed under reduced pressure. The resulting solid **29** was precipitated by crystallization from THF/hexane to obtain a pale yellow solid (2.89 g, 82%).

*$^1$H-NMR (300 MHz, $CDCl_3$)* δ (ppm): 10.11 (s, 3H, CHO), 8.89 (d, 3H, *J* = 2.0 Hz, PyrH), 8.02 (dd, 3H, *J* = 8.0 Hz, *J*= 2.0 Hz, PyrH), 7.97 (d, 6H, *J* = 8.25 Hz, ArH), 7.83 (d, 6H, *J* = 8.25 Hz, ArH), 7.72 (d, 3H, *J* = 8.0 Hz, PyrH), 4.09 (s, 6H, $CH_2$).

*(ESI-MS)* (m/z): $[M+H]^+$ calculated for $[C_{39}H_{30}N_4O_3+H]^+$ = 603.23; found = 603.24.

### 5.2.3 General procedure for the synthesis of the Complex TPMA•Zn

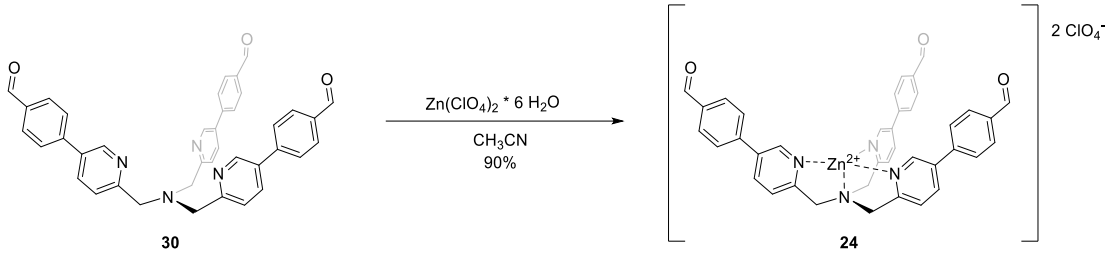


30 24

To a suspension of ligand **30** (100 mg, 0.17 mmol) in acetonitrile (15 ml), zinc (II) perchlorate hexahydrate was added (40.5 mg, 0.17 mmol). The solution was stirred at room temperature for 1 hour and the reaction was followed by $^{1}$H-NMR and ESI-MS. At the end of the reaction diethyl ether (25 ml) was added obtaining quantitatively a crystalline solid, then centrifuged and dried. Complex **24** results as a pale yellow solid (128 mg, 90%).

*$^{1}$H-NMR (400 MHz, $D_2O$)* δ (ppm): 8.74 (d, *J* = 2.2 Hz, 6H, PyrH), 8.28 (dd, *J* = 8.3, 2.2 Hz, 6H, PyrH), 7.72 (d, *J* = 8.3 Hz, 6H, PyrH), 7.49 (d, *J* = 8.1 Hz, 12H, ArH), 7.38 (d, *J* = 8.1 Hz, 12H, ArH), 5.26 (s, 12H, $CH_2$ amine TPMA), 4.40 – 4.22 (m, 12H, $CH_2$ TPMA )

### 5.2.4 Synthesis of Cage 28

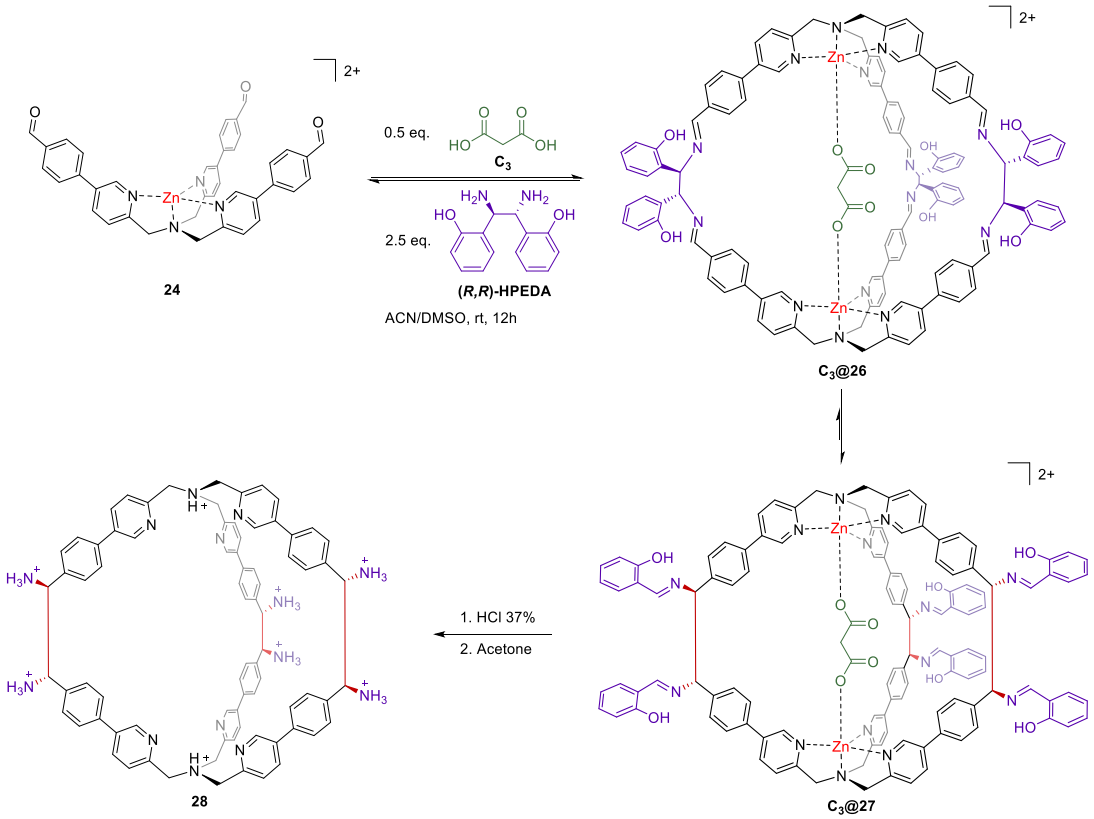


To 30 ml (60 µmol) of a solution 0.002 M of complex **24** in $CH_3CN$, 3 ml (30 µmol) of a solution 0.01 M of malonic acid in $CH_3CN$ and 7.5 ml (150 µmol) of a solution 0.02 M of 1,2-diphenylethylenediamine in $CH_3CN$/DMSO were added. The mixture was left reacting for 12 hours at room temperature. After having removed $CH_3CN$ by evaporation, the product, still dissolved in DMSO, was treated with 3 ml of concentrated HCl 37% and stirred for 1 hour. Then, 50 mL of acetone were added to the solution, leading to the quantitative precipitation of a crystalline solid, which was subsequently centrifuged, dried and checked via $^1$H-NMR. Product **28** results as a pale yellow solid (80.8 mg, 90% yield).

$^{1}$*H-NMR (400 MHz, D2O)* δ (ppm): 8.74 (d, *J* = 2.2 Hz, 6H, PyrH), 8.28 (dd, *J* = 8.3, 2.2 Hz, 6H, PyrH), 7.72 (d, *J* = 8.3 Hz, 6H, PyrH), 7.49 (d, *J* = 8.1 Hz, 12H, ArH), 7.38 (d, *J* = 8.1 Hz, 12H, ArH), 5.26 (s, 12H, $CH_2$ ammine TPMA), 4.40 – 4.22 (m, 12H, $CH_2$ TPMA ).

### 5.2.5 Complexation of the stable Cage 28 with Zn

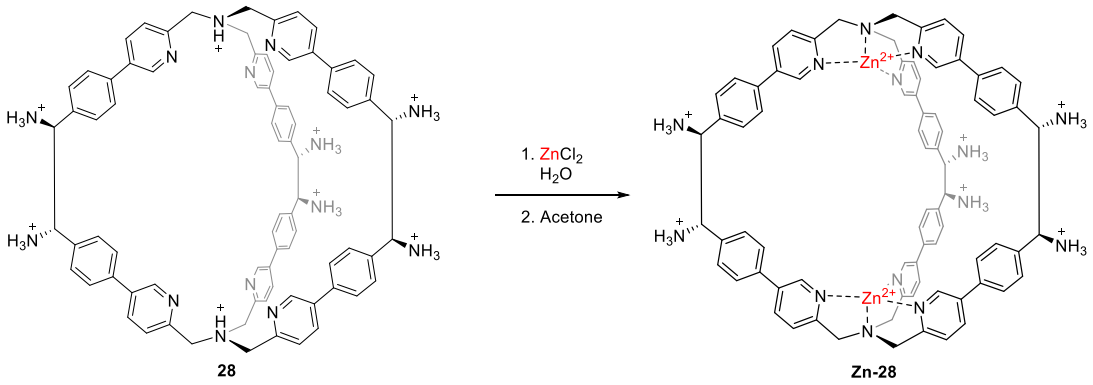


To a solution of cage **28** (25 mg, 0.013 mmol) in water (5 ml), 5 mg (0.026 mmol) of $ZnCl_2$ were added. The solution was stirred at room temperature for 1 hour and the reaction was followed by $^1$H-NMR and ESI-MS. At the end of the reaction acetone (50 ml) was added obtaining quantitatively a crystalline solid, that was subsequently centrifuged and dried.

*$^1$H-NMR (400 MHz, D2O)* δ (ppm): 9.28 (d, *J* = 2.1 Hz, 6H, PyrH), 8.32 (dd, *J* = 8.3, 2.1 Hz, 6H, PyrH), 7.80 (d, *J* = 8.1 Hz, 6H, ArH), 7.69 (d, *J* = 8.2 Hz, 6H, PyrH), 7.26 (d, J = 8.0 Hz, 6H, Pyr), 5.09 (s, 6H, CH amine), 4.47 – 4.17 (m, 12H, $CH_2$TPMA)

*(ESI-MS)* (m/z): $[M]^{2+}$ calculated for $[C_{39}H_{30}N_4O_3Zn_2]^{2+}$ = 706.3; found = 706.2.

### 5.2.6 Complexation of the stable Cage 28 with Cu

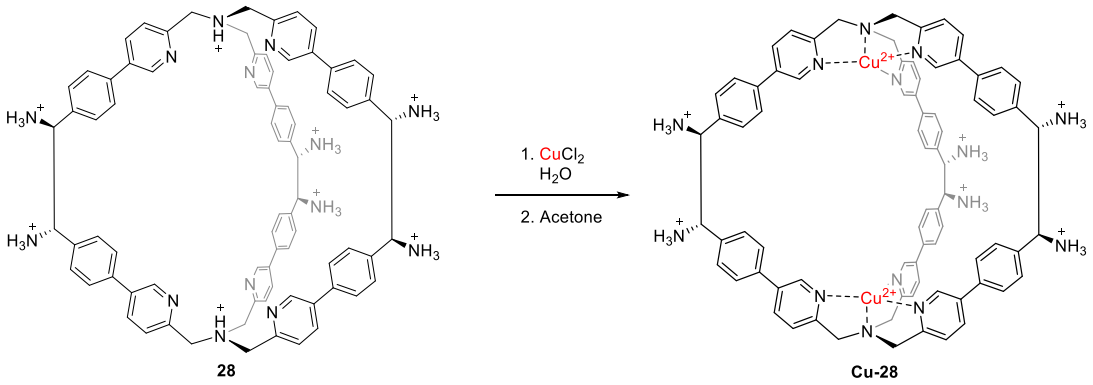


14 mg (0.026 mmol) of $CuCl_2$ were added to a solution of cage **28** (25 mg, 0.013 mmol) in water (5 ml). The solution was stirred at room temperature for 1 hour and the reaction was followed by ESI-MS. At the end of the reaction acetone (50 ml) was added obtaining quantitatively a crystalline solid, that was subsequently centrifuged and dried.

*(ESI-MS)* (m/z): $[M+H]^{2+}$ calculated for $[C_{39}H_{30}N_4O_3Cu_2]^{2+}$ = 704.6; found = 700.2.

### 5.3 Electrochemical titration of Cage 28 with $CuCl_2$

For the electrochemical titration experiment of Cage **28** with $CuCl_2$ a three electrodes setup was used with a Glassy carbon (3 mm diameter) as WE, a graphite rod separated from the WE compartment by a glass frit as CE and a standard saturated calomel as RE. First cyclic voltammetries (CVs) of the cage were recorded in 5 mL of water using 8.25 mg (0.5 mM, 2.5 μmol) of Cage **28** in the absence of copper, only using 0.108 g (0.1 M, 49 mmol) of tetraethylammonium tetrafluoroborate ($Et_4NBF_4$) as supporting electrolyte. Then, other cyclic voltammetries were recorded after the addition of 10 μL aliquots of a 0.1 M solution of $CuCl_2$ up to a total volume of Cu of 30 μL. At this point, 5 μL aliquots were added up to a total Cu volume of 65 μL, in order to be more precise in the determination of the point corresponding to the calculated stoichiometric ratio

1:2 of Cage **28** : Cu. After each addition the solution was degassed and left under vigorous magnetic stirring for about 10 minutes and then the voltammetries were recorded in a quite environment.

| *Entry* | *$V_{tot}$ $CuCl_2$ (mL)* | *$CuCl_2$ equiv.* | *$CuCl_2$ mmol* |
|---|---|---|---|
| *1* | 10 | 0.4 | 1 |
| *2* | 20 | 0.8 | 2 |
| *3* | 30 | 1.2 | 3 |
| *4* | 35 | 1.4 | 3.5 |
| *5* | 40 | 1.6 | 4 |
| *6* | 45 | 1.8 | 4.5 |
| *7* | 50 | 2 | 5 |
| *8* | 55 | 2.2 | 5.5 |
| *9* | 60 | 2.4 | 6 |
| *10* | 65 | 2.6 | 6.5 |

## 5.4 Cyclic voltammetries at different scan rates

A 4 mL water solution containing 1 mM of Cage **28** (13.2 mg, 4 μmol), 2 mM of $CuCl_2$ (1.1 mg, 8 μmol) and 0.2 M of NaBr (82 mg, 0.8 mmol) was analyzed by cyclic voltammetries at different scan rates starting from a scan rate of 20 mV/s up to 1000 mV/s in order to calculate the diffusion coefficient (D) and hydrodynamic radius ($R_{hyd}$). The electrochemical cell was equipped with a Glassy carbon as working electrode, a graphite rod separated from the WE compartment by a glass frit as counterelectrode and a standard saturated calomel as reference. With the values of $I_p$ obtained for each trial, a graph was made as a function of the corresponding scan rate.

| *Entry* | *Scan rate (mV)* | *$I_{pc}$ (mA)* |
|---|---|---|
| *1* | 20 | -1.17 |
| *2* | 50 | -1.33 |
| *3* | 100 | -1.70 |
| *4* | 200 | -2.43 |
| *5* | 500 | -4.37 |
| *6* | 1000 | -6.90 |

## 5.5 Cyclic voltammetries at different concentrations of the catalyst

The same solution and setup were used to perform cyclic voltammetries decreasing the concentration of the **Cu-28** catalyst starting from 1 mM **28** and 2 mM $CuCl_2$, up to 0.0625 mM of cage **28** and 0.125 mM $CuCl_2$. After each voltammetry, 2 mL of solution were removed from the electrochemical cell and 2 mL of $H_2O$ were added in order to halve the concentration of the catalyst. To keep the concentration of the supporting electrolyte constant at 2 mM for all voltammetries, 79 mg of NaBr were added after each diluition.

| *Entry* | *Cu-28 conc (mM)* | *$I_{pc}$ (mA)* |
|---|---|---|
| *1* | 1 | -2.47 |
| *2* | 0.5 | -1.86 |
| *3* | 0.25 | -1.71 |
| *4* | 0.125 | -0.73 |

## 5.6 Cyclic Voltammetry

All experiments were conducted in collaboration with Prof. Abdirisak Ahmed Isse and Dr. Marco Fantin in our department. For the setup of the reaction a 5-neck electrochemical cell was used, equipped with three electrodes.

*Working electrode (WE):* Glassy Carbon (GC) disc (3 mm diameter) was employed as working electrode for cyclic voltammetry. GC is commonly used because of its low electrical resistance and adsorption coefficient that prevents the adsorption of molecules on its surface, reducing the risk of electrode passivation and the corresponding drop in active area.

*Counter electrode (CE):* the electrode was a graphite rod separated from the WE compartment by using a glass frit and a layer of methylcellulose gel saturated with 0.1 M *n*-$Bu_4NBF_4$ in dimethylformamide (DMF).

*Reference electrode (RE):* an Ag/AgI/ *n*-$Bu_4NI$ was used as reference; it was prepared using an Ag thread and a glass frit with methylcellulose gel saturated with a solution of 0.1 M *n*-$Bu_4NI$ in DMF.

All experiments were conducted in 7.2 mL of water as solvent using NaBr 0.1 M as supporting electrolyte. The environment into the cell was well deoxygenated through

a continuous nitrogen flow, thermostated at 25 °C and the solution stirred with a magnetic bar.

### 5.6.1 General procedure for the study of oligo (ethylene glycol) methyl ether methacrylate (OEOMA) monomers polymerization catalyzed by Cu-28 complex

#### 5.6.1.1 Cyclic voltammetry of the Cu-28 complex

Redox properties of Cage **Cu-28** were investigated in water by cyclic voltammetry (CV). The ligand **28** was complexed in situ with a solution 0.1 M $CuCl_2$ in a 1:2 Cage **28** : $CuCl_2$ stoichiometric ratio. After setting up the electrochemical cell with the three electrodes, 13.2 mg (0.5 mM, 4 µmol) of the ligand Cage **28** were added to a solution 0.1 M of NaBr (79 mg, 0.8 mmol) in water (7.2 mL) and complexed with 80 µL (1 mM, 8 µmol) of a solution 0.1 M of $CuCl_2$. The solution was deoxygenated and stirred for 30 minutes and then a cyclic voltammetry was recorded in a quite environment (i.e. unstirred solution) allowing the process to be diffusion-controlled.

The voltammetry was recorded at a scan rate of 200 mV/s and potential range of 700 mV to 0 mV vs Ag/AgI.

#### 5.6.1.2 Cyclic voltammetry in the presence of the monomer

A second cyclic voltammetry was recorded for each experiment after the addition of 0.8 mL (10 % v/v) of monomer. The experimental parameters were kept constant and the solution was stirred and degassed for 5 minutes before recording. A reversible peak couple corresponding to one electron transfer was observed for the Cu catalyst in each monomer. From the values of $E_{pc}$ and $E_{pa}$, cathodic and anodic peak potentials respectively, the half-wave potential ($E_{1/2}$) was calculated in order to choose the suitable potential to apply ($E_{app}$) for the polymerization of each type of monomer.

$E_{1/2} = (E_{pc} + E_{pa}) / 2$

The monomers chosen are oligo (ethylene glycol) methyl ether methacrylate (OEOMA) with different chain lengths.

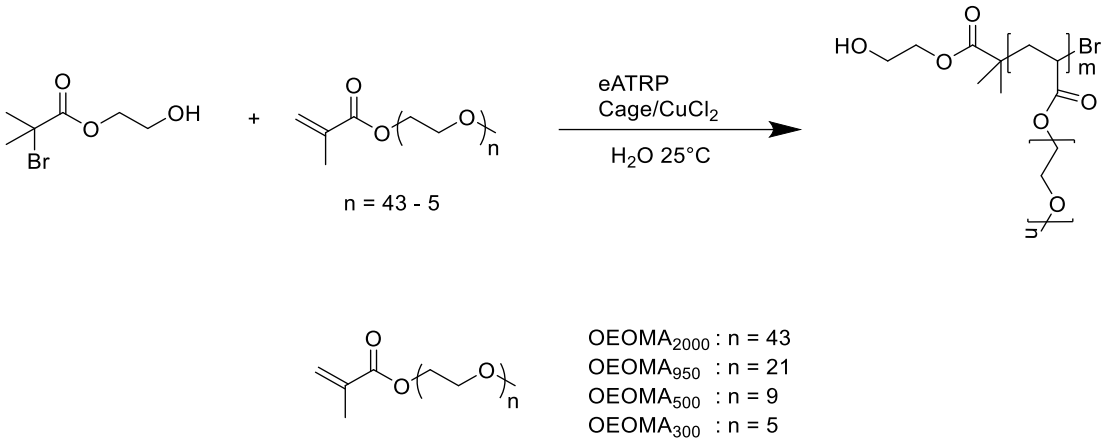


*OEOMA$_{2000}$:* Before being used the monomer was passed on basic alumina to remove the inhibitor. 0.8 mL (0.054 M, 0.4 mmol) were added to the solution. From the cyclic voltammetry recorded, the values of $E_{pc}$ and $E_{pa}$ were obtained and $E_{app}$ was therefore chosen.

$E_{1/2}$ = (302.1 mV + 456.6 mV) / 2 = 379.35 mV vs Ag/AgI

$E_{app} = E_{1/2}$ – 120 mV = 379.35 mV – 120 mV = 259.35 mV vs Ag/AgI

*OEOMA$_{950}$:* Before being used the monomer was dissolved in THF and passed over basic alumina, then precipitate with hexane and filtered on buchner to remove the inhibitor. 0.88 g (0.116 M, 0.9 mmol) of the solid monomer were added to the solution. From the cyclic voltammetry recorded, the values of $E_{pc}$ and $E_{pa}$ were obtained and $E_{app}$ was therefore determined:

$E_{app} = E_{1/2}$ = (225.8 mV + 418.0 mV) / 2 = 320.0 mV vs Ag/AgI

*OEOMA$_{500}$:* Before being used the monomer was passed on basic alumina to remove the inhibitor. 0.8 mL (0.216 M, 1.7 mmol) were added to the solution. From the cyclic voltammetry recorded, the values of $E_{pc}$ and $E_{pa}$ were obtained and $E_{app}$ was therefore chosen.

$E_{1/2}$ = (362.0 mV + 543.0 mV) / 2 = 452.0 mV vs Ag/AgI

$E_{app}$ = $E_{1/2}$ – 120 mV = 452.0 mV – 120 mV = 332.0 mV vs Ag/AgI

*OEOMA$_{300}$:* Before being used the monomer was passed on basic alumina to remove the inhibitor. 0.8 mL (0.054 M, 0.4 mmol) were added to the solution. From the cyclic

voltammetry recorded, the values of $E_{pc}$ and $E_{pa}$ were obtained and $E_{app}$ was therefore determined:

$E_{app} = E_{1/2}$ = (376.0 mV + 205.0 mV) / 2 = 290.0 mV vs Ag/AgI

#### 5.6.1.3 Cyclic voltammetry in the presence of the initiator

Another cyclic voltammetry was recorded after the addition of the polymerization initiator, keeping a potential range of 700 mV to 0 mV vs Ag/AgI and a scan rate of 200 mV/s. Even in this case, the solution was stirred and degassed for 5 minutes before recording.

2-hydroxyethyl 2-bromoisobutyrate (HEBiB) was chosen as initiator and 2.5 µL (2 mM, 16 µmol) were added to the solution containing **Cu-28** complex and the monomer. The process can be described by the following electrocatalytic cycle:

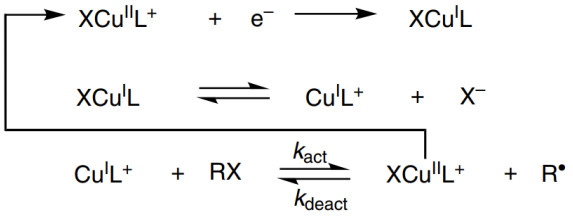


The $XCu^{II}L^+$ complex is reduced to $XCu^{I}L$ at the WE, after which it can partially dissociate to $Cu^{I}L^+$, the ATRP activator complex. $Cu^{I}L^+$ quickly reacts with the alkyl halide to for a radical and to reform $XCu^{II}L^+$, closing the catalytic cycles.

In all cases, is it possible to see an enhancement of the cathodic current and the disappearance of the anodic peak, corresponding to the reoxidation of Cu(I) to Cu(II), indicating the fast activation of RX and the beginning of the polymerization process.

### 5.6.2 Polymerization of OEOMA monomers using Cu-28 as catalyst

The 7.2 mL water solution containing 0.5 mM of Cage **28** ligand, 1 mM of $CuCl_2$, 0.1 M of NaBr, 10% v/v of monomer and 2 mM of HEBiB was used for the polymerization processes. The 5-neck electrochemical cell was equipped with 3 electrodes.

*Working electrode (WE):* platinum mesh electrode was used (area ca. 10 $cm^2$). Before every polymerization the electrode was subjected to a cleaning and activation process, consisting of 100-200 scanning cycles (speed 0.2 $Vs^{-1}$) between the potentials -0.65 V and 0.6 V vs SCE (saturated calomel electrode) in a 0.5 M solution sulphuric acid in bi-distilled water.

*Counter electrode (CE):* the electrode was a graphite rod separated from the WE compartment by using a glass frit and a layer of methylcellulose gel saturated with 0.1 M *n*-$Bu_4NBF_4$ in dimethylformamide (DMF).

*Reference electrode (RE):* Ag/AgI/ *n*-$Bu_4NI$ was used as reference, glass frit with methylcellulose gel saturated with a solution of 0.1 M *n*-$Bu_4NI$ in DMF.

The environment into the cell was well deoxygenated through a continuous nitrogen flow, thermostated at 25 °C and the solution stirred with a magnetic bar throughout the duration of the reaction. For each polymerization an appropriate $E_{app}$ was applied at the WE and the process was followed for 4 hours and during the process, periodic sampling of the solution in the cell was carried out using a single-use syringe previously degassed with nitrogen flow. The sample taken before starting the polymerization (t = 0) was analyzed only by 600 MHz $^1$H-NMR for the determination of the conversion. The other samples were taken after t = 30, 60, 120, 180 and 240 min and were properly treated and analyzed by 600 $^1$H-NMR and gel permeation chromatography (GPC).

*$^1$H-NMR NMR analysis:* 50 µL of solution were taken from the reaction mixture and diluted with 400 µL of Deuterium oxide ($D_2O$) and 30 µL (0.01 M) solution of DMSO in $D_2O$ as internal standard.

*GPC analysis:* The samples for GPC analysis were diluted with a 10 mM LiBr solution in DMF and then filtered through a neutral alumina layer and a 0.2 µm porosity PTFE filter (VWR) to eliminate the catalyst present in the sample and any other particle that could damage the column.

The degree of polymerization (DP) was calculated using the formula:

DP = [Monomer] / [Initiator]

The Theoretical Molecular weight ($Mn_{th}$) was calculated using the formula:

$Mn_{th} = MM_{Monomer} \times DP) + MM_{Initiator}$

| ***Entry*** | ***Monomer*** | **$DP_{target}$** | **$Mn_{th}$** |
|---|---|---|---|
| ***1*** | *$OEOMA_{2000}$* | 27 | 54211 |
| ***2*** | *$OEOMA_{950}$* | 58 | 55311 |
| ***3*** | *$OEOMA_{500}$* | 108 | 54211 |
| ***4*** | *$OEOMA_{300}$* | 170 | 51211 |

*$OEOMA_{2000}$:*

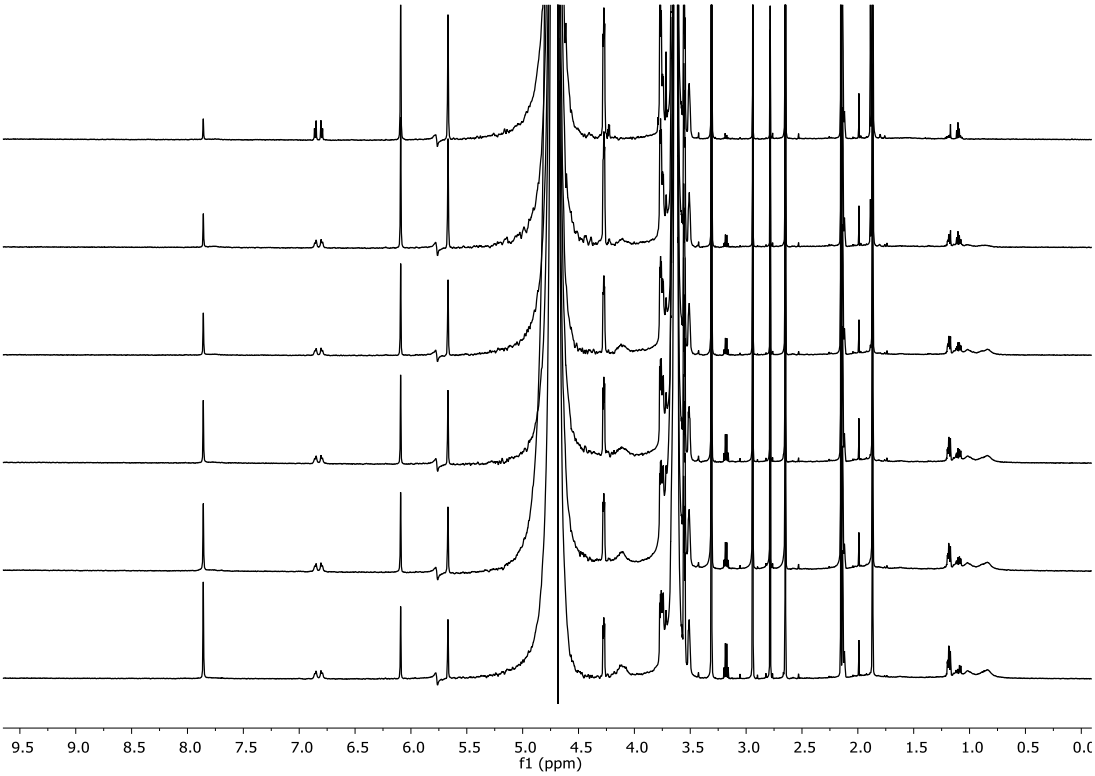


**Figure 49** 600 MHz $^1$H-NMR spectra stacking for the polymerization reaction of $OEOMA_{2000}$ monomer catalyzed by **Cu-28**. From top to bottom spectra recorded at time = 0, 30min, 1 hour, 2 hours, 3 hours and 4 hours. Integrals corresponding to the monomer, 6.10 ppm and 5.67 ppm signals, and polymer, signals between 1.3-0.7 ppm, have been used to determine the conversion. Integrals are referred to the internal standard DMSO-$d_6$ signal at 2.67 ppm.

*OEOMA$_{950}$:*

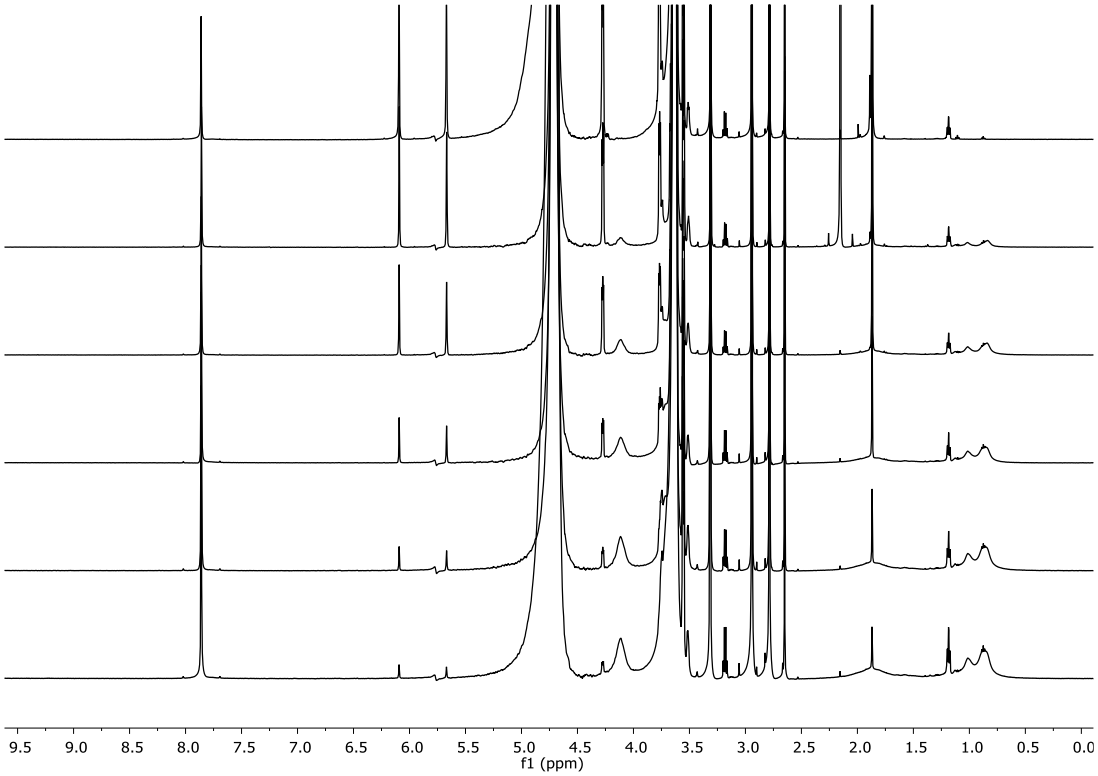


**Figure 50** 600 MHz $^{1}$H-NMR spectra stacking for the polymerization reaction of OEOMA$_{950}$ monomer catalyzed by **Cu-28**. From top to bottom spectra recorded at time = 0, 30min, 1 hour, 2 hours, 3 hours and 4 hours. Integrals corresponding to the monomer, 6.10 ppm and 5.67 ppm signals, and polymer, signals between 1.3-0.7 ppm, have been used to determine the conversion. Integrals are referred to the internal standard DMSO-$d_6$ signal at 2.67 ppm.

*OEOMA$_{500}$:*

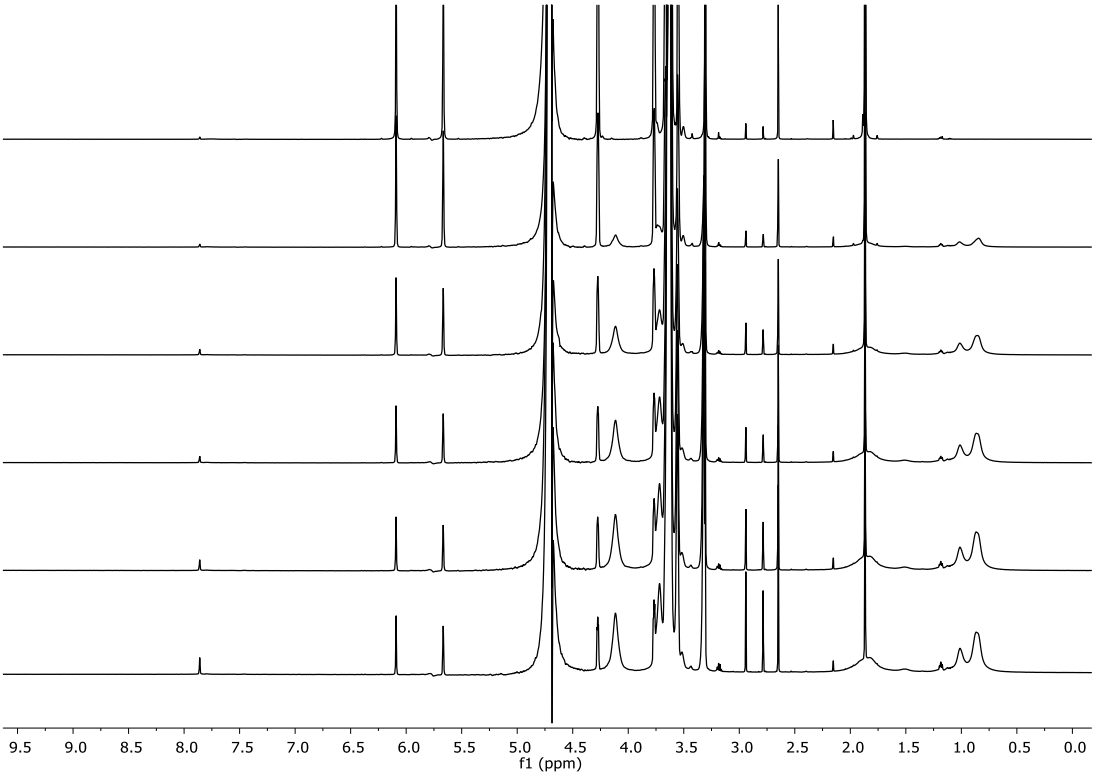


**Figure 51** 600 MHz $^1$H-NMR spectra stacking for the polymerization reaction of OEOMA$_{500}$ monomer catalyzed by **Cu-28**. From top to bottom spectra recorded at time = 0, 30min, 1 hour, 2 hours, 3 hours and 4 hours. Integrals corresponding to the monomer, 6.10 ppm and 5.67 ppm signals, and polymer, signals between 1.3-0.7 ppm, have been used to determine the conversion. Integrals are referred to the internal standard DMSO-$d_6$ signal at 2.67 ppm.

OEOMA$_{300}$:

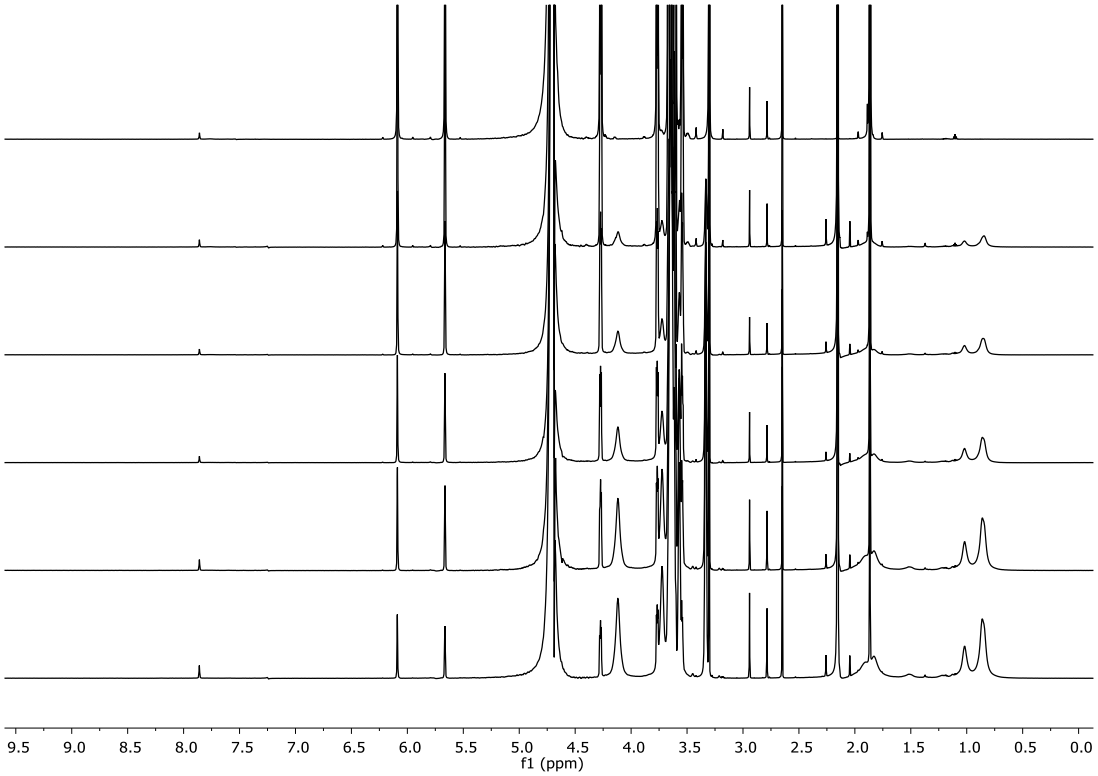


**Figure 52** 600 MHz $^{1}$H-NMR spectra stacking for the polymerization reaction of OEOMA$_{300}$ monomer catalyzed by **Cu-28**. From top to bottom spectra recorded at time = 0, 30min, 1 hour, 2 hours, 3 hours and 4 hours. Integrals corresponding to the monomer, 6.10 ppm and 5.67 ppm signals, and polymer, signals between 1.3-0.7 ppm, have been used to determine the conversion. Integrals are referred to the external standard DMSO-$d_6$ signal at 2.67 ppm.

### 5.6.3 General procedure for the study of oligo (ethylene glycol) methyl ether methacrylate (OEOMA) monomers polymerization catalyzed by Cu/TPMA complex

#### 5.6.3.1 Cyclic voltammetry of the $Cu^{II}$/TPMA complex

Redox properties of **Cu/TPMA** were investigated in water by cyclic voltammetry (CV). The **TPMA** ligand was complexed in situ with a solution 0.1 M $CuCl_2$ in a 1:1 **TPMA** : $CuCl_2$ stoichiometric ratio. After setting up the electrochemical cell with the three electrodes, 2.32 mg (1 mM, 8 µmol) of the **TPMA** ligand were added to a solution 0.1 M of NaBr (79 mg, 0.8 mmol) in water (7.2 mL) and complexed with 80 µL (1 mM, 8 µmol) of a solution 0.1 M of $CuCl_2$. The solution was deoxygenated and stirred for 30 minutes and then a cyclic voltammetry was recorded in a quite environment (i.e. unstirred solution) allowing the process to be diffusion-controlled.
The voltammetry was recorded at a scan rate of 200 mV/s and potential range of 500mV to -100 mV vs Ag/AgI.

#### 5.6.3.2 Cyclic voltammetry in the presence of the monomer

A second cyclic voltammetry was recorded for each experiment after the addition of 0.8 mL (10 % v/v) of monomer. The experimental parameters were kept constant and the solution was stirred and degassed for 5 minutes before recording. A reversible peak couple corresponding to one electron transfer was observed for each monomer. From the values of $E_{pc}$ and $E_{pa}$, cathodic and anodic peak potentials respectively, the half-wave potential ($E_{1/2}$) was calculated in order to choose the suitable potential to apply ($E_{app}$) for the polymerization of each type of monomer.

$E_{1/2} = (E_{pc} + E_{pa}) / 2$

The monomers chosen are oligo (ethylene glycol) methyl ether methacrylate (OEOMA) with different chain lengths.

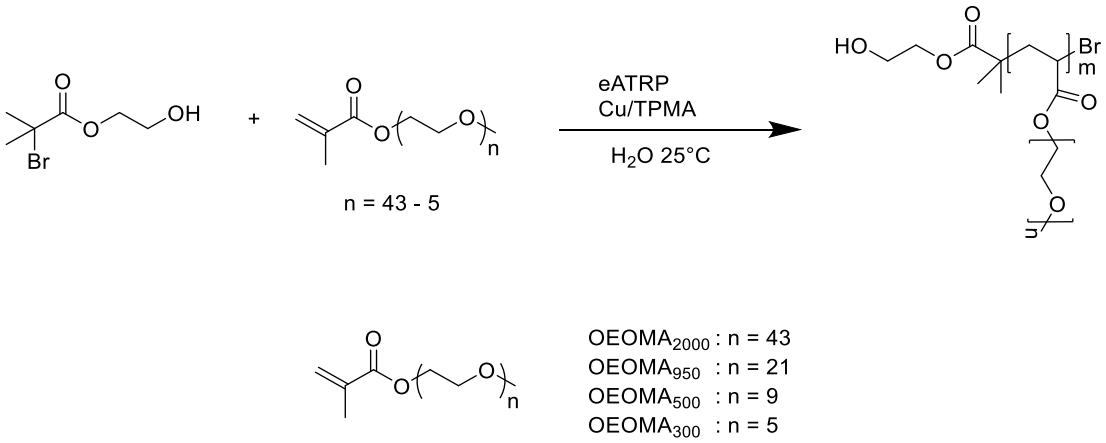


*OEOMA$_{2000}$:* After removing the inhibitor, 0.8 mL (0.054 M, 0.4 mmol) were added to the solution. From the cyclic voltammetry recorded, the values of $E_{pc}$ and $E_{pa}$ were obtained and $E_{app}$ was therefore chosen.

$E_{app} = E_{1/2}$ = [(157.3 mV + 278.3 mV) / 2 ] + 60 mV = 278 mV vs Ag/AgI

*OEOMA$_{950}$:* After removing the inhibitor. 0.88 g (0.116 M, 0.9 mmol) of the solid monomer were added to the solution. From the cyclic voltammetry recorded, the values of $E_{pc}$ and $E_{pa}$ were obtained and $E_{app}$ was therefore determined.

$E_{app} = E_{1/2}$ = [(175.0 mV + 253.0 mV) / 2] + 60 mV = 274.0 mV vs Ag/AgI

*OEOMA$_{500}$:* after removing the inhibitor. 0.8 mL (0.216 M, 1.7 mmol) were added to the solution. From the cyclic voltammetry recorded, the values of $E_{pc}$ and $E_{pa}$ were obtained and $E_{app}$ was therefore chosen.

$E_{app} = E_{1/2}$ = [(208.0 mV + 280.0 mV) / 2] + 60 mV = 304.0 mV vs Ag/AgI

*OEOMA$_{300}$:* After removing the inhibitor. 0.8 mL (0.340 M, 2.7 mmol) were added to the solution. From the cyclic voltammetry recorded, the values of $E_{pc}$ and $E_{pa}$ were obtained and $E_{app}$ was therefore determined.

$E_{app} = E_{1/2}$ = [(207.0 mV + 267.0 mV) / 2] + 60 mV = 297.0 mV vs Ag/AgI

#### 5.6.3.3 Cyclic voltammetry in the presence of the initiator

Another cyclic voltammetry was recorded after the addition of the polymerization initiator, keeping a potential range of 500 mV to -100 mV and a scan rate of 200 mV/s. Even in this case, the solution was stirred and degassed for 5 minutes before recording. 2-hydroxyethyl 2-bromoisobutyrate (HEBiB) was chosen as initiator and 2.5 μL (2 mM, 16 μmol) were added to the solution containing the $Cu^{II}$/**TPMA** complex and the monomer. In all cases, is it possible to see the disappearance of the anodic peak, corresponding to the reoxidation of Cu(I) to Cu(II), indicating the beginning of the polymerization process.

### 5.6.4 Polymerization of OEOMA monomers using Cu/TPMA as catalyst

The 7.2 mL water solution containing 1 mM of **TPMA** ligand, 1 mM of $CuCl_2$, 0.1 M of NaBr, 10% v/v of monomer and 2 mM of HEBiB was used for the polymerization processes. The 5 necks electrochemical cell was equipped with 3 electrodes.

*Working electrode (WE):* platinum mesh electrode was used. Before every polymerization the electrode was subjected to a cleaning and activation process, consisting of 100-200 scanning cycles (speed 0.2 $Vs^{-1}$ ) between the potentials -0.65 V and 0.6 V vs SCE (saturated calomel electrode) in a 0.5 M solution sulphuric acid in bi-distilled water.

*Counter electrode (CE):* glass frit with methylcellulose gel saturated with 0.1 M *n*-$Bu_4NBF_4$ in dimethylformamide (DMF) and a graphite mine immersed.

*Reference electrode (RE):* Ag/AgI/ *n*-$Bu_4NI$ was used as reference, glass frit with methylcellulose gel saturated with a solution of 0.1 M *n*-$Bu_4NI$ in DMF.

The environment into the cell was well deoxygenated through a continuous nitrogen flow, thermostated at 25 °C and the solution stirred with a magnetic bar throughout the duration of the reaction. Each polymerization was followed for 4 hours and during the process, periodic sampling of the solution in the cell was carried out using a single-use syringe previously degassed with nitrogen flow. The sample taken before starting the polymerization (t = 0) was analyzed only by 600 MHz $^1$H-NMR for the determination of the conversion. The other samples were taken after t = 30, 60, 120, 180 and 240 min and were properly treated and analyzed by 600 $^1$H-NMR and gel permeation chromatography (GPC).

*[1]H-NMR NMR analysis:* 50 µL of solution were taken from the solution and diluted with 400 µL of Deuterium oxide ($D_2O$) and 30 µL (0.01 M) solution of DMSO in $D_2O$ as internal standard.

*GPC analysis:* The samples for GPC analysis were diluted with a 10 mM LiBr solution in DMF and then filtered through a neutral alumina layer and a 0.2 µm porosity PTFE filter (VWR) to eliminate the catalyst present in the sample and any other particle that could damage the column.

The degree of polymerization (DP) was calculated using the formula:

DP = [Monomer] / [Initiator]

The Theoretical Molecular weight ($Mn_{th}$) was calculated using the formula:

$Mn_{th} = ( MM_{Monomer} \times DP) + MM_{Initiator}$

| ***Entry*** | ***Monomer*** | **$DP_{target}$** | **$Mn_{th}$** |
|---|---|---|---|
| ***1*** | *$OEOMA_{2000}$* | 27 | 54211 |
| ***2*** | *$OEOMA_{950}$* | 58 | 55311 |
| ***3*** | *$OEOMA_{500}$* | 108 | 54211 |
| ***4*** | *$OEOMA_{300}$* | 170 | 51211 |

*$OEOMA_{2000}$:*

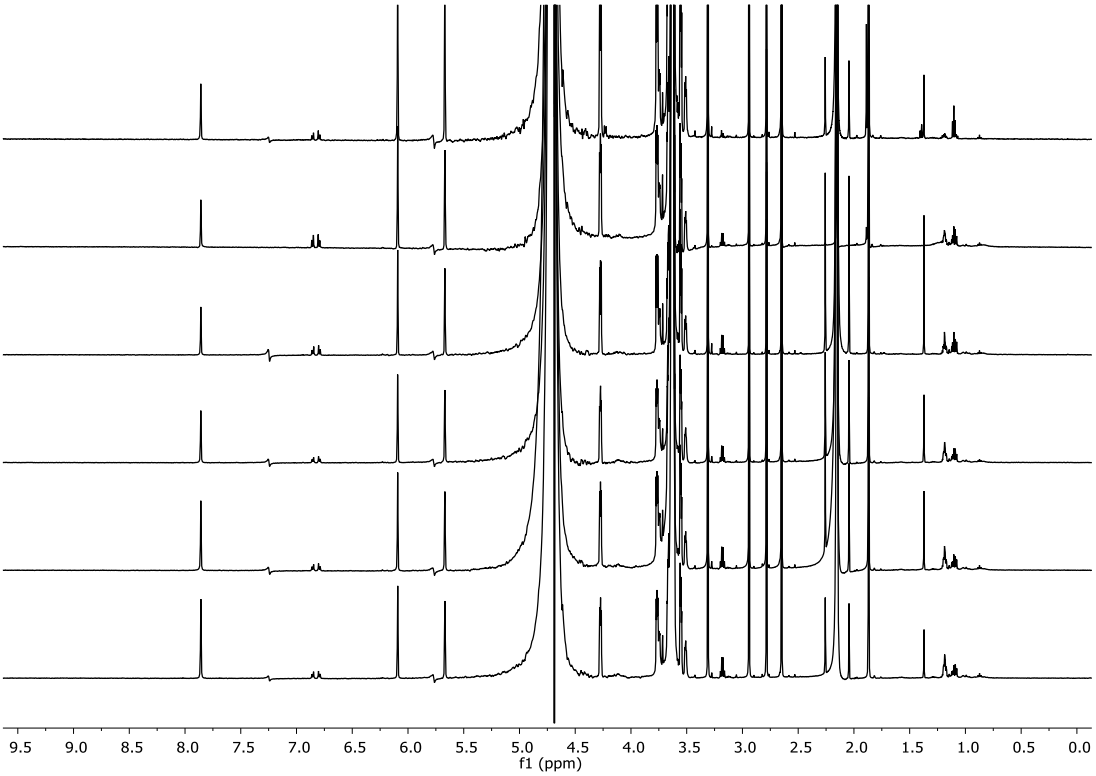


**Figure 53** 600 MHz $^1$H-NMR spectra stacking for the polymerization reaction of $OEOMA_{2000}$ monomer catalyzed by **Cu/TPMA**. From top to bottom spectra recorded at time = 0, 30min, 1 hour, 2 hours, 3 hours and 4 hours. Integrals corresponding to the monomer, 6.10 ppm and 5.67 ppm signals, and polymer, signals between 1.3-0.7 ppm, have been used to determine the conversion. Integrals are referred to the internal standard DMSO-$d_6$ signal at 2.67 ppm.

*OEOMA$_{950}$:*

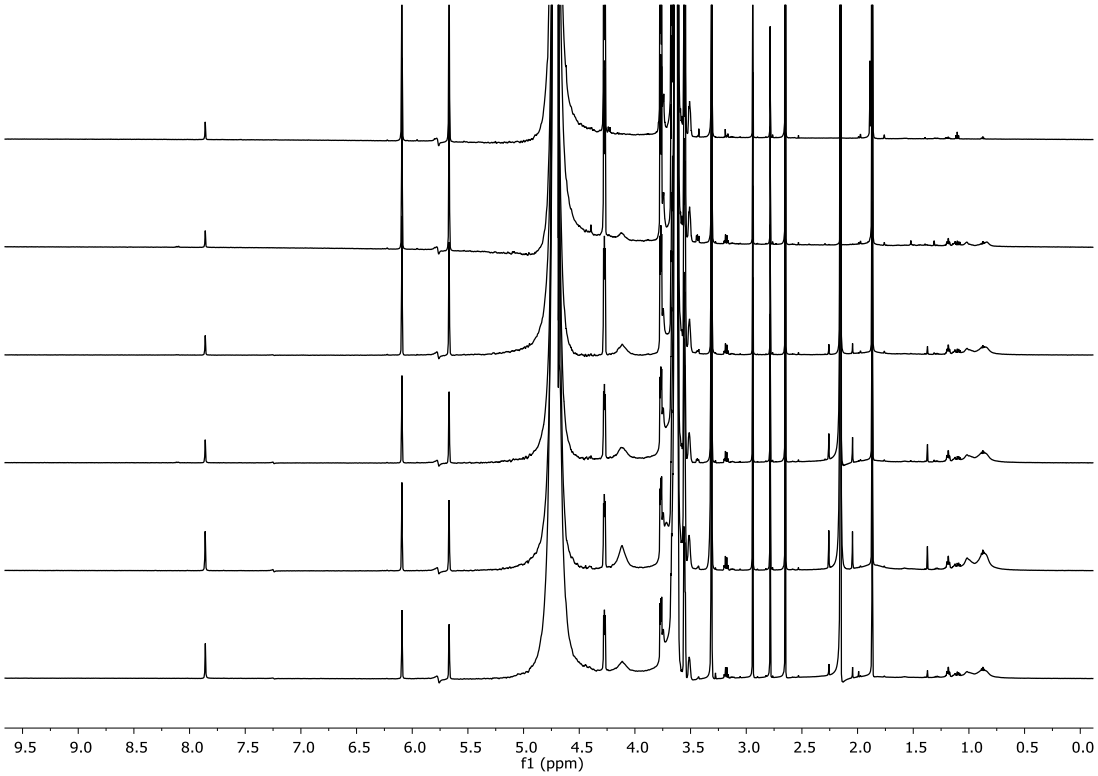


**Figure 54** 600 MHz $^{1}$H-NMR spectra stacking for the polymerization reaction of OEOMA$_{950}$ monomer catalyzed by **Cu/TPMA**. From top to bottom spectra recorded at time = 0, 30min, 1 hour, 2 hours, 3 hours and 4 hours. Integrals corresponding to the monomer, 6.10 ppm and 5.67 ppm signals, and polymer, signals between 1.3-0.7 ppm, have been used to determine the conversion. Integrals are referred to the internal standard DMSO-$d_6$ signal at 2.67 ppm.

*$OEOMA_{500}$:*

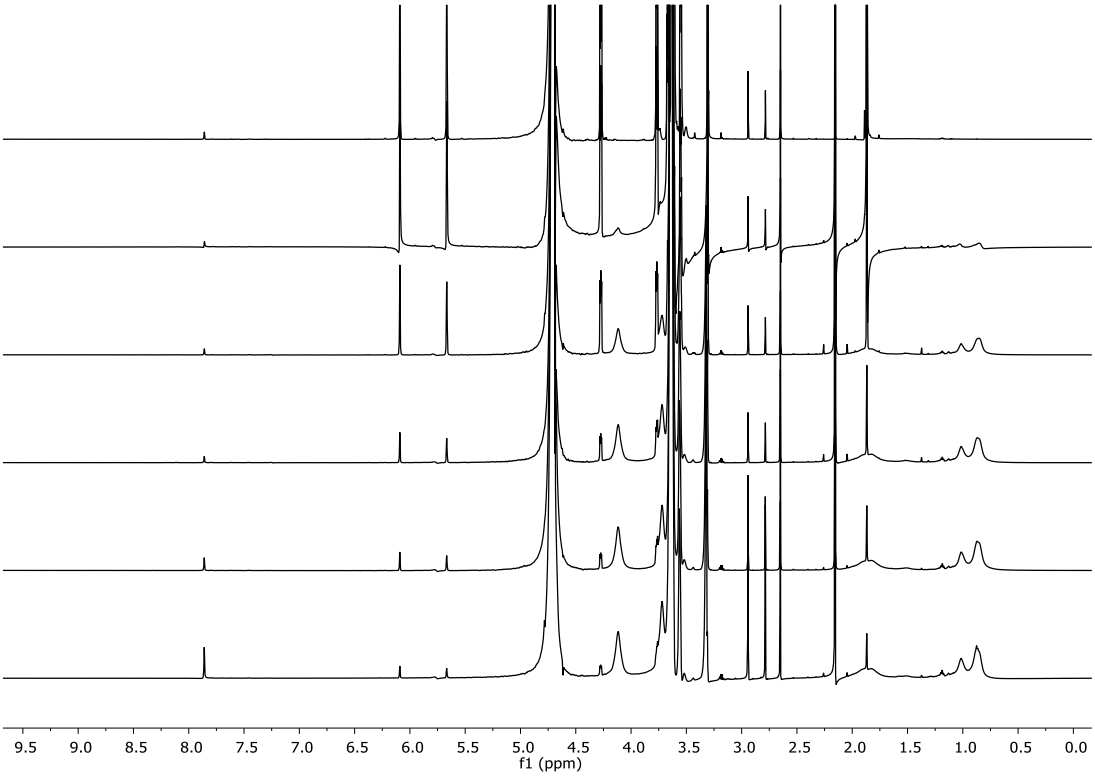


**Figure 55** 600 MHz $^{1}$H-NMR spectra stacking for the polymerization reaction of $OEOMA_{500}$ monomer catalyzed by **Cu/TPMA**. From top to bottom spectra recorded at time = 0, 30min, 1 hour, 2 hours, 3 hours and 4 hours. Integrals corresponding to the monomer, 6.10 ppm and 5.67 ppm signals, and polymer, signals between 1.3-0.7 ppm, have been used to determine the conversion. Integrals are referred to the internal standard DMSO-$d_6$ signal at 2.67 ppm.

*OEOMA$_{300}$:*

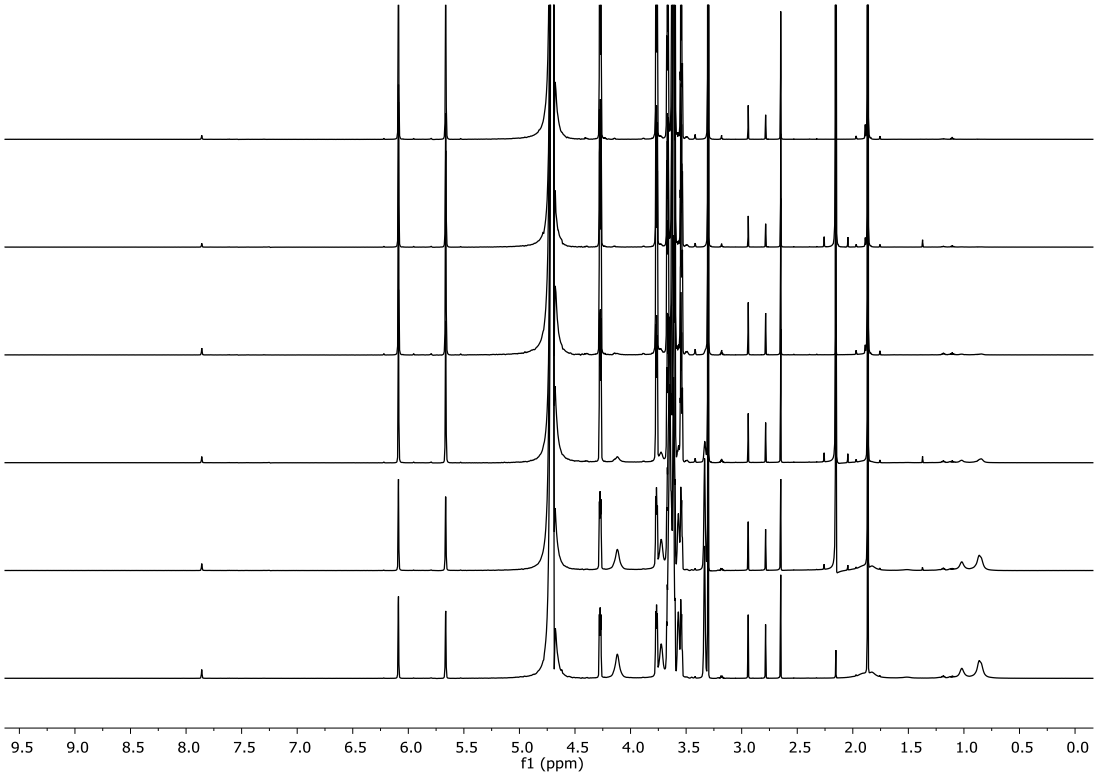


**Figure 56** 600 MHz $^{1}$H-NMR spectra stacking for the polymerization reaction of OEOMA$_{300}$ monomer catalyzed by **Cu/TPMA**. From top to bottom spectra recorded at time = 0, 30min, 1 hour, 2 hours, 3 hours and 4 hours. Integrals corresponding to the monomer, 6.10 ppm and 5.67 ppm signals, and polymer, signals between 1.3-0.7 ppm, have been used to determine the conversion. Integrals are referred to the internal standard DMSO-$d_6$ signal at 2.67 ppm.

## 5.7 General procedure for the study of methacrylic acid monomer polymerization catalyzed by Cu/Cage complex

For the setup of the reaction a 5 necks electrochemical cell was used, equipped with three electrodes.

*Working electrode (WE):* Glassy Carbon (GC) disc (3 mm diameter) was employed as working electrode for kinetic analysis. GC is commonly used because of its low electrical resistance and adsorption coefficient that prevents the adsorption of molecules on its surface, reducing the risk of electrode passivation and the corresponding drop in active area.

*Counter electrode (CE):* the electrode was assembled using a glass frit with methylcellulose gel saturated with 0.1 M *n*-$Bu_4NBF_4$ in dimethylformamide (DMF) and a graphite mine immersed.

*Reference electrode (RE):* standard saturated calomel electrode (SCE)

All experiments were conducted in 7.2 mL of water as solvent using NaBr 0.1 M as supporting electrolyte. The environment into the cell was well deoxygenated through a continuous nitrogen flow, thermostated at 25 °C and the solution stirred with a magnetic bar.

### 5.7.1 Cyclic voltammetry of the Cage-28 complex at different acidic pH

Redox properties of Cage **Cu-28** were investigated in water by cyclic voltammetry (CV) at different acidic pH values. The ligand Cage **28** was complexed in situ with a solution 0.1 M $CuCl_2$ in a 1:2 Cage **28** : $CuCl_2$ stoichiometric ratio. After setting up the electrochemical cell with the three electrodes, 13.2 mg (0.5 mM, 4 μmol) of the ligand Cage **28** were added to 7.2 mL of water and complexed with 80 μL (1 mM, 8 μmol) of a solution 0.1 M of $CuCl_2$. The solution was deoxygenated and stirred for 30 minutes and then a cyclic voltammetry was recorded in a quite environment (i.e. unstirred solution) allowing the process to be diffusion-controlled.

The voltammetry was recorded at a scan rate of 200 mV/s and potential range of 300 mV to -500 mV vs SCE. The reaction conditions of each experiment at different pH values are shown in Table 1.

| *Entry* | *pH* | *Acid* | **Supporting electrolyte** |
|---|---|---|---|
| ***1*** | 2.5 | | 5 mM NaCl |
| ***2*** | 1.1 | HOTf | 5 mM NaCl |
| ***3*** | 0.8 | HOTf | 5 mM NaCl |
| ***4*** | 0.8 | HCl | 5 mM NaCl |

**Table 3** Reaction conditions for all the experiments at different acidic pH values. Entry 1) Natural pH of the Cu/Cage catalyst, no acid has been added in this case, 2) pH = 1.1 obtained by adding to the solution 400 µL of triflic acid (HOTf), 3) pH = 0.8 obtained by adding to the solution 1800 µL of triflic acid, 4) pH = 0.8 obtained by adding to the solution 1500 µL of chloridric acid (HCl). All experiment were conducted using 5 mM NaCl as supporting electrolyte.

### 5.7.2 Cyclic voltammetry in the presence of the monomer

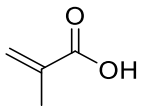


A second cyclic voltammetry was recorded for each experiment after the addition of 0.8 mL (10 % v/v, 1.18 M, 9.5 mmol) of methacrylic acid. The experimental parameters were kept constant and the solution was stirred and degassed for 5 minutes before recording. A reversible peak couple was observed in all cases, corresponding to one electron transfer.

### 5.7.3 Cyclic voltammetry in the presence of the initiator

Another cyclic voltammetry was recorded after the addition of the polymerization initiator, keeping a potential range of 300 mV to -500 mV and a scan rate of 200 mV/s. Even in this case, the solution was stirred and degassed for 5 minutes before recording. 2-hydroxyethyl 2-bromoisobutyrate (HEBiB) was chosen as initiator and 2.5 µL (2 mM, 16 µmol) were added to the solution containing Cage **Cu-28** complex and the monomer. In all cases, is it possible to see the disappearance of the anodic peak, corresponding to the reoxidation of Cu(I) to Cu(II), indicating the beginning of the polymerization process.

### 5.7.4 Polymerization of Methacrylic acid using Cage Cu-28 as catalyst

The 7.2 mL water solution containing 0.5 mM of Cage **28** ligand, 1 mM of $CuCl_2$, 5 mM of NaCl, 10% v/v of methacrylic acid and 2 mM of HEBiB was used for the polymerization processes. The 5 necks electrochemical cell was equipped with 3 electrodes.

*Working electrode (WE):* platinum mesh electrode was used. Before every polymerization the electrode was subjected to a cleaning and activation process, consisting of 100-200 scanning cycles (speed 0.2 $Vs^{-1}$ ) between the potentials -0.65 V and 0.6 V vs SCE (saturated calomel electrode) in a 0.5 M solution sulphuric acid in bi-distilled water.

*Counter electrode (CE):* glass frit with methylcellulose gel saturated with 0.1 M *n*-$Bu_4NBF_4$ in dimethylformamide (DMF) and a graphite mine immersed.

*Reference electrode (RE):* standard saturated calomel electrode (SCE).

The environment into the cell was well deoxygenated through a continuous nitrogen flow, thermostated at 25 °C and the solution stirred with a magnetic bar throughout the duration of the reaction. Each polymerization was followed for 4 hours and during the process, periodic sampling of the solution in the cell was carried out using a single-use syringe previously degassed with nitrogen flow. The sample taken were analyzed only by 600 MHz $^1$H-NMR for the determination of the conversion. The samples were taken after t = 0, 30, 60, 120, 180 and 240 min.

A standard applied potential ($E_{app}$) of – 350 mV vs SCE was used for each polymerization process.

*$^1$H-NMR NMR analysis:* 50 µL of solution were withdrawn from the solution and diluted with 400 µL of Deuterium oxide ($D_2O$) and 30 µL (0.01 M) solution of DMSO in $D_2O$ as internal standard.

The degree of polymerization (DP) was calculated using the formula:

DP = [Monomer] / [Initiator] = 1.18 M / 0.002 M = 590

The Theoretical Molecular weight ($Mn_{th}$) was calculated using the formula:

$Mn_{th}$ = ( $MM_{Monomer}$ x DP) + $MM_{Initiator}$ = ( 86.06 g/mol x 590 ) + 211 g/mol = 50986 g/mol

*Polymerization at pH 2.5:*

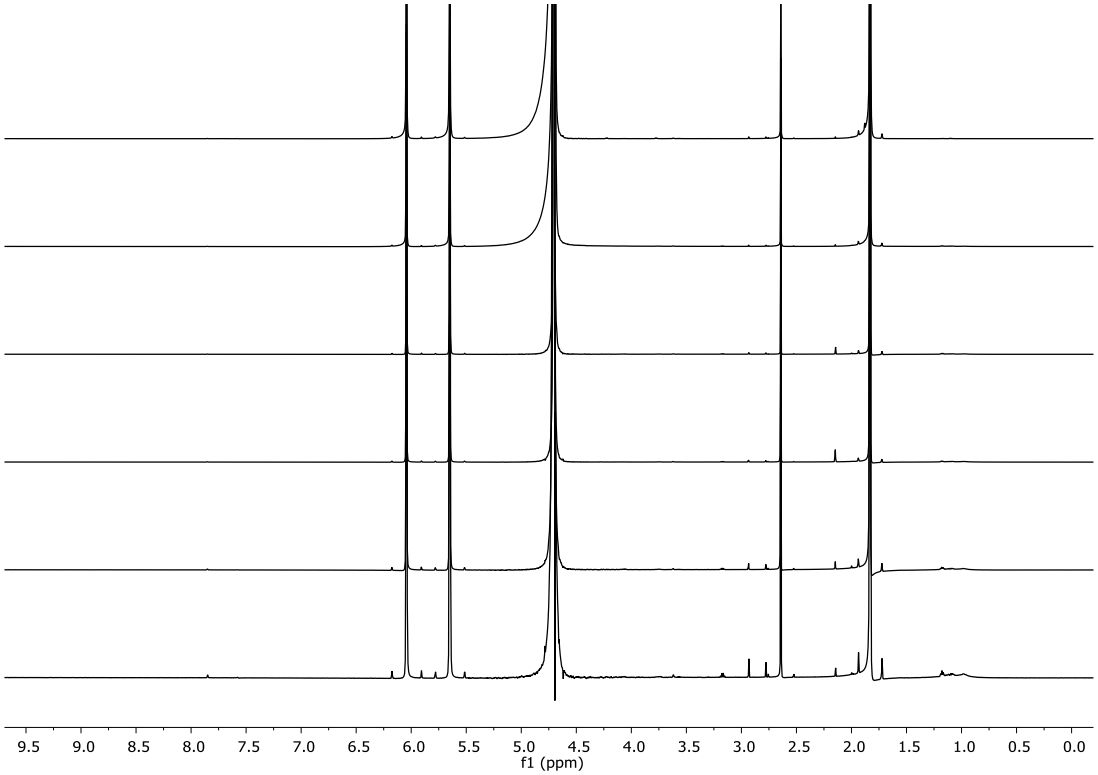


**Figure 57** 600 MHz $^{1}$H-NMR spectra stacking for the polymerization reaction of methacrylic acid catalyzed by Cage **Cu-28** referred to Entry 1 Table 1 experiment. From top to bottom spectra recorded at time = 0, 30min, 1 hour, 2 hours, 3 hours and 4 hours. Integrals corresponding to the monomer, 6.06 ppm and 5.67 ppm signals, and polymer, signals between 1.3-0.7 ppm, have been used to determine the conversion. Integrals are referred to the internal standard DMSO-$d_6$ signal at 2.67 ppm.

*Polymerization at pH 1.1 with HOTf:*

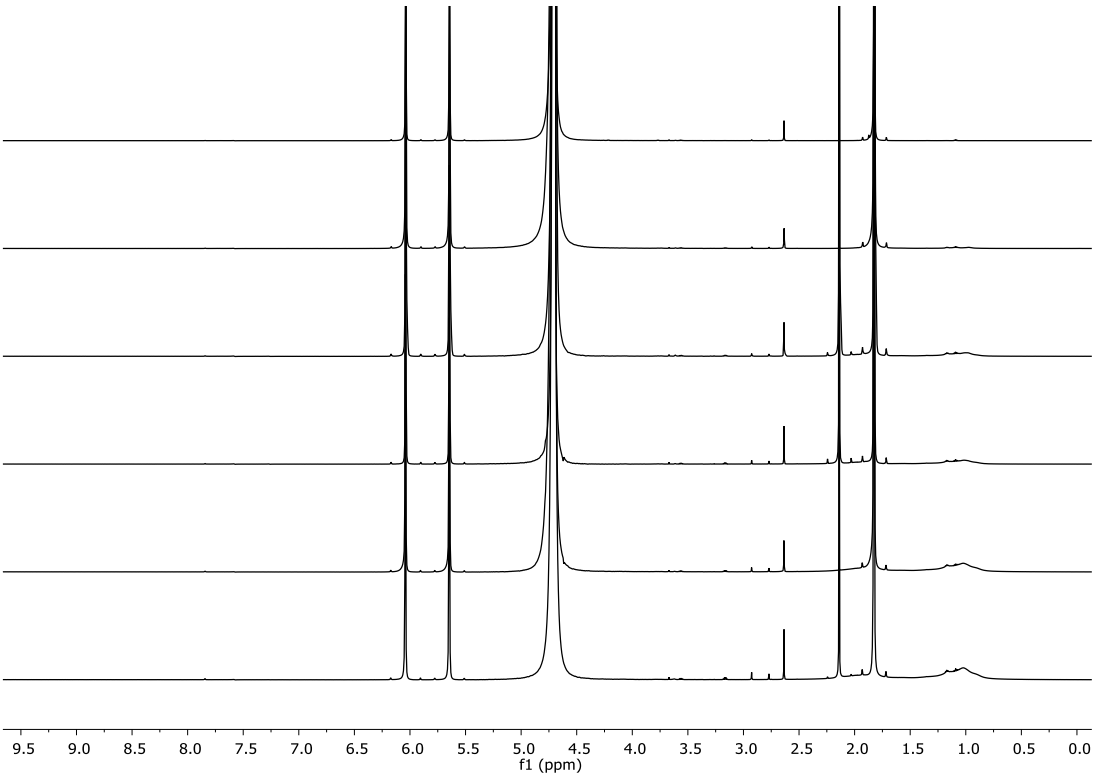


**Figure 58** 600 MHz $^{1}$H-NMR spectra stacking for the polymerization reaction of methacrylic acid catalyzed by Cage **Cu-28** referred to Entry 2 Table 1 experiment. From top to bottom spectra recorded at time = 0, 30min, 1 hour, 2 hours, 3 hours and 4 hours. Integrals corresponding to the monomer, 6.06 ppm and 5.67 ppm signals, and polymer, signals between 1.3-0.7 ppm, have been used to determine the conversion. Integrals are referred to the internal standard DMSO-$d_6$ signal at 2.67 ppm.

*Polymerization at pH 0.8 with HOTf:*

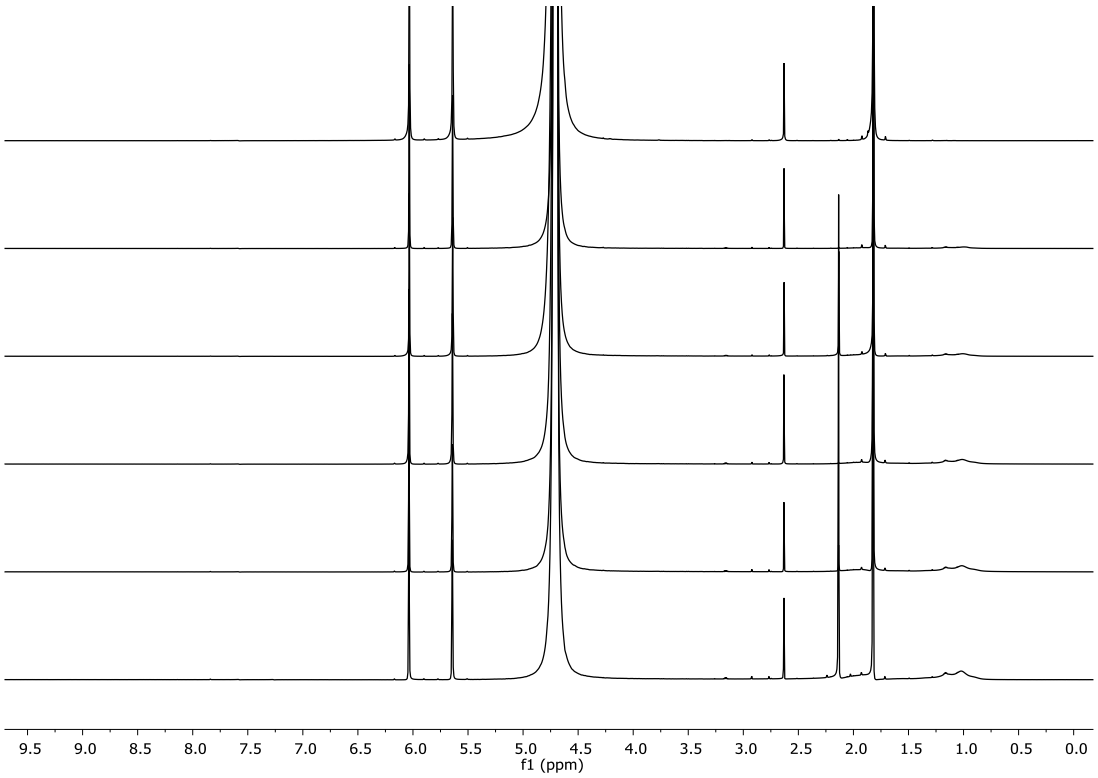


**Figure 59** 600 MHz $^{1}$H-NMR spectra stacking for the polymerization reaction of methacrylic acid catalyzed by Cage **Cu-28** referred to Entry 3 Table 1 experiment. From top to bottom spectra recorded at time = 0, 30min, 1 hour, 2 hours, 3 hours and 4 hours. Integrals corresponding to the monomer, 6.06 ppm and 5.67 ppm signals, and polymer, signals between 1.3-0.7 ppm, have been used to determine the conversion. Integrals are referred to the internal standard DMSO-$d_6$ signal at 2.67 ppm.

*Polymerization at pH 0.8 with HCl:*

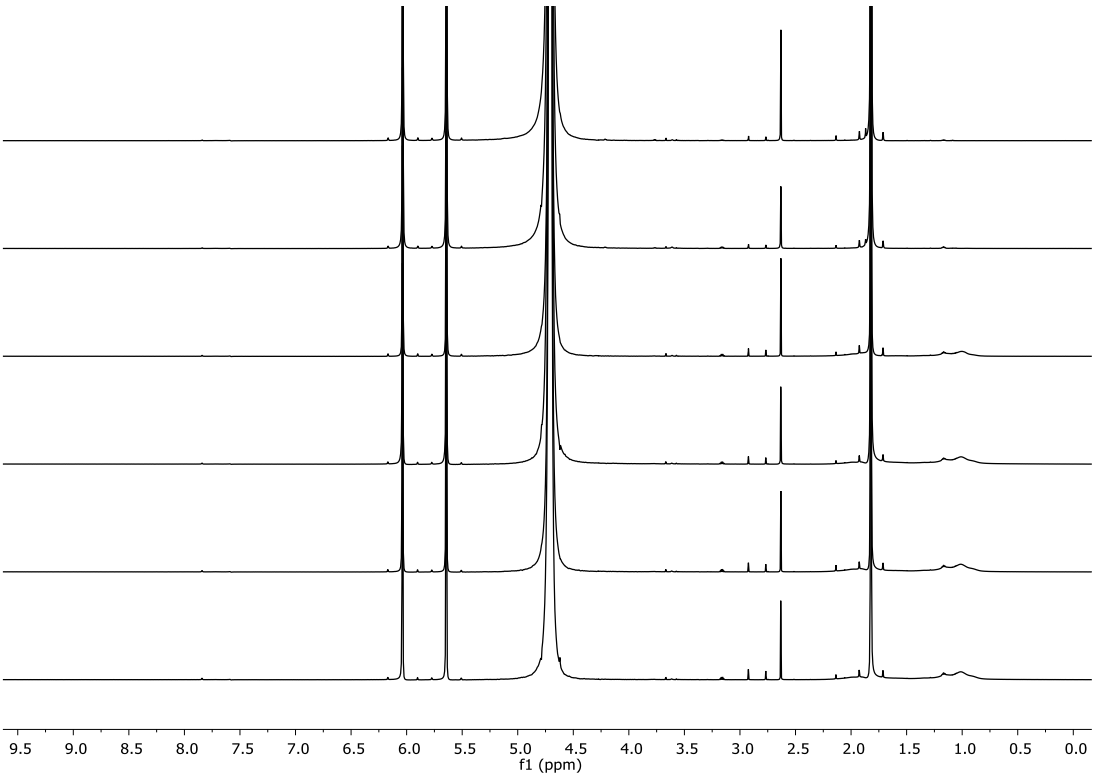


**Figure 60** 600 MHz $^{1}$H-NMR spectra stacking for the polymerization reaction of methacrylic acid catalyzed by Cage **Cu-28** referred to Entry 4 Table 1 experiment. From top to bottom spectra recorded at time = 0, 30min, 1 hour, 2 hours, 3 hours and 4 hours. Integrals corresponding to the monomer, 6.06 ppm and 5.67 ppm signals, and polymer, signals between 1.3-0.7 ppm, have been used to determine the conversion. Integrals are referred to the internal standard DMSO-$d_6$ signal at 2.67 ppm.

# 6 REFERENCES


(1) Yoon, T. P.; Jacobsen, E. N. Privileged Chiral Catalysts. *Science (80-. ).* **2003**, *299* (5613), 1691–1693.

(2) Leenders, S. H. A. M.; Gramage-Doria, R.; De Bruin, B.; Reek, J. N. H. Transition Metal Catalysis in Confined Spaces. *Chem. Soc. Rev.* **2015**, *44* (2), 433–448.

(3) Blackman, A. G. Tripodal Tetraamine Ligands Containing Three Pyridine Units: The Other Polypyridyl Ligands. *Eur. J. Inorg. Chem.* **2008**, No. 17, 2633–2647.

(4) M.M. da Mota, J. Rodgers, S. M. N. The Co-Ordination Number of Transition Metal Ions. Part VII. An Evaluation of Steric Factors in the Stabilization of High Spin Five-Co-Ordinate Nickel(II) Complexes of Multidentate TPMA Ligands. *Chem. Soc. Rev.* **1969**, 2036–2044.

(5) Anderegg, G.; Hubmann, E.; Podder, N. G.; Wenk, F. No Title. *Helv. Chim. Acta* **1977**, *60*, 123–140.

(6) Abdel-Magid, A. F.; Carson, K. G.; Harris, B. D.; Maryanoff, C. A.; Shah, R. D. Reductive Amination of Aldehydes and Ketones with Sodium Triacetoxyborohydride. Studies on Direct and Indirect Reductive Amination Procedures. *J. Org. Chem.* **1996**, *61* (11), 3849–3862.

(7) D.G. Lonnon, D.C. Craig, S. B. C. Rhodium, Palladium and Platinum Complexes of Tris(Pyridylalkyl)Amine and Tris(Benzimidazolylmethyl)Amine N4-Tripodal Ligands. *Dalt. Trans.* **2006**, 3785–3797.

(8) Szajna, E.; Dobrowolski, P.; Fuller, A. L.; Arif, A. M.; Berreau, L. M. NMR Studies of Mononuclear Octahedral Ni(II) Complexes Supported by Tris((2-Pyridyl)Methyl)Amine-Type Ligands. *Inorg. Chem.* **2004**, *43* (13), 3988–3997.

(9) Diebold, A.; Hagen, K. S. Iron(II) Polyamine Chemistry: Variation of Spin State and Coordination Number in Solid State and Solution with Iron(II) Tris(2-Pyridylmethyl)Amine Complexes. *Inorg. Chem.* **1998**, *37* (2), 215–223.

(10) Natali, M.; Badetti, E.; Deponti, E.; Gamberoni, M.; Scaramuzzo, F. A.; Sartorel, A.; Zonta, C. Photoinduced Hydrogen Evolution with New Tetradentate Cobalt(Ii) Complexes Based on the TPMA Ligand. *Dalt. Trans.* **2016**, *45* (37), 14764–14773.

(11) Benazzi, E.; Begato, F.; Niorettini, A.; Destro, L.; Wurst, K.; Licini, G.; Agnoli,

S.; Zonta, C.; Natali, M. Electrocatalytic Hydrogen Evolution Using Hybrid Electrodes Based on Single-Walled Carbon Nanohorns and Cobalt(Ii) Polypyridine Complexes. *J. Mater. Chem. A* **2021**, *9* (35), 20032–20039.

(12) Carmo dos Santos, N. A.; Lorandi, F.; Badetti, E.; Wurst, K.; Isse, A. A.; Gennaro, A.; Licini, G.; Zonta, C. Tuning the Reactivity and Efficiency of Copper Catalysts for Atom Transfer Radical Polymerization by Synthetic Modification of Tris(2-Methylpyridyl)Amine. *Polymer (Guildf).* **2017**, *128*, 169–176.

(13) Chan, S. L. F.; Lam, T. L.; Yang, C.; Lai, J.; Cao, B.; Zhou, Z.; Zhu, Q. Cobalt(II) Tris(2-Pyridylmethyl)Amine Complexes [Co(TPA)X]+bearing Coordinating Anion (X = Cl−, Br−, I−and NCS−): Synthesis and Application for Carbon Dioxide Reduction. *Polyhedron* **2017**, *125*, 156–163.

(14) Chan, S. L. F.; Lam, T. L.; Yang, C.; Yan, S. C.; Cheng, N. M. A Robust and Efficient Cobalt Molecular Catalyst for CO2 Reduction. *Chem. Commun.* **2015**, *51* (37), 7799–7801.

(15) You, L.; Pescitelli, G.; Anslyn, E. V.; Di Bari, L. An Exciton-Coupled Circular Dichroism Protocol for the Determination of Identity, Chirality, and Enantiomeric Excess of Chiral Secondary Alcohols. *J. Am. Chem. Soc.* **2012**, *134* (16), 7117–7125.

(16) Aktar, M. A.; Alam, M. M.; Al-Amin, A. Q. Global Economic Crisis, Energy Use, CO2 Emissions, and Policy Roadmap amid COVID-19. *Sustain. Prod. Consum.* **2021**, *26*, 770–781.

(17) Tong, L.; Zong, R.; Thummel, R. P. Molecular Cobalt Complex. *J. Am. Chem. Soc.* **2014**, 5–8.

(18) Schroder, K.; Mathers, R. T.; Buback, J.; Konkolewicz, D.; Magenau, A. J. D.; Matyjaszewski, K. Substituted Tris(2-Pyridylmethyl)Amine Ligands for Highly Active ATRP Catalysts. *ACS Macro Lett.* **2012**, *1* (8), 1037–1040.

(19) Fantin, M.; Isse, A. A.; Bortolamei, N.; Matyjaszewski, K.; Gennaro, A. Electrochemical Approaches to the Determination of Rate Constants for the Activation Step in Atom Transfer Radical Polymerization. *Electrochim. Acta* **2016**, *222*, 393–401.

(20) Wang, J.-S.; Matyjaszewski, K. Controlled /“ Living ” Radical Polymerization . Atom Transfer Radical Polymerization in the Presence of Pi-Cl. *J. Am. Chem.*

*Soc.* **1995**, *117* (6), 5614–5615.

(21) Sawamoto, M.; Higashimura, T. (Triphenylphosphine)Ruthenium(II)/ Methylaluminum. **1995**, *2* (Ii), 1721–1723.

(22) Matyjaszewski, K.; Paik, H. J.; Zhou, P.; Diamanti, S. J. Determination of Activation and Deactivation Rate Constants of Model Compounds in Atom Transfer Radical Polymerization1. *Macromolecules* **2001**, *34* (15), 5125–5131.

(23) Bortolamei, N.; Isse, A. A.; Magenau, A. J. D.; Gennaro, A.; Matyjaszewski, K. Controlled Aqueous Atom Transfer Radical Polymerization with Electrochemical Generation of the Active Catalyst. *Angew. Chemie - Int. Ed.* **2011**, *50* (48), 11391–11394.

(24) Zhang, G.; Mastalerz, M. Organic Cage Compounds-from Shape-Persistency to Function. *Chem. Soc. Rev.* **2014**, *43* (6), 1934–1947.

(25) Kang, J. and J. R. Molecular Capsule. **1997**, *385* (January), 50–52.

(26) Heinz, T.; Rudkevich, D. M.; Rebek, J. Pairwise Selection of Guests in a Cylindrical Molecular Capsule of Nanometre Dimensions. *Nature* **1998**, *394* (6695), 764–766.

(27) Fujita, D.; Suzuki, K.; Sato, S.; Yagi-Utsumi, M.; Yamaguchi, Y.; Mizuno, N.; Kumasaka, T.; Takata, M.; Noda, M.; Uchiyama, S.; Kato, K.; Fujita, M. Protein Encapsulation within Synthetic Molecular Hosts. *Nat. Commun.* **2012**, *3* (May), 2–8.

(28) Höger, S. Shape-Persistent Macrocycles: From Molecules to Materials. *Chem. - A Eur. J.* **2004**, *10* (6), 1320–1329. https://doi.org/10.1002/chem.200305496.

(29) Cook, T. R.; Stang, P. J. Recent Developments in the Preparation and Chemistry of Metallacycles and Metallacages via Coordination. *Chem. Rev.* **2015**, *115* (15), 7001–7045.

(30) Zhou, H. C. J.; Kitagawa, S. Metal-Organic Frameworks (MOFs). *Chem. Soc. Rev.* **2014**, *43* (16), 5415–5418.

(31) Yamashina, M.; Tanaka, Y.; Lavendomme, R.; Ronson, T. K.; Pittelkow, M.; Nitschke, J. R. An Antiaromatic-Walled Nanospace. *Nature* **2019**, *574* (7779), 511–515.

(32) Chemistry A European J - 2018 - Tan - Supramolecular Coordination Cages for Asymmetric Catalysis.Pdf.

(33) Angew Chem Int Ed - 2020 - Guo - Visible Light Photocatalysis of Asymmetric

2 2 Cycloaddition in Cage Confined Nanospace.

(34) Caulder, D. L.; Powers, R. E.; Parac, T. N.; Raymond, K. N. The Self-Assembly of a Predesigned Tetrahedral M4L4 Supramolecular Cluster. *Angew. Chemie - Int. Ed.* **1998**, *37* (13–14), 1840–1843.

(35) Fiedler, D.; Bergman, R. G.; Raymond, K. N. Supramolecular Catalysis of a Unimolecular Transformation: Aza-Cope Rearrangement within a Self-Assembled Host. *Angew. Chemie* **2004**, *116* (48), 6916–6919.

(36) Z.J. Wang, K.N. Clary, R.G. Bergman, K. N. R. and F. D. T. Z.J. *Nat. Chem.* **2015**, 100–103.

(37) Fang, Y.; Powell, J. A.; Li, E.; Wang, Q.; Perry, Z.; Kirchon, A.; Yang, X.; Xiao, Z.; Zhu, C.; Zhang, L.; Huang, F.; Zhou, H. C. Catalytic Reactions within the Cavity of Coordination Cages. *Chem. Soc. Rev.* **2019**, *48* (17), 4707–4730.

(38) Guo, J.; Xu, Y.-W.; Li, K.; Xiao, L.-M.; Chen, S.; Wu, K.; Chen, X.-D.; Fan, Y.-Z.; Liu, J.-M.; Su, C.-Y. Regio- and Enantioselective Photodimerization within the Confined Space of a Homochiral Ruthenium/Palladium Heterometallic Coordination Cage. *Angew. Chemie* **2017**, *129* (14), 3910–3914.

(39) Chen, S.; Chen, L.-J. Metal–Organic Cages: Applications in Organic Reactions. *Chemistry (Easton).* **2022**, *4* (2), 494–519.

(40) Bravin, C.; Badetti, E.; Scaramuzzo, F. A.; Licini, G.; Zonta, C. Triggering Assembly and Disassembly of a Supramolecular Cage. *J. Am. Chem. Soc.* **2017**, *139* (18), 6456–6460.

(41) Rowan, S. J.; Cantrill, S. J.; Cousins, G. R. L.; Sanders, J. K. M.; Stoddart, J. F. *Dynamic Covalent Chemistry*; 2002; Vol. 41.

(42) Acharyya, K.; Mukherjee, P. S. Organic Imine Cages: Molecular Marriage and Applications. *Angew. Chemie* **2019**, *131* (26), 8732–8745.

(43) Joyce, L. A.; Maynor, M. S.; Dragna, J. M.; Da Cruz, G. M.; Lynch, V. M.; Canary, J. W.; Anslyn, E. V. A Simple Method for the Determination of Enantiomeric Excess and Identity of Chiral Carboxylic Acids. *J. Am. Chem. Soc.* **2011**, *133* (34), 13746–13752.

(44) Bravin, C.; Badetti, E.; Puttreddy, R.; Pan, F.; Rissanen, K.; Licini, G.; Zonta, C. Binding Profiles of Self-Assembled Supramolecular Cages from ESI-MS Based Methodology. *Chem. - A Eur. J.* **2018**, *24* (12), 2936–2943.

(45) Begato, F.; Penasa, R.; Licini, G.; Zonta, C. Straight from the Bottle! Wine and

Juice Dicarboxylic Acids as Templates for Supramolecular Cage Self-Assembly. *Chem. Commun.* **2021**, *57* (78), 10019–10022.

(46) Mastalerz, M.; Schneider, M. W.; Oppel, I. M.; Presly, O. A Salicylbisimine Cage Compound with High Surface Area and Selective CO2/CH4 Adsorption. *Angew. Chemie - Int. Ed.* **2011**, *50* (5), 1046–1051.

(47) Kim, H.; Nguyen, Y.; Yen, C. P. H.; Chagal, L.; Lough, A. J.; Kim, B. M.; Chin, J. Stereospecific Synthesis of C2 Symmetric Diamines from the Mother Diamine by Resonance-Assisted Hydrogen-Bond Directed Diaza-Cope Rearrangement. *J. Am. Chem. Soc.* **2008**, *130* (36), 12184–12191.

(48) Kim, H. J.; Kim, H.; Alhakimi, G.; Jeong, E. J.; Thavarajah, N.; Studnicki, L.; Koprianiuk, A.; Lough, A. J.; Suh, J.; Chin, J. Preorganization in Highly Enantioselective Diaza-Cope Rearrangement Reaction. *J. Am. Chem. Soc.* **2005**, *127* (47), 16370–16371.